Ca' Foscari University of Venice

Master's Degree Programme in

Conservation Science and Technology for Cultural Heritage

Final Thesis

Alteration and protection methods for glass in Cultural Heritage

Multi-analytical investigation into the composition effects for glass alteration under atmospheric and immersion conditions, and a study of two possible protection methods based on zinc salts and silica nanoparticles

Graduand
Anna Piccolo
matriculation number 870194

Supervisors
Robert Carlyle Pullar
Odile Majérus
Giulia Franceschin
Arianna Traviglia

Academic year 2021/2022

Ca' Foscari University of Venice

Master's Degree Programme in

Conservation Science and Technology for Cultural Heritage

Final Thesis

Alteration and protection methods for glass in Cultural Heritage

Multi-analytical investigation into the composition effects for glass alteration under atmospheric and immersion conditions, and a study of two possible protection methods based on zinc salts and silica nanoparticles

Graduand

Anna Piccolo

matriculation number 870194

Supervisors

Robert Carlyle Pullar

Odile Majérus

Giulia Franceschin

Arianna Traviglia

Academic year 2021/2022

Contents

Abstract

The composition effect on glass alteration was studied through a multi-analytical approach focused on plate and powder replicas. These were synthesised in a way to simplistically represent different glass formulations typically found in Cultural Heritage objects. Mixed alkali glass, characteristic of Medieval central Europe, was reproduced and studied in comparison with other compositions for which the alkali/alkaline earth ratio was systematically varied. Artificial ageing tests under both atmospheric and immersion conditions were carried out to investigate the different behaviours of the studied glass. The difference between stable and unstable compositions resulted straightforward as the latter easily presented flakes and salts formation upon ageing. The analytical results revealed they had undergone a severe hydration and, in some cases, also a change in the silica structure. Carbonate salts formed on samples surfaces as a secondary phenomenon, which was assessed to be temperature dependent. The ageing under immersion conditions resulted less aggressive, causing an incongruent dissolution that affected only a very thin layer of the material surface. Two possible methods for glass protection were also studied: one based on zinc salts and the other on a hydrophobic sol-gel coating. While the former was tested on plate samples, for the latter silica nanoparticles of different dimensions were synthesised and characterised as a preliminary step of the product formulation.

1. Frames and aims of the thesis

This work results from two internship projects, one held at the Research Institute of Chimie Paris (IRCP) and the other at the Italian Institute of Technology (IIT), both having as main focus the preservation and protection of glass against water alteration. The role of composition in glass durability, the difference between the ageing under atmospheric and immersion conditions and the protection efficacy of a zinc-salts based deposit were questioned in the former, as a continuation of the research started with Fanny Alloteau and Valentina Valbi and in the frame of the PhD project of Amandine Serve and the internship of Thalie Law. Saint Gobain Research (SGR) and the Centre de Recherche et de Restauration des Musées de France (C2RMF) were involved in this project, which comprised the study of twelve different compositions and targeted both industrial and Cultural Heritage (CH) glass. In this thesis, a focus on the latter is presented with the aim of shedding light on the mechanisms governing the alteration of CH glass objects, whether exposed to a humid atmospheric environment or immersed in water, and ultimately providing conservators with useful information and practical means of mitigating their degradation. Such objectives are common to the research conducted at the IIT, where the formulation of a silica-based coating with improved hydrophobicity is underway. In the frame of a project on Roman ancient glass preservation involving the post-doc fellow Giulia Franceschin and the PhD students Stefano Centenaro and Roberta Zanini, one of the very first steps of the protective development is here treated: the synthesis of silica nanoparticles (NPs) to be included in the coating. Its main objective being the advancement of the production protocol, the study on the method for silica NP synthesis was intertwined with the research conducted by the PhD student Neva Stucchi concerning the formulation of nano-structured consolidants for stone materials. In the present thesis, a contribution to the protocol optimisation is proposed and is aimed at determining a reproducible and efficient method for synthesising homogeneously spherical nanoparticles with tunable and definite size distributions. This would ease the protective formulation by allowing the control of NP production according to the experimental needs and could help determining the most convenient paths to follow if big quantities of material will be involved. Both the branches of this thesis work being quite vast, only sparkles of the composite wholes are tackled here. Without the claim of solving big questions on glass conservation, this work brings out a contribution, together with the testimony of two research projects that are still ongoing in Paris and Venice.

2. Introduction

Despite its early appearance in human culture [1–3], glass encloses manifold riddles to scholars and is still a matter of debate in the recent literature. Its hardness and transparency resulting from the firing of sand, it is not surprising that glass needed tremendous technological skills to be developed and that nowadays it requires equally scientific efforts for being understood. Glassmaking originated probably about 4500 years ago in Egypt, Mesopotamia or Syria, when the control over fire was such that elevated temperatures could be reached and crystalline silica could be converted into an amorphous material [3, 4]. Yet, this was not composed of pure SiO_2, as plant ashes were included in the mixture to lower the melting temperature and hence render glassmaking feasible for the available technology and favour workability [3, 4]. This way, oxides of mainly alkali and alkaline earth ions, that strongly impact on the melt viscosity and the liquidus temperature, were introduced in the composition and became part of the glass structure. According to the model developed by Zachariasen [5], this occurs through a depolymerisation of the silica network: some bonds between silicon and oxygen are broken for letting the so-called network modifiers in the structure and giving rise to non-bridging oxygens (NBO) [6, 7]. To describe the polymerisation degree of glass, the Q^n notation is commonly used, where Q indicates a silicate tetrahedron (SiO_4) and n the number of bridging oxygens bound to the Si atom (zero to four) [8, 9]. As the quantity and kind of network modifiers have a direct effect on the abundance and arrangement of the different Q^n species, glass composition is a parameter of paramount importance for the resulting structural cohesion of the material. Based on the size and charge of the cations, the network adjusts in complex and unique arrangements where the ion repulsions are minimised [4].

If on one hand the alkali ions have the role of *fluxes*, meaning that they lower melting and working temperature, on the other, they are generally agreed to be at the core of glass alteration, as they are loosely bound to the silica network and highly soluble in water [10]. The role of the different cations in glass durability is still not clear and it would rather be more appropriate to consider the whole composition, the structure being dependent on the relative amounts of the components [11]. What cannot be contested is the experimental evidence that the most severe alteration phenomena are observed to occur on glass with specific ranges of composition. These are generally labelled as *unstable* and mainly consist of two domains of glasses: one characterised by high SiO_2 content (equal or higher of about 70 mol%), high percentages of alkalis ($M_2O \sim 20$ mol%, M standing for *metal*) and low amounts of alkaline earth ions ($MO < 10$ mol%), and the other containing less SiO_2 (< 65 mol%) and more

alkalis and alkaline earth ions ($MO > 20$ mol% and M_2O around $15 - 20$ mol%) [12–14]. These are shown in Fig. 2.1 as *domains 1* (blue) and *2* (red), respectively. The latter group includes the so-called potash-lime-silica glass, which is well renowned for its poor resistance to degradation phenomena and was introduced in central Europe starting from the Middle-Ages, when glassmakers used inland trees (probably beechwood) and fern ashes in the starting batch [12, 14–16]. This was rich in lime, potash and magnesia and was probably chosen for its local availability. Natron (mineral containing mainly hydrated sodium carbonate) from Egypt or maritime Na-rich plant ash were instead used by Romans, whose high soda and high lime glass (yellow in Fig. 2.1) is renowned for its impressive durability [4, 15].

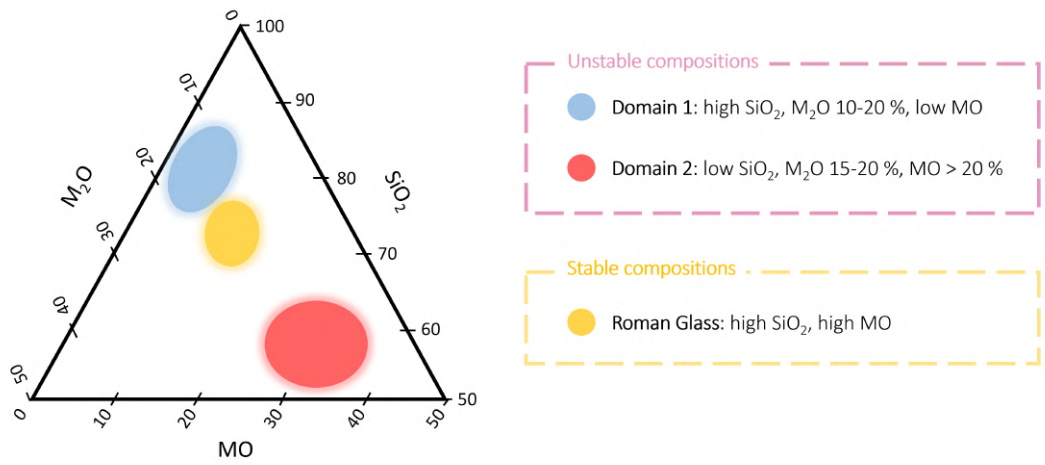

Figure 2.1: Ternary plot for representing glass compositions, built after the one proposed by Newton [17]. The molar percentages of SiO_2, M_2O and MO (M standing for *metal*) are reported as variables, and the diagram regions related to the glass compositions discussed in the text are indicated with different colours.

Whilst stable compositions such as that of Roman glass are generally retrieved in good state of conservation, unstable glasses often show severe signs of degradation, even if they are quite recent and/or stored under atmospheric conditions. This is the case of several items (such as objects, glazes or enamels) in historic glass museum collections, which have been reported to display evident changes in their appearance and sometimes to be physically damaged (see examples reported in Fig. 2.2)[1, 4, 11, 18–25]. The aesthetics is generally spoiled through a loss of the original transparency, which is replaced by a dull or cloudy effect [14, 16, 24, 26]. Salts deposits can be found on the glass surface as a consequence of alteration, and water droplets may form in the thereby named *sweating* or *weeping* glasses, due to the strong hygroscopic character of some alkali salts [18, 26]. Not only the appearance, but

also the physical resistance is jeopardised in an advanced stage of alteration, when crizzling (i.e. fine surface crazing) occurs. Manifesting with intricate interweavings of cracks, this phenomenon can ultimately lead to flake formation [14–16, 18, 20, 23, 27–30]. Delaminations curl upward from the glass surface and can be easily spalled away, so that material loss takes place [18, 19, 21, 24, 31]. While the mentioned symptoms are mainly related to the ageing under atmospheric conditions, typical signs of degradation for buried glasses are the presence of opaque surface crusts and the arising of iridescence [4]. The latter phenomenon affects both the aspect and the cohesion of glass and is recognisable as a rainbow effect on the glass surface. This stems from the interaction of light with the exfoliated material: a multitude of colours can be seen due to the interference among rays of light reflected by alternating layers of altered glass and air [4, 31–34].

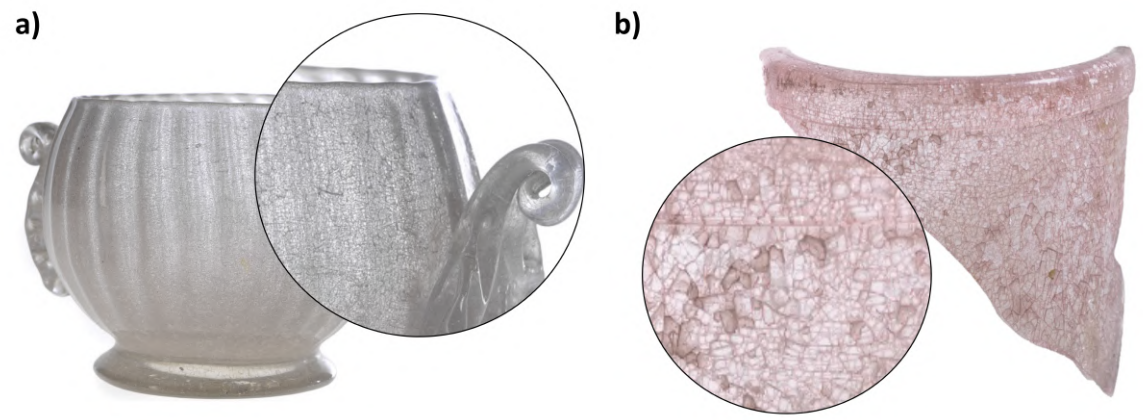

Figure 2.2: Photographs of ancient glass objects presenting visible signs of alteration, ©C2RMF, Anne Maigret. **(a)** Round ribbed sugar bowl (Venice, 18th century); **(b)** fragment of a blown glass oil dish (Burgundy, 18th century), both conserved at the Musée des Arts Décoratifs, Paris [35]

Being governed by multiple parameters, glass alteration is an extremely complex phenomenon that is still not fully understood [1, 12, 15, 16]. Both the composition and the weathering conditions play important roles in determining the degree and outcomes of degradation processes, which are diverse [31]. Whether under immersion or atmospheric conditions, glass alteration always occurs due to interaction with water [2, 12, 24, 31, 36]. Extensive research has been undertaken to disclose the chemical mechanisms involved in the corrosion processes occurring when glass is immersed in solution. Even if this is chiefly studied in the field of nuclear waste containment [21, 37–40], it is of great interest in the frame of CH, being fundamental for understanding the phenomenology of the degradation of archaeological glass both submerged in water basins or buried in damp soils [11, 15, 41]. Three competing phenomena are generally agreed to occur simultaneously, to be closely inter-related and con-

tribute in the overall so-called leaching process: ion exchange, glass hydration and network hydrolysis [7, 10, 12, 20, 31, 32, 36, 38, 42–45]. The ionic exchange involves protons from water and alkali ions of glass and leads to the formation of silanol ($Si-OH$) groups and to the leaching of network modifiers towards the surface.* The term *interdiffusion* is often used, so as to describe the concurrent inwards diffusion of protons from water and outward diffusion of alkalis from the glass. The process is reported in Eqs. (2.1) and (2.2), where the symbol $\equiv$ stands for three bonds of silicon with bridging or non-bridging oxygen atoms.

$$\equiv Si-O^- M^+ + H^+ \longrightarrow \equiv Si-OH + M^+ \tag{2.1}$$

$$\equiv Si-O^- M^+ + H_3O^+ \longrightarrow \equiv Si-OH + H_2O + M^+ \tag{2.2}$$

Silanol groups are also formed through glass hydration and hydrolysis, as shown in Eqs. (2.3) and (2.4), respectively. The one or the other reaction takes place according to the structure of the silica network: if there is enough space for molecular water to diffuse in glass (voids larger than 0.7 nm), hydration occurs, otherwise water penetration accomplishes through hydrolysis reactions [40, 45]. Since bridging bonds are broken, the glass structure is deeply modified by hydrolysis and, eventually, glass dissolution can take place. In addition, glass alteration is enhanced by the rise in pH originating from the leaching process itself: on one hand, the dissolution process (Eqs. (2.5) and (2.6)) is kinetically favoured as OH^- groups are better nucleophiles than H_2O, and, on the other, silica dissolution is thermodinamically facilitated by the increased solubility of silicic acid, existing as $Si(OH)_3O^-$ and $Si(OH)_2{O_2}^{2-}$ ions [39, 46–48]. A structural rearrangement can then take place through the condensation of silanols and consequent repolymerisation [36, 45]. Overall, the illustrated processes result in the partial dissolution of the surface material, the leaching of network modifiers and the formation of a silica rich, hydrated and porous layer, usually named *gel* [7, 9, 10, 38, 40, 45, 46, 49, 50].

$$\equiv Si-O^- M^+ + H_2O \longrightarrow \equiv Si-OH + M^+ + OH^- \tag{2.3}$$

$$\equiv Si-O-Si + H_2O \longrightarrow \equiv Si-OH + HO-Si \equiv \tag{2.4}$$

*The term *leaching* has a literal meaning here, while elsewhere in the text (as above) it indicates the overall alteration process that includes ion exchange, hydration and hydrolysis of glass.

$$\equiv \mathrm{Si} - \mathrm{O} - \mathrm{Si} + \mathrm{O\,H^-} \longrightarrow \equiv \mathrm{Si} - \mathrm{O^-} + \mathrm{O\,H} - \mathrm{Si} \equiv \tag{2.5}$$

$$\equiv \mathrm{Si} - \mathrm{O^-} + \mathrm{H_2\,O} \longrightarrow \equiv \mathrm{Si} - \mathrm{O\,H} + \mathrm{H\,O^-} \tag{2.6}$$

Glass alteration under immersion conditions is often described as a three stage process, where at the beginning (stage 1) ion exchange and network dissolution occur quite rapidly following the *forward rate*, subsequently the reactions are slowed down in stage 2 with the *residual rate* and finally, in some cases, the alteration can accelerate again in stage 3 [36–38, 40, 51]. The considerable rate drop described in such a model for the second phase of the alteration process stems from the passivating role of the gel layer formed in stage 1 and the saturation in Si of the solution. Depending on the glass composition and the alteration conditions, one of the two causes may be predominant. Nevertheless, this does not always happen and the residual rate may not be too different from the forward rate [7, 36, 37, 40, 52].

Water plays a key role as well in glass atmospheric alteration, albeit in the form of moisture adsorbed on the surface [16, 21, 24]. The percentage relative humidity (RH %) is, therefore, a fundamental parameter for the unfolding of glass weathering: the higher its value, the more dramatic the hydration of glass [12, 53]. Compared to that under immersion conditions, fewer studies are dedicated to glass atmospheric ageing [21, 28, 40]. Yet, this represents a very critical topic in the field of CH, especially for museum collections. Notwithstanding the involved chemical processes are generally described as analogous to those of the alteration in water [10, 12, 20, 23, 26], crucial differences make the two phenomena have distinct outputs, so that it is hardly possible to predict the behaviour under atmospheric conditions of a given glass based on what observed in water solution [31, 40]. The main reason for this is the lower water availability in the case of atmospheric conditions, which makes the time of exposure to moisture and the environmental parameters gain significant importance [12, 16, 31]. Water molecules have to be first physisorbed on glass surface to consequently take part in the competing reactions of hydration, hydrolysis and ion exchange [16, 21, 31]. Given the relatively low water availability, more time is required for solvating network modifier ions, so that the hydrolysis reaction is probably favoured with respect to interdiffusion. Furthermore, according to molecular dynamics simulations, water molecules in the unsaturated conditions of the atmospheric environment are bound or adsorbed in such a way that their solvation properties are mitigated [31, 54]. Ion mobility is therefore limited and, instead of the dissolution occurring under immersion conditions, a redistribution of alkali and alkaline earth ions takes place in the alteration layer [21, 31, 40]. Part of them may reach the glass surface and give rise to

salt crystallisation by interacting with atmospheric agents, such as carbon dioxide or pollutants - in the case of an external or uncontrolled environment [12, 22, 55]. Most frequently, calcium carbonates are found in monitored atmosphere, meaning that a preferential leaching of Ca^{2+} ions occur. According to Alloteau et al. [21, 31], as a consequence of the poor water solvation properties, the more negative their hydration enthalpy, the more mobile the cations in the silica network, because they are more efficiently solvated. Overall, the atmospheric ageing seems to be more dangerous for glass than that in liquid water both because of the retention of alkalis in the structure and because of the more unstable environment it entails. For instance, fluctuations in RH% are likely favouring crizzling and flaking: the partial drying of the hydrated glass determines volume contractions in the fragile glass surface layers, which cannot accommodate the mechanical stress and hence crack [1, 11, 24, 31].

Great care must be taken for glass conservation and determining the best storage conditions is quite critical. In this sense, research on glass alteration under atmospheric conditions results to be considerably helpful for selecting the most appropriate humidity, temperature, lighting and air circulation settings in museum display cases [23, 24, 31]. In order to avoid thermal or physical shocks in the material, these would better be kept rather constant, and excessively dry conditions should be avoided to prevent hydrated glass from cracking [19, 31]. Very often, micro-climate control is the only preventive measure taken by museum curators and conservators, as the protectives and consolidants proposed so far still present some disadvantages [24]. Quite challenging is the fulfilment of the conservation requirements, which claim that a protective should be nontoxic, compatible with the substrate, reversible as much as possible, easily applicable and readily available. Moreover, small quantities of material would better be used and the physical and optical integrity of the treated artifact must be preserved [14, 18, 56]. A variety of organic coatings has been proposed and employed in the past years. These comprised, for instance, products made of acrylic or epoxy resins, and were mostly chosen starting from the 1970s among the protectives already used for stone materials [14, 16, 24, 31, 56]. Due to their low compatibility with glass and their tendency to yellow via photo-oxidation, such treatments have been progressively abandoned [18].

In the last decades, silica coatings synthesised by sol-gel process have been developed. Such protectives represent a competitive option, as they are transparent, highly compatible with the glass substrate and they can be easily applied without any curing step either by dip coating or spray [14, 16, 18, 56, 57]. Even if not reversible, the protection treatment with silica coating can be quite thin (about 200 nm thick) and could be periodically repeated without compromising the aesthetics of the glass artifact [14, 16, 57]. Accelerated ageing tests performed on mock-samples treated with sol-gel silica coating confirmed the efficacy of the

protection, showing that the ion exchange process is slowed down and the consequent crizzling or flaking are avoided [16]. Even if they are already quite affirmed in the conservation field [57], silica coatings could be further improved in order to provide a superior and long lasting protective effect. Water being the main reason for glass alteration, it would be beneficial to convey hydrophobic properties to the coating. This would lower the wettability of the material surface and hence inhibit water penetration [58, 59]. An astonishing natural example of such property comes from lotus leaves, which remain clean and dry in aquatic environments thanks to their superhydrophobicity. The thereby named *lotus effect* derives from the superficial structure of the leaves, characterised by rounded micrometric protrusions: these minimise the adhesion of water drops to the surface, hence preventing them from spreading and letting them slip away together with any dust deposit [58, 60, 61]. It would be appealing to reproduce similar surface structures in protective coatings in order to confer analogous self-cleaning and hydrophobic properties to ancient glass. Starting from a silica sol-gel coating, a compatible material to provide the desired roughness would be $Si\,O_2$ nanoparticles. These would allow the preservation of the coating transparency, as their size may be tuned in order to not exceed 100 nm, which is roughly the limit below which any feature is invisible to the naked eye [62]. Furthermore, branched structures may be attained through self assembly of NPs with different diameters and the hydrophobic character would likely be enhanced [60, 62]. The Stöber process constitutes an easy and convenient method for silica NP synthesis and is therefore widely employed [63–65]. Since its introduction in 1968 [66], many attempts have been made for deepening the knowledge on the kinetics of the reactions involved in such protocol and ultimately determine how to repeatably use it for the production of mono-dispersed spherical NPs with desired sizes [64, 65, 67, 68]. This would confer additional advantages to the already simple, customisable and cost-effective Stöber method [65]. Its accomplishment is based on the reaction of Tetraethyl orthosilicate (TEOS, $Si(O\,Et)_4$) with water in low-molecular-weight alcoholic solution and under ammonia catalysis. In such conditions, silica NP synthesis can be simplistically described as consisting of a first hydrolysis of TEOS (Eq. (2.7)) and the subsequent condensation of the so-produced monomers (Eq. (2.8)) [63, 64, 66–68].

$$Si(O\,Et)_4 + H_2\,O \longrightarrow (O\,Et)_3\,Si(O\,H) + Et\,O\,H \tag{2.7}$$

$$(O\,Et)_3\,Si(O\,H) + H_2\,O \longrightarrow Si\,O_2 + 3\,Et\,O\,H \tag{2.8}$$

An alternative treatment for the protection of CH glass was recently proposed by Alloteau et al. [18, 31, 35, 69, 70] as an adaptation of a protocol already employed for the protection of float glass in the industrial field or of glasswares against the damage caused through dishwasher

cleaning. This consists of applying a very small quantity of zinc salts onto the glass surface and therefore requires little and non-toxic material, is rather simple and low cost [69]. As it is commonly done for industrial float glass protection, the application through spray may be chosen in the case of museum objects due to its ease of execution. This was tested and proven to be effective on pristine glass when subsequently artificially aged [18, 31]. About 0.1 to 1.5 $\mu g/cm^2$ were found to be sufficient for a satisfactory protection, hence testifying for the low amounts of material required in this approach [69]. Alkali ions resulted stabilised in the glass network and the alteration processes were slowed down thanks to this protective deposit [69, 70]. Still, the mechanisms through which zinc ions make glass more durable are unclear: it is proposed that either they enhance glass resistance by assuming the role of network formers and giving rise to a passivating layer, or they render the surface more hydrophobic by creating a diffusion barrier. Possibly, multiple effects contribute to the protective action: Zn^{2+} ions can precipitate with OH^- groups and hence (I) determine a lowering of the pH, (II) render the surface less hydrophilic and (III) create a highly insoluble layer [69]. Alloteau et al. have shown that after the treatment, Zn^{2+} ions are partially chemisorbed, physisorbed and included in crystalline precipitates on the glass surface, the first phenomenon being favoured by a moderate heating step and being the main one responsible for the protection efficacy [69]. Further research is necessary to deepen the knowledge on how the zinc salts treatment works and to determine whether it would represent a suitable proposal for museum conservators. In their studies, Alloteau et al. obtained unsatisfactory results when treating pre-aged samples and when the protective was applied at room temperature [69]. Therefore, the efficacy of the zinc salts treatment on already altered glass has to be further tested, as well as the relevance and possible avoidance of the heating step.

Notwithstanding the extensive and thorough research conducted in the last decades, a number of questions on glass alteration and protection methods are still open. In this thesis, multiple issues are treated, concerning different aspects of such a wide field of research. The composition effects on alteration were addressed by focusing on glass rich in silica and having alkalis and alkaline earths in quantities below 20 mol%, belonging to the *domain 1* (see Fig. 2.1). Previous studies on such glass have revealed that alkaline earth ions were unexpectedly mobile, while alkalis were retained in the hydrated layer [13]. On the other hand, it is generally agreed that the higher the ratio of MO to M_2O contained in the glass, the higher the stability of the material against alteration [2, 4, 20]. In order to investigate on how these two aspects can relate to one another and be both truthful, ageing tests were performed on glasses with different compositions specifically prepared for the present work. Furthermore, the same approach was adopted to analyse the role of potassium and question the common

belief that sees the latter as responsible for the poor durability of glass. Not only was the ageing of glass studied under atmospheric conditions, but a dissolution experiment was also implemented, to compare the alteration occurring on the very same glass compositions when exposed to the atmosphere or immersed in water. This choice stemmed from the limited literature dedicated to both the atmospheric alteration and its direct comparison with the ageing under immersion conditions. Some critical aspects of the zinc- and silica-based protection methods were also addressed. For the former, additional insights compared to those provided by Alloteau et al. [18, 69] were explored: the protection efficacy on already aged glass and the possibility of combining the treatment with a step of water rinsage. In the case of the latter method, a reproducible protocol for the synthesis of monodispersed spherical nanoparticles of tunable size was sought. Such control on the production procedure would constitute a useful tool for the protection treatment development.

Knowing more about the mechanisms governing the ageing processes and shedding light on the composition effect would help customise the conservation measures to the specific glass artifacts. Deeply related to such issues is the formulation of effective and easily applicable protective treatments. More studies are therefore needed to ultimately contribute in preserving the unique and fascinating testimonies of glass technology that are part of our common Cultural Heritage.

3. Experimental

3.1 Materials

In this study, plate and powder glass samples were considered in order to investigate both the surface and the bulk alteration processes. It was thus possible to employ different characterisation techniques which required samples to be either in the form of granules or of flat surfaces. Their composition (Table 3.1, Fig. 3.1) was intentionally decided to be a simplified representation of those of Cultural Heritage glass. In order to facilitate the analysis of the role played by the main components of ancient glass, the number of oxides contained was reduced to six: SiO_2, Al_2O_3, MgO, CaO, Na_2O and K_2O. The starting composition was glass PA0, previously studied by Fanny Alloteau and representing a model for mixed alkalis (Na and K) glass similar to that of late-medieval Limoges enamels [13, 71]. By varying the ratio of alkaline earth on alkalis (R, defined in Table 3.1 caption), the series PA0, PA1 and PA2 was created. Whilst the content of SiO_2 and Al_2O_3 is kept constant in such compositions, the value of R is progressively higher along the sequence. In order to investigate the role of potassium, a further composition was implemented: this is labelled PA0noK and has the same composition of PA0, except that all K_2O is replaced by Na_2O. Compositions PK and B were previously studied by Fanny Alloteau [13] and are models of a potash rich and a Roman glass, respectively. They were considered for some of the investigations to support the results and enable meaningful comparisons.

Table 3.1: Compositions (nominal for PK and B and resulted from EDX analyses for the others) of the model glass samples considered in this study, the quantity of the different oxides being reported in molar percentage. PA0, PA1 and PA2 constitute a series of compositions with a progressively increasing value of R (ratio of alkaline earth to alkalis was calculated as $R = \frac{CaO+MgO}{Na_2O+K_2O}$). PA0noK instead is related to PA0 composition in that it differs only for the nature of the alkalis it contains, R being the equal.

Name	**Form**	**%mol**						**R**
		SiO_2	Al_2O_3	MgO	CaO	Na_2O	K_2O	
PA0	plates + powder	74.27	0.49	1.24	5.58	11.11	7.31	0.37
PA1	powder	74.48	0.53	1.98	9.05	7.82	5.18	0.85
PA2	plates + powder	75.32	0.52	2.46	11.19	6.46	4.05	1.30
PA0noK	plates + powder	74.35	0.51	1.19	5.68	18.26	0.01	0.38
PK	plates	81.70	0.20	0.30	2.30	1.60	13.90	0.17
B	plates	67.00	1.50	4.60	8.10	17.50	1.40	0.67

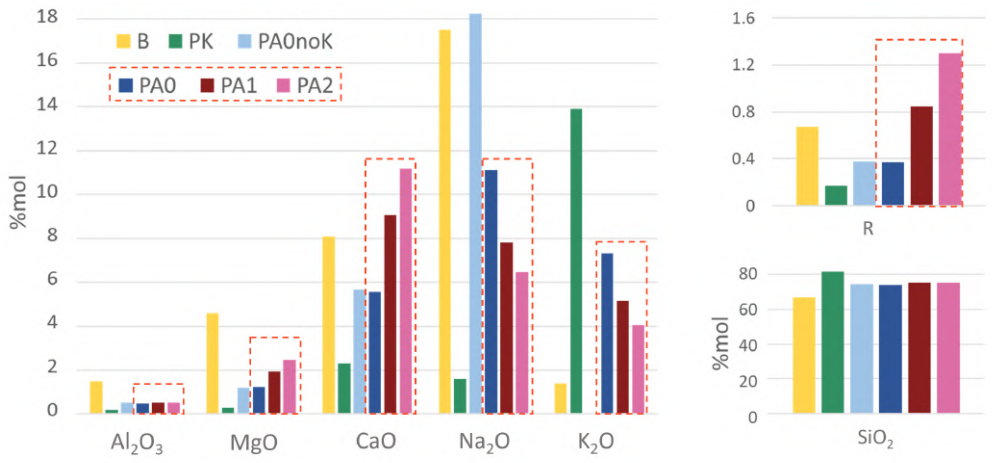

Figure 3.1: Bar charts overview of the glass samples compositions. The series of PA0, PA1 and PA2 is highlighted with dashed red boxes.

Starting from glass blocks synthesised by Saint-Gobain Recherche (France), plate samples were and cut with dimensions of either $1 \times 1 \times 0.3$ cm^3 (PA0, B) or $1.3 \times 1.3 \times 0.3$ cm^3 (PA2, PA0noK) and polished by an external company (Opticad, France) by using a water-based 1 μm diamond suspension. Some complications were assessed to have occurred in latter procedure, as scratches and small holes were detected on the surfaces of the samples: as their presence could affect the intensity and spatial distribution of the surface alteration phenomena, each sample was labelled with a different name. This way, it was possible to achieve a better tracking of the changes occurring during the ageing processes. For each plate sample, the surface with less defects was chosen for the investigations and the opposite one was marked by engraving a cross with a diamond tip.

Calibrated powders of $20 - 63$ μm size fraction were produced by PRIMEVerre: such granulometry was selected to have a specific surface (S) that would allow for kinetic studies in the frame of a two weeks ageing. If on one hand rather high values of S are necessary for a proper alteration of the material to take place, on the other these should be sufficiently low to let the process occur slowly enough to enable the study of its kinetics. Therefore, a compromise between these two necessities was seeked.

Poly(methyl methacrylate) (PMMA) boxes were employed for sample plates storage, two of their compartments being filled with silica gel beads in order to keep the environment dry. Controlled storage conditions were implemented by placing such containers as well as those for the powders (polypropylene tubes) in a hermetic box made of acrylic resin (Fig. 3.2). Silica gel beads were put on its lower tray and a TESTO data logger was used to monitor the

temperature and the relative humidity (RH%). These varied in the range of $20 - 25$°C and $25 - 55$ RH%, respectively.

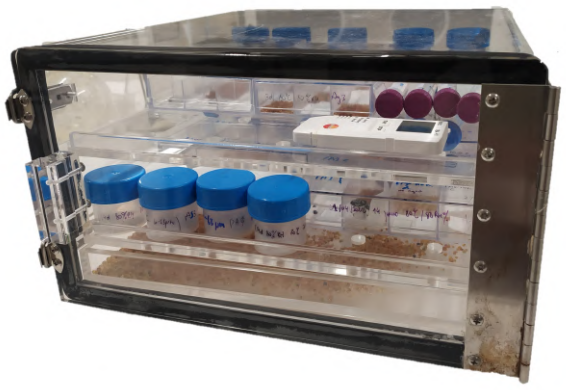

Figure 3.2: PTFE box used for sample storage. Silica beads were placed on its lower level and a TESTO data logger was used to monitor the ambient temperature and RH%.

3.2 Methods

3.2.1 Mock-up samples preparation

Plates samples were thoroughly cleaned before each experiment and analysis in order to remove organic contaminations or the alteration products that could have naturally formed after production. The cleaning procedure was optimised starting from the one used by Alloteau et al.[69] and was carefully monitored by comparing the appearance of the surface before and after the treatment with optical microscopy and by assessing the absence of organic residues after washing via infrared spectroscopy. Samples were first washed for ca. 30 seconds in a 0.3 M solution of ultrapure Sodium Dodecyl Sulphate (SDS, ROTH), then rinsed with milliQ water and ultrasonically washed in absolute ethanol for 10 minutes. Due to the high sensitivity to humidity of some samples, the final washing step with milliQ water proposed in [69] was not included. Samples were dried with a gentle flux of warm air (ca. 40°C) and by robbing with dry nonwoven cleanroom wipers (TechniCloth® TX612) so that to remove the eventual ethanol stains.

3.2.2 Composition effect study

The role of composition on glass atmospheric alteration mechanisms was studied by artificially ageing the samples for different time spans at monitored temperature and relative

humidity (RH) levels. Samples were multi-analytically characterised before and after such alteration treatments in order to assess the degree and kind of resulting alteration and comparisons were made among the different compositions. Ageings at 80°C and 80 RH% were performed with durations of 18 hours, 3, 7 and 14 days in a climatic chamber (WEISS WKL34). Starting from 21°C and 35 RH%, a ramp of three hours was used both for reaching the dwell and for going back to the initial conditions. In order to perform it in parallel with those at 80°C, an ageing test of 14 days at 60°C, 80 RH% was carried out by placing the samples in a hermetic box made of acrylic resin containing a saturated solution of KCl (Honeywell Fluka™), inside an oven (memmert UFB 400). Such experimental conditions were set up to provide the needed level of relative humidity [72] which was further checked with a data logger: the actual RH% measured at 60°C was 77 RH%.

Samples were characterised by visual and optical microscopy observations right after their withdrawal from the climatic chamber/oven so that to assess the immediate effect of the accelerated ageing process only. Other analyses were performed the earliest possible, based on the instrument availability, and the time passed before the measurements acquisition was taken into account. This was aimed at considering separately the effects of accelerated and natural ageings, the former occurring in the climatic chamber or oven and the latter taking place subsequently, during sample storage.

As the alteration kinetics are highly affected by temperature, artificial ageings are probably considerably different from the natural ones [21, 23]. Nonetheless, high temperatures were employed in the present study in order to accomplish the experiments within the time frame of the project. Even if they are not directly relatable to the real ones, the effects of artificial ageing are usually better measurable and can provide information on glass durability and degradation processes. In particular, durable or unstable compositions are likely such both at high and ambient T.

3.2.3 Dissolution experiment

The ageing under immersion conditions was investigated by following a procedure inspired by that of Tournié et al [73]. For each glass composition about 2 grams of calibrated powder were put in a polytetrafluoroethylene (PTFE) hermetic jar containing 500 mL of milliQ water pre-heated to 80°C. A plate sample of the same composition was also immersed and placed on a PTFE holder not to stay in contact with the underlying powder and to expose its whole surface to the alteration mechanisms. An accelerated ageing test of 2 weeks was performed on such systems by employing an oven and fixing the temperature to 80°C. Water samples

of 15 mL were collected using clean plastic syringes after different time periods. These were shorter in the initial stages of the experiment in order to better track the first and most meaningful phase of the dissolution kinetics. Syringe filters with a pore size of 0.45 μm were used to withdraw the water samples prior to storage at about 4°C, to retain all the remaining granules of powder and prevent the dissolution process from continuing. It is important to point out that the solution was well mixed and allowed to deposit before the withdrawals, and that each sampling was compensated in the jars by adding 80°C milliQ water until bringing up to the initial volume. At the end of the ageing process, under-vacuum filtering was performed using a Büchner funnel to recover the glass powder from the solution. Both plate and powder samples were washed with milliQ water and dried before being analysed.

3.2.4 Zinc salts treatment

As an extension of Alloteau et al. work [18, 69], the efficacy of the zinc salt treatment was tested on both pristine and pre-aged samples by varying the ageing durations with respect to the previous studies. Among the already tested solutions, the one observed to be the most effective was chosen for the present investigations: a concentration of 9 mM in zinc was obtained by ultrasonically dissolving 675.8 mg of zinc nitrate hexahydrate ($Zn(N\,O_3)_2\ 6\ H_2\,O$, Sigma-Aldrich) in 250 mL of absolute ethanol. In order to favour a homogeneous dissolution, the low foaming non-ionic surfactant Pluronic F-127 (BASF) was added in a concentration of ca. 0.015 g/L. The solution was applied onto the samples surfaces with commercial perfume atomiser bottles: this would be an easy and feasible methodology for museum conservators and was thus preferred to the more effective but less practical immersion method [69]. Two sprays at a distance of about 10 cm were sufficient to completely cover the plates area, which were subsequently dried with the help of a 40°C air flux. However, due to the hygroscopic nature of the salts formed on the surface, it was not possible to achieve a complete drying.

For each glass composition, four plate samples were pre-aged in the climatic chamber with an 18 hour process including a 12 hour dwell at 80°C and 80 RH%. Among these, three were subsequently treated alternatively with a first rinsing and the following application of the zinc salt solution, or with only one of the two steps. The rinsing step was included as it well simulated the washing treatment usually performed in museums by restorers [70] and was observed to positively affect the durability of glass by reducing the quantity of alkalis retained in the hydrated layer [13, 25, 74]. It was implemented by separately immersing the samples in a fixed volume of milliQ water for 5 minutes and subsequently rinsing them with additional milliQ water, which was collected in the same container and weighed in order to allow quantitative analyses. Samples were finally dried with nonwoven cleanroom wipers and

the rinsing water was stored at about 4°C before being analysed. Two additional samples for each composition were used for testing the zinc salt treatment on pristine glass. These were not pre-aged and only one of the two was subjected to the protection method test. Finally, all the samples were artificially aged for 7 days at 80°C and 80 RH% in the climatic chamber (see schematic reported in Fig. 3.3 for clarity).

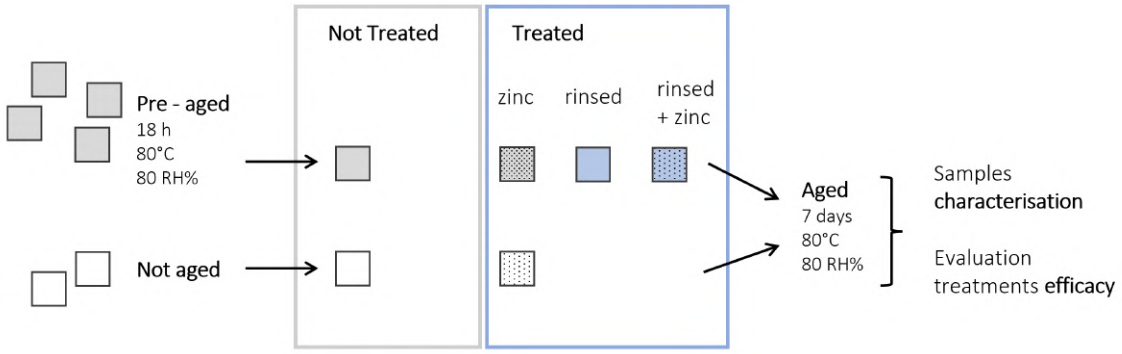

Figure 3.3: Schematic of the analytical method used for the study of the zinc salt treatment for glass protection.

3.2.5 Synthesis of silica nanoparticles

As a preliminary step for the formulation of a hydrophobic sol-gel silica coating, the synthesis of silica nanoparticles (NPs) was performed repeatedly by Stöber method in order to develop an efficient and reproducible protocol for obtaining NPs with homogeneous spherical shape and controlled average size and size distribution. The reaction between Tetraethyl orthosilicate (TEOS, Sigma-Aldrich) and water was carried out in pure ethanol (Sigma-Aldrich, purity $\leq$99.8%) with ammonia (Sigma-Aldrich, solution 32%) as a catalyst. Ethanol was first poured into a PTFE 250 mL round-bottom flask by using a calibrated cylinder, while MilliQ water and ammonia were subsequently added with the help of micropipettes. An AREC.X digital ceramic hot plate stirrer (Velp scientifica SRL) was employed and a stirring rate between 400 and 800 revolutions per minute (rpm) was kept for the whole synthesis duration. After about ten minutes of stirring, TEOS was added dropwise into the solution, so that to spread it as homogeneously as possible. The system was let to react for about 24 hours, the temperature and RH% of the surrounding environment (laboratory hood) being periodically checked by means of a digital hygrometer by Extech instruments. Temperatures between 19 and 24°C and RH ranging from 35 to 87 % were registered during the different syntheses. The temperature effect on the nucleation rate - and hence the particles size - was neglected, as the T range was quite low and restricted [75–77].

The substances involved in the reaction were introduced in quantities which varied according to the desired nanoparticle size, the volume of reaction kept constant to 100 mL. Starting from the molar ratios used by Stucchi et al. [78] for synthesising 50 and 100 nm NPs, modifications in the relative amounts were introduced with the aim of obtaining sizes of 200 and 25 nm. Syntheses were labelled by adding the expected size of particles (200, 100, 50 and 25) to the suffix SN, standing for silica nanoparticles. As can be seen in Table 3.2, the molarity of ammonia was the key parameter to change for regulating the size of the NPs: the concentration of TEOS and water were kept constant and the quantity of ethanol was adjusted to make the total volume be always the same. Repeated syntheses were performed for the different molar ratios with the aim of testing both the reproducibility of the method and the distinct effect of two protocols for NP washing (see below). The molarity (M) of water, TEOS and ethanol was changed for the syntheses SN100a and SN25a and b: these were single trials aimed at checking the role of the reagents and solvent relative quantities, hence they were not repeated. For the latter cases, concentrations were varied in ranges for which ethanol, water and TEOS are miscible [79].

Table 3.2: Molarity (M) of milliQ water, ammonia, TEOS and ethanol used for synthesising silica NPs. The expected size, name and number of synthesis repetitions are reported for each quantity combination.

M (mol/L)				Expected Size	Synthesis Name	Repetitions
H_2O	NH_3	TEOS	EtOH			
4.935	1.652	0.113	14.510	200	SN200	3
4.935	0.826	0.113	14.840	100	SN100	3
2.468	0.413	0.057	15.983	100	SN100a	1
4.935	0.413	0.113	15.005	50	SN50	3
4.935	0.207	0.113	15.088	25	SN25	2
14.950	0.207	0.113	11.988	25	SN25a	1
9.969	0.207	0.113	13.530	25	SN25b	1

The pH was monitored at different stages of the synthesis by using pH-indicator strips (MQuant® Supelco, pH 6.5 - 10.0). In all the cases, the addition of ammonia into the solution made the pH range between 9 and 9.5, and no change was noticed throughout the synthesis process. The obtained suspension was subsequently brought to neutrality via a series of washing cycles aimed at removing ammonia. Two methods were adopted for cleaning the suspensions: that employed by Stucchi et al. [78] and an experimental one, entailing the use of Amicon®Ultra-15 Centrifugal Filters (Fig. 3.4). In the former case, the suspension was transferred into 50 mL centrifuge tubes by Sorfa, where a solution 50:50 % in volume of ethanol (75% purity) and milliQ water was added. After mixing with both a vortex mixer at about 2400 rpm and the ultrasonic bath for ca. 5 minutes, the tubes were centrifuged at

9500 rpm (corresponding to ca. 6498 relative centrifugal force, RCF, in the used centrifuge, a Centrisart®G-16C Refrigerated Benchtop Centrifuge) for 30 minutes in the first washing and 15 minutes for the following ones. Once separated, most of the solvent was removed from the nanoparticles and the 50:50 solution EtOH:H_2 O was added again to start a new washing. The pH of the removed solvent solution was measured with pH-indicator strips to monitor the advancement of the cleaning process: when a value between 6.8 and 7.1 was registered, the removal of ammonia was considered complete. Generally, three or more washing cycles were performed, the last one by using ethanol only, instead of the 50:50 solution. Nanoparticles were finally dried by covering centrifuge tubes with pierced aluminum foil to allow solvent evaporation, and leaving them in the oven at 60°C for 24 hours.

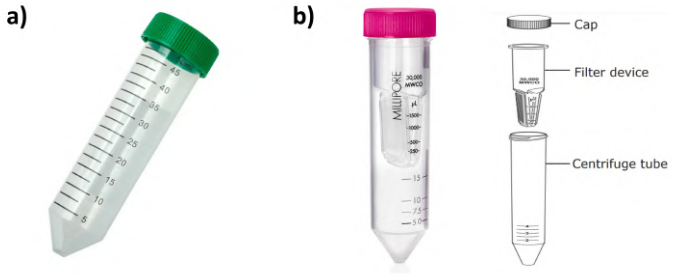

Figure 3.4: **(a)** 50 mL Sorfa centrifuge tube used for the washing method by Stucchi et al.; **(b)** picture and schematic of the Amicon® Ultra-15 Centrifugal Filters used for the new washing method. Images are taken from the providers' websites [80, 81].

This washing method was quite fast and efficient, but it did not work well for NPs smaller than 100 nm. In the case of 50 nm particles, the suspensions had to be centrifuged one hour per cycle for the NPs to sink to the bottom of the tubes. Thereby the necessity of another method for particles of 50 and 25 nm diameter. Amicon centrifugal filters, usually dedicated to bio-molecules, were chosen with the aim of separating the solvent of synthesis from the obtained NPs by keeping the system in suspension as much as possible. As the volume percentage in ethanol had to be lower than 70% for ensuring the integrity of the filters membranes, an adapted milliQ water volume was added to the synthesis batch prior to the washing with Amicon tubes (in this step, the pH was observed to rise up about a value of 10). For the same reason, the washings could not be performed with pure ethanol, only the solution 50:50 EtOH:H_2 O could be employed. The suspension was first concentrated via a centrifuge of 10 minutes at 4500 RCF and then transferred, with the use of a Pasteur pipette, into a PTFE beaker for the washing step. After adding the 50:50 EtOH:H_2 O solution, mixing was performed with 5 minutes in the ultrasonic bath. Once the suspension was transferred again into the Amicon tubes, it was concentrated through centrifuge (10 minutes, 4500 RCF)

and the pH of the ultrafiltrate collected at the bottom of the tubes was measured. The same procedure was repeated until reaching neutrality, the material concentrated in the Amicon filter reservoir being systematically mixed with the use of a Pasteur pipette. At the end of the washing procedure, the clean suspension was recovered with a Pasteur pipette by adding some milliQ water for avoiding substantial material losses.

The Amicon method resulted to be longer compared to the other, due to the initial larger volume of suspension and higher pH given by the addition of water, together with the limited capacity of the filter devices. Furthermore, in order to have sufficient space and not to damage the membranes with the ultrasonic bath, it was necessary to transfer the suspension from the Amicon tubes into a beaker for mixing with the washing solution.

The yield for the two methodologies was evaluated by comparing the mass of dry NPs obtained per each synthesis to the theoretical mass of product. Based on the assumption that TEOS fully converts into silica NPs [82], the latter was approximated to the mass of $Si\,O_2$ formed through the reactions of hydrolysis and consequent condensation of TEOS in water (Eqs. (2.7) and (2.8)) and was thus computed by considering the moles of silica to be equal to those of TEOS added for the NP synthesis. While the washing method with ordinary centrifuge tubes resulted in dry nanoparticles, the other entailed the preservation of the suspension condition. Therefore, after adequate mixing in an ultrasonic bath to ensure the homogeneity of the suspensions, aliquots had to be withdrawn and dried for yield evaluation. Two alternative methods were tested to remove the liquid: drying in oven at 60°C and lyophilisation. The latter alternative was abandoned after a trial where a considerable loss of material for the 50 and 25 nm NPs was assessed. The pressure change entailed in such process was too abrupt and caused the small NPs to move out of the samples containers. As a consequence, the slower but safer drying in the oven was preferred.

3.3 Characterisation techniques

A multitude of analytical techniques was implemented for this study and is hereafter described. The techniques employed for the investigations on glass samples are first discussed in ascending order of invasiveness, whereas those dedicated to the characterisation of syntesised silica NP are presented in the last paragraph of this section.

3.3.1 Optical Microscopy (OM)

A Keyence VHX - 5000 digital microscope was employed for characterising the samples in their appearance before and after every step of the experimental procedure. This instrument is

provided with a LCD monitor and allows to perform length measures on the samples. Images were acquired in reflection mode by a CMOS camera equipped with an 1/1.8-inch CMOS image sensor (virtual pixels: 1600 (H) × 1200 (V)) and both Z20 and Z500 objectives were used.

3.3.2 Spectroscopic analyses

In order to evaluate the level of hydration of the plate samples, both transmission and attenuated total reflection (ATR) Fourier transform infrared spectroscopy (FT-IR) were employed. Such choice pointed at combining the fast and bulk-related analyses given by the former and the high surface sensitivity of the latter technique [83, 84]. Transmission FT-IR was performed with a Bruker Tensor 27 IR instrument, endowed with a Deuterated Lanthanum α Alanine doped TriGlycine Sulphate (DLaTGS) detector. Such analyses allowed for the study of the OH bands only (range 4000 - 2000 cm^{-1}), as below 2000 cm^{-1} the signal is saturated due to the strong absorption of the bulk glass [83]. Spectra were acquired with 64 scans and 4 cm^{-1} resolution and a background was registered every 4 sample measurements. A Nicolet iS50 FTIR spectrometer endowed with a liquid N_2-cooled mercury cadmium telluride (MCT) detector was used for ATR-FTIR analyses. Spectra were registered in the range 4000 - 700 cm^{-1}, even though a particular attention was reserved to the range 4000 - 1500 cm^{-1} for evaluating the hydration level. As the signal intensity is considerably lower in ATR compared to transmission FTIR, spectra were acquired with 256 scans, the resolution being still 4 cm^{-1}. Two or three spectra were collected per each altered sample immediately after one of a reference of the same composition, in order to enable meaningful comparisons. The background was measured every two acquisitions to correct for the possible changes in environmental humidity. FTIR measurements could not be performed on the very unstable compositions that presented flaking phenomena upon ageing: transmission spectra would be distorted as the optical path would change due to the presence of flakes, while the mild force exerted by the instrument probe for ATR-FTIR analyses would imply irreversible damage on the cracked samples.

Raman spectra were collected on pristine and weathered plate samples as well as on flakes formed upon ageing. A Renishaw inVia Raman instrument equipped with a Leica confocal microscope system was used, employing a Nd-YAG green laser (532 nm, power of 100 mV). Prior to the measurements on samples, the instrument was calibrated using a monocrystalline Si standard, generating a single peak at 520.5 cm^{-1}. Spectra were registered in the range $3800 - 100$ cm^{-1} with an acquisition time of 30 seconds, laser power of 50 mV and 4 scans. As it works in the visible range of the electromagnetic spectrum, this technique enabled

measurements to be performed at μm scale and allowed for a higher spatial precision compared to infrared spectroscopy. Information about the glass structure and hydration level as well as about the nature of the alteration salts formed could be gained with these analyses by comparing the experimental results with spectra from the literature or databases. Due to the minimal space dividing the sample from the microscope objectives, such technique could not be employed on flaked samples without the risk of damaging them. Hence, measurements were performed on the flakes detached from the plates surface. In order to enable a thorough comparison among the results, spectra were normalised by taking the peak at about 1100 cm^{-1} (stretching of Q^3 species, see section 4.1.1) as a reference: by considering its maximum ($y_{\max 1100}$) and the minimum value at higher wavenumbers ($y_{\min 1100}$), the intensities of each spectrum were transformed as follows:

$$\text{Normalised}(y) = \frac{y - y_{\min 1100}}{y_{\max 1100} - y_{\min 1100}}$$

3.3.3 Scanning Electron Microscopy - Energy Dispersive X-ray Spectroscopy (SEM-EDX)

The surface state of plate samples was examined with SEM analyses using a JEOL JSM-7800F. Samples were fixed on carbon tapes over metal cylinders and covered with a 1 nm - thick layer of platinum. The electrical contact was ensured by applying colloidal graphite (PELCO®) and a gentle air flux was used to remove the isopropanol residues. In the case of altered samples, some of the formed flakes were detached from the plates and placed on separate carbon tapes: a thorough investigation was performed by analysing flakes both as isolated and as still bound to the underlying glass. For images acquisition, a vacuum less than or equal to 10^{-4} Pa and a voltage of 7 KeV were used, the current was set to 1.63 nA and the working distance (WD) to 9.5 mm. Images were acquired by collecting secondary electrons. Not only such investigations were useful to assess the material's porosity or to characterise the alteration salts formed on the glass, but also they allowed for an evaluation of the flakes thickness: average values were calculated based on measurements performed on different flake edges. Elemental quantitative analyses were also performed through EDX with the system Bruker QUANTAX 400: acquisitions were made with a x1000 magnification and by employing a constant voltage of 15 KeV, which is low enough to allow the analyses to be limited to low depths in the material. To assess their reproducibility, measurements were performed as triplicates on different areas of the same examined region. In the case of samples where flakes had formed after the ageing tests, EDX data were acquired both above and below flakes (see Fig. 3.5 for clarity). Quantification was carried out by using the STRATAGem

data-processing software and by modelling glass plates as stacks of different layers of known thickness: alteration layer/Pt. Data were obtained in the form of percentages in molar atomic normalised quantities. For each triplet of measures averages were computed and considered for calculating the % molar oxides quantities. Based on the related stoichiometry, the % molar atomic quantity of oxygen given by all the oxides could be derived. Such measure was subtracted to that provided by the instrument for oxygen to get the % molar of oxygen in excess and thus of incorporated water (level of hydration). The % mass oxides quantities were calculated by multiplying the % molar oxides quantities by the molar mass (MM) of the oxides and subsequently normalised for their sum.

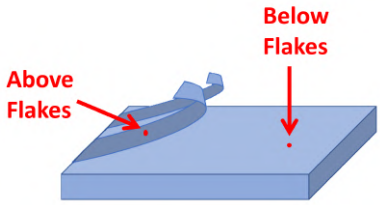

Figure 3.5: Schematic of a plate glass sample where flakes have formed after artificial ageing. Red arrows and points indicate the areas considered as above and below flakes for SEM-EDX analyses.

3.3.4 Time of Flight Secondary Ions Mass Spectrometry (ToF-SIMS)

In order to investigate the mechanisms of alteration in depth, ToF-SIMS analyses were performed by Antoine Seyeux (IRCP) on pristine and aged plate samples which did not present flakes or excessive alteration salts on their surface. Such technique being extremely sensitive, it enabled to acquire depth profiles on the material surface with a spatial resolution of a few nanometers. A Tof-SIMS V instrument (Ion-Tof company) was employed: this was equipped with a LMIG Bi^+ ion emitter (25 keV, 0.3 pA) for the analysis, a $O_2{}^+$ ion beam (2 keV, 150 nA) for in-depth abrasion, and an unfocused electron beam of some eV for neutralising the charge. As it required the usage of a very high vacuum (10^{-6} Pa), this analytical technique could determine irreversible damage to the samples and was thus employed only in the final stages of the experimental procedure, after performing the other less invasive analyses. Two or three measures were acquired for each analysed sample, to check the reproducibility and compensate for possible charge effects. Each measurement cycle was composed of 50 μs of analysis (pulsed beam and flight of ions in the ToF detector), 5 s of sputtering, and a pause of 4 s to avoid surface charging. The sputtering zone was 100 $\times$ 100 μm and determined the formation of a 300 $\times$ 300 μm crater. The depth of the latter was measured through mechanical profilometry to determine the sputtering rate: this was found to be ca. 0.77 and 0.79 nm/s

for PA0 and PA0noK, respectively. By assuming the abrasion rate to be constant regardless of the density of the altered/pristine material, the resulting profiles obtained in the form of *counts* vs *time* were converted into *counts* vs *depth* to gain more meaningful information from the analyses. The resulting counts for the different cations were normalised with respect to the $^{28}Si^{+}$ signal intensity registered for the pristine glass.

3.3.5 Characterisation of powder samples: Thermogravimetric analysis (TGA) and Nuclear Magnetic Resonance (NMR) spectroscopy

Chemical and structural information on pristine and altered glass was gained by analysing powders with TGA and NMR. The former was performed with a NETZSCH's STA 449 F3 Jupiter® thermal analyzer on about 100 mg of powder per sample held in an alumina crucible. These were heated with a ramp starting from 20°C and reaching 1000°C with a speed of 10°C/min and then cooled down to room temperature at the same rate under nitrogen flux. A correction of the measurements was carried out by considering as a baseline the curve acquired for a reference empty alumina crucible. Such analyses allowed to quantify the mass fraction of free and bound water as well as the one of carbonates, if present. The temperature range from 150 to 600 °C was considered for the loss of bound water, while the region below 150°C and the one between 600 and 800°C were attributed to physisorbed water and carbonates, respectively [13, 85]. The weight percentages were related to the whole mass of the analysed sample. In order to allow comparisons between TGA and EDX results, the weight percentage of bound water was calculated as the ratio of the % weight loss in the range 150-600°C to the % wt of the whole sample, the physisorbed water and carbonates excluded.

Bruker Avance I and Avance II spectrometers, operating at magnetic fields of 7.02 T (300WB) and 11.72 T (500WB), respectively, were employed for the collection of ^{1}H and ^{29}Si magic-angle spinning (MAS) NMR spectra of glass powders. These analyses were conducted by Thibault Charpentier (NIMBE service of CEA Saclay) by packing about 100 mg of powder in 4-mm outer-diameter ZrO_2 rotor, and spinning from 10 kHz (7.02 T) to 12.5 kHz (11.72 T) using Bruker CPMAS probes. The complete nuclear magnetisation relaxation was attained by applying a recycle delay from 20 to 200 s for the ^{29}Si nucleus and of ca. 1 s in the case of ^{1}H. For the latter, the Hahn echo-pulse sequence (90-TE–180-TE-Acq) with a rotorsynchronised echo delay TE was used for spectra acquisition.

3.3.6 Analyses on water samples: pH measurements and Inductively Coupled Plasma Atomic Emission Spectroscopy (ICP-AES)

A pH metre Eutech Instruments pH 510 was employed for the characterisation of the water samples before acidifying them for ICP analyses.

ICP-AES analyses were performed on water samples collected from the dissolution experiment and from the rinsing step carried out in the frame of the zinc salt treatment test. A Thermo Scientific iCap 6000 instrument equipped with an Argon plasma was employed and the axial mode was preferred as to have a higher sensitivity. Water samples were acidified with nitric acid 68% supplied by VWR Chemicals prior to the analyses. Volumes of 250 and 500 μL of acid were added to 15 and 30 mL samples, respectively, in order to obtain a concentration of HNO_3 of about 1 %. The content of Si, Na, K, Ca and Mg in the acidified solutions was quantified to evaluate dissolution degree. For each element, 3 or 4 emission wavelengths were considered and calibration curves were built based on the signals obtained for standards diluted in 5 different concentrations. The absolute error for the measures was calculated by multiplying the obtained concentrations for the Relative Standard Error (RSE) calculated by the instrument as:

$$RSE = \sqrt{\left(\sum_{i=1}^{n}\left[\frac{x_i' - x_i}{x_i}\right]^2\right)/(n-p)}$$

where x_i is the known concentration of the calibration level i, x_i' is the measured concentration at level i, n is the number of calibration points, and p is the number of terms in the fitting equation (linear = 2, quadratic = 3).

Starting from the obtained concentration values, the normalised mass loss of element i ($NL(i)$, measured in g/m^2), was calculated as follows, according to the literature [73, 86–89]:

$$NL(i) = \frac{C(i) \times V}{m \times S \times x_i}$$

where $C(i)$ [g/L] is the concentration of the element i in the water sample, V [L] is the volume of water in which the dissolution experiment was carried out, m [g] is the mass of the powder glass sample considered, S [m^2/g] the specific surface and x_i the atomic mass fraction of the element i in the glass. Two main approximations were made to calculate $NL(i)$: (1) only the powder samples were considered, neglecting the coupons (when present) and (2) the specific surface was assumed to be 2000 cm^2/g based on the data reported by Alloteau [35]. A higher precision for the latter value will be gained once the Brunauer-Emmett-Teller (BET) method

will be employed for measuring the powder specific surface (planned for the pursuit of the research project). Starting from the normalised mass loss, the equivalent thickness ($ET(i)$, measured in m) for sodium and silicon was calculated by dividing $NL(i)$ by the density of glass [7, 21, 52, 86]. Based on the information given by the samples provider, the latter was approximated to be 2.5 g/cm^3 for all the compositions. Water samples taken at the end of the ageing test were considered for these calculations, so that to infer about the depth of silica network dissolution ($ET(Si)$) and the thickness of the leached layer ($ET(Na)$) [21].

3.3.7 Characterisation of synthesised silica nanoparticles: Dynamic Light Scattering (DLS) and Transmission Electron Microscopy (TEM)

Silica nanoparticles were characterised in terms of dimensions and shape through DLS and TEM. Dynamic Light Scattering analyses were carried out by using a Malvern Zetasizer Ultra system, equipped with a He-Ne (633 nm) laser, and provided information about the nanoparticles hydrodynamic diameter. Given that such investigations required samples to be in suspension, for dry nanoparticles some mg of product were mixed with about 1 mL of milliQ water. Homogenisation was attained through ultrasonic bath and vortex mixer right before the analyses. NP suspensions were then introduced in polystyrene cuvettes (10 × 10 × 45 mm, Sarstedt) for DLS characterisation. Five measures per sample were registered and the average intensity size distribution was considered for data evaluation. The choice of studying the instrumental outputs in the form of *intensity* vs *size* plots was aimed at evaluating the results without any additional elaboration of the signal. As bigger particles are emphasised in such representations due to their strong scattering, the results were not used for a quantitative but rather for a qualitative analysis, which took into account the limitations of the technique. The number or volume distributions were not examined in this work to avoid misleading transformations of the collected signal [90].

Information about the actual particles diameter and on the shape of NPs was gained through Transmission Electron Microscopy analyses, which were carried out by Luca Leoncino (Electron Microscopy Facility, IIT @ Genova Morego). A JEM-1400Plus microscope equipped with a thermionic source (LaB6) was employed and images were acquired by operating at 120 kV in Bright Field (BF) mode. Prior to the analyses, dry NPs were ground in an agate mortar for breaking any aggregates, and put in suspension with milliQ water. These, as well as silica NPs that had been washed with the Amicon filters, were diluted in milliQ water and mixed through ultrasound sonication. About 8 μL per sample were dropcasted onto carbon film on Cu grid which had been previously plasma cleaned (Ar + O_2, forward RF 5W, 1 min). Finally, samples were dried at room temperature on filter paper and inserted in the

microscope on a quartet specimen holder. About 10 images were acquired per each sample in order to have a quite representative picture of the particles size distribution. The latter was evaluated through image processing with ImageJ software: the NP diameter was manually measured along 2 or 3 axes per particle and histograms were built using Origin software and considering 300 measures per synthesis.

4. Results

4.1 Composition effect on CH glass atmospheric alteration

The ageing tests on plate samples allowed for a subdivision by mere naked eye observation into stable and unstable compositions. PA0 and PA0noK glasses underwent severe alteration phenomena, whereas glasses of types B and PA2 did not show evident changes upon ageing. The content in $Si\,O_2$ and $Al_2\,O_3$ being constant for all the compositions, what distinguishes the first couple from the second is the amount of alkalis with respect to that of alkaline earths: this is higher for PA0 and PA0noK compared to B and PA2 glasses. The composition of PA0noK resulted to be the most critical, as signs of alteration could be noticed even prior to the artificial ageing tests. Samples of such glass type presented salts of different dimensions and morphologies quite homogeneously spread on their surface: some examples are shown in Fig. 4.1a,b , whereas the OM image of glass PA0 before washing is reported in Fig. 4.1c for comparison purposes. The salts detected on PA0noK glass could be easily removed with the washing protocol and indicated that a natural alteration process occurred during the time gap of about two months between the production of the samples (cut and polished) and the analyses performed in the present study.

Mainly by considering the effects on the most unstable glass compositions, a kinetics of alteration phenomena could be recognised for the ageing tests with 80 RH% and 80°C. Furthermore, the temperature effect previously observed by Alloteau et al.[91] was assessed by comparing the results obtained with the 80 RH% 60°C ageing. The two topics will be separately presented in the following paragraphs.

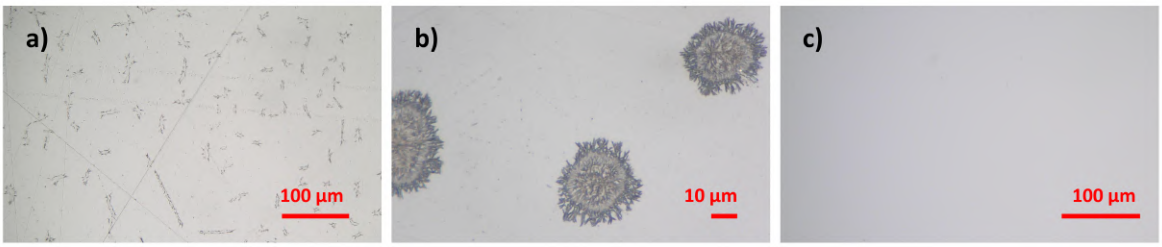

Figure 4.1: OM images of samples surface before cleaning: **(a)** elongated and **(b)** spherical salts detected on PA0noK, **(c)** surface of PA0 glass, not affected by salts crystallisation.

4.1.1 Alteration kinetics with 80 RH%, 80°C ageings

Samples of glass types PA0 and PA0noK behaved very similarly upon ageing at 80 RH% and 80°C as they both formed flakes when subjected to 3, 7 or 14 days ageing tests. Eighteen hours, instead, were not sufficient for such a phenomenon to occur, but they highlighted some differences between the two compositions. PA0noK glass presented extended iridescence along the edges (Fig. 4.2a), whereas PA0 barely had this effect around few defects on the corners. Microscopy observations showed how this had widely occurred on PA0noK samples, thus revealing the fragile nature of such glass type. With the 3-days ageing, iridescence manifested along cracks. These curled upwards and evolved into flakes only few hours after taking the samples out of the climatic chamber (Fig. 4.2b,c). While for PA0noK flakes were quite wide, PA0 glass formed thin and long lamellae* and some perpendicular brighter lines appeared on its surface (Fig. 4.2d). The flakes thickness was measured through SEM and assessed to increase proportionally with the duration of ageing. PA0noK samples presented thicker lamellae and a more rapid enlargement with time compared to PA0 ones (Table 4.1). The scatter plot built based on data of Table 4.1 and the optical microscopy images of Fig. 4.3 schematically represent the kinetics of alteration. Side images enable to assess the flakes' curvature: as their thickness increased, the lamellae appeared to be less flexible and to lie closer to the surface.

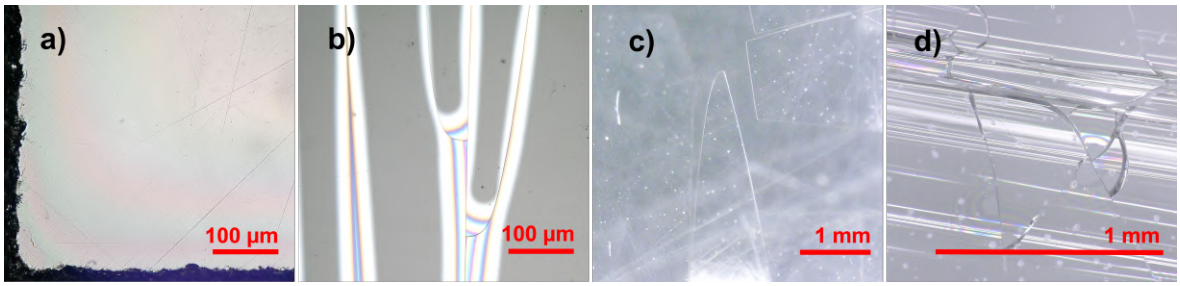

Figure 4.2: **(a)** Iridescence formed on PA0noK glass after 18 hours ageing at 80 RH% 80°C; **(b)** cracks and iridescence before flakes formation on PA0 after 3 days ageing at 80 RH% 80°C; **(c)** flakes of PA0noK after 3 days ageing at 80 RH% 80°C; **(d)** bright lines extending perpendicularly with respect to the flakes on PA0 after 14 days ageing at 80 RH% 80°C.

Not only did flakes change in width as the time of ageing increased, but they also presented a different structure. SEM observations on samples artificially aged for 3 and 7 days showed the lamellae to be quite smooth on the upper face and to have a rough and porous surface on the lower side(Fig. 4.4a,b). The ageing of 14 days, instead, caused the flakes to crack and thus to present several fractures both on their surface and edges (Fig. 4.4c,d). This could be due to

*The term *lamella/ae* is hereafter used as a synonym for flake/s

their thickness, which also prevented them from being flexible and curling up. Considerable must have been the physical stress induced by the physisorbed water removal in such wide hydrated layers. The cracking testifies for their fragility, which hindered the accommodation of the volume contraction.

Table 4.1: Thickness of flakes formed upon ageing on PA0noK and PA0 glass. Average measures are reported together with the relative uncertainty.

Ageing time (days)	Flakes thickness (μm)	
	PA0noK	**PA0**
3	13 ± 2	10 ± 2
7	30 ± 2	23 ± 2
14	67 ± 2	57 ± 2

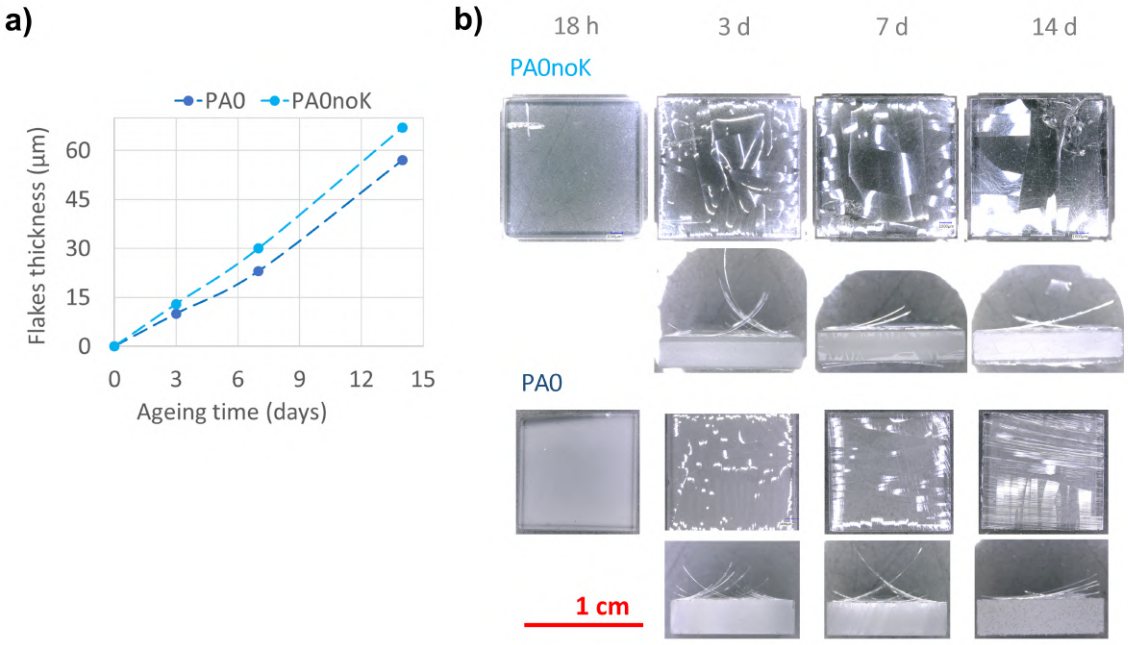

Figure 4.3: **(a)** Scatter plot based on data from Table 4.1 (the uncertainty - 2 μm - is smaller than the size of the filled circles in the plot): thickness of flakes formed on PA0 and PA0noK samples after ageings of 3, 7 and 14 days with 80 RH% and 80°C; **(b)** optical microscopy photographs of PA0 and PA0noK samples after ageing tests with 80 RH% and 80°C of durations 18 hours ("h"), 3, 7 and 14 days ("d").

By observing at high magnification through the electron microscope, other interesting aspects could be noticed. Scratches deriving from the polishing of samples were well visible, even below the flakes. Considering that this was assessed in all the aged plates and that the thickest flakes were measured to be ca. 67 μm wide, it is possible to affirm that the

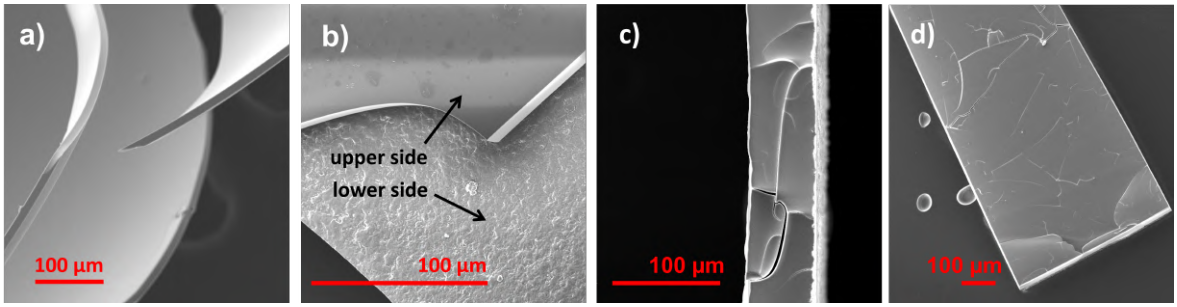

Figure 4.4: Secondary electrons SEM images of flakes formed after atmospheric ageing at 80°C, 80 RH% of **(a)** 3 days on PA0noK, **(b)** 7 days on PA0, and after 14 days on **(c)** PA0noK (edge) and **(d)** on PA0 glasses. The image shown in **(b)** was taken on two overlapping flakes: one on its normal orientation, the upper side upwards, and the other flipped.

scratches have affected the material until at least that distance from the surface. Another hypothesis could envisage that the hydration process proceeded homogeneously on the sample plate through hydrolysis. The latter, having a surface-limited kinetics, might have allowed the external contour (including the scratches) to be conserved during the in-depth unfolding of alteration, so that, as a final outcome, the surface reappeared scratched below the detached flakes. In any case, scratches do not seem to have played a role in the cracking of glass. As can be seen in Fig. 4.5a, crevices did not coincide with scratches profiles. On the other hand, such irregularities were preferential locations for salts growth (Fig. 4.5b). This had been as well observed by De Bardi et al. [16] and might be due to the higher quantity of moisture that could be hosted by the hollows compared to the smooth regions of the surface.[†]

Salts with sizes in the magnitude order of about 200 nm were detected to be spread homogeneously on PA0 and PA0noK glass samples aged at 80°C and 80 RH%. These can be seen in Fig. 4.5c and d. In the latter image, another type of salt that was found multiple times on the studied samples is displayed: it consisted of a network of wavy structures similar to trees roots, which branched out from a central core. Salts of this kind were detected throughout the surface of aged samples in different dimensions and diversified morphology. Furthermore, the elongated salts seen on PA0noK samples before the washing step were found (see 4.1 and Fig. 4.5e). These are similar to the ones referred to as *butterfly-shaped* by Falcone et al. [93] and as *crow's paws* (from the French *pattes de corneille*) by Fanny Alloteau [35]. The gain in intensity of the signals for sodium and carbon in EDX results for the detected salts suggested they all consisted of different species of sodium carbonate. This is in accordance with what was concluded by Falcone and Alloteau [35, 93]. Nevertheless, it cannot be excluded that the

[†]Water condensation was favoured in the highly negative curvature of the scratches, in accordance with Laplace's law of capillarity [92].

enrichment in metals other than sodium are hardly detectable with EDX and some of the observed salts are composed of mixed carbonates (likely of sodium and calcium).

Based on the conducted analyses, it was not possible to identify a relation between the salts formation and the duration of ageing. Similar salts were found both on PA0 and PA0noK aged for 3, 7 and 14 days. A parameter that may be more relevant is the time passed after the end of the removal of the samples from the climatic chamber. As it was observed by Alloteau et al. [13, 21], salts have probably formed as a second step and have slowly grown during storage. Such hypothesis was corroborated by the observation of some salts located where different cracks meet (Fig. 4.5f). This suggests their formation occurred after the fissuring of glass, hence subsequently to the end of the ageing test.

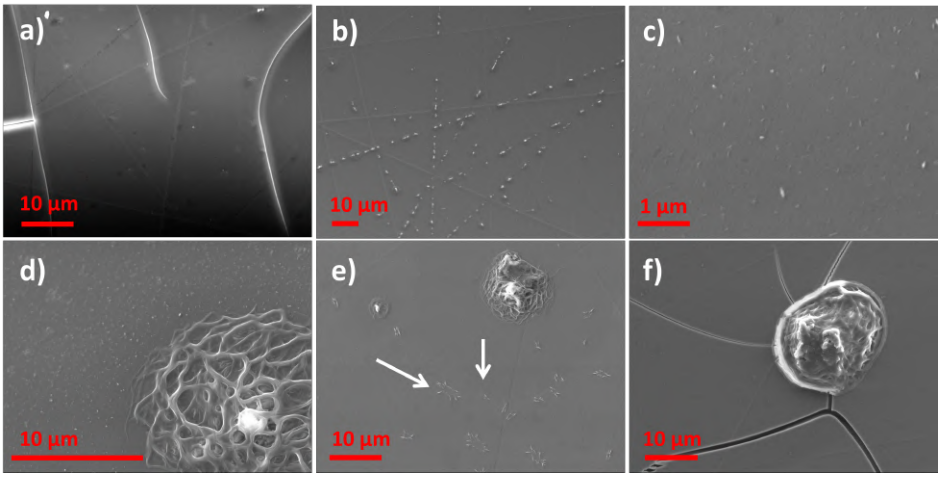

Figure 4.5: Secondary electrons SEM images of **(a)** the cracks and polishing scratches outlines on the surface of PA0noK after the 14-days ageing at 80°C, 80 RH%; **(b)** salts formed along scratches on PA0noK aged 3 days at 80°C, 80 RH%; **(c)** small salts spread homogeneously on the flakes formed on PA0 after the 3-days ageing; **(d)** salts with different morphologies and dimensions on PA0 glass after the 14-days ageing; **(e)** salts on PA0 aged 7 days (*crow's paws* salts are highlighted with arrows); **(f)** salt formed at the intersection of multiple cracks on PA0noK aged 7 days.

Due to the flakes formation with the 3, 7 and 14 days ageing at 80°C and 80 RH%, infrared spectra could be collected only for samples aged for 18 hours at the same temperature and moisture conditions. Transmission spectra did not show any change after the ageing test for all the glass types except for PA0noK. For the latter, $O-H$ stretching bands at about 3500 and 2800 cm^{-1} [8, 83, 94–97] presented an increase in intensity with ageing, indicating the hydration of the material (Fig. 4.6a). Such signals are ascribable to the stretching vibrations of $(Si)O-H$ groups whose association to non-bridging oxygen is weak and strong, respectively [35, 83, 95–97].

A higher sensitivity could be gained with ATR-FTIR analyses, which allowed for the

detection of the occurred surface hydration on the other glass types. The broad band centered at about 3200 cm^{-1} can be ascribed to $O-H$ stretching modes of silanol groups of the glass and molecular water [2, 12, 83, 98–104]. Given the varying degrees of hydrogen bonding associated to such species, the signal results in quite a wide band characterised by multiple shoulders. Upon ageing, this band gained intensity, as did the signals at about 2300 and 1640 cm^{-1} assigned to silanol groups stretching and molecular water bending, respectively [2, 12, 96, 99–104]. As can be seen from Fig. 4.6b,d,e , such change was quite remarkable for PA0noK, whereas for glasses PA0 and B it was way less evident. The stability of composition B enabled the ATR-FTIR analyses to be carried out on such glass also after the 7-days ageing at 80°C and 80 RH%. An increase in OH-related bands can be noticed, together with the appearance of a band at about 1445 cm^{-1} (Fig. 4.6e). This signal was registered also for PA0noK aged for 18 hours and points to the formation of carbonate salts (stretching CO_3^{2-} [43, 101–105]). Interestingly, the OH band registered for glass B presented stronger signal intensities at high wavenumbers compared to that of PA0 and PA0noK. This suggests that the OH groups in the last two are more bound and, therefore, are involved in hydrogen bondings with NBOs, even after ageing. Such interpretation is in accordance with what was pointed out by Alloteau et al. regarding PA0 glass: upon ageing under atmospheric conditions alkalis are retained in the structure and are likely favouring the progression of the alteration processes [13].

A further confirmation that PA0noK glass underwent a more severe alteration is given by the change in intensity and position of the signals given by $Si-O$ bonds vibrations in the region $1130-750$ cm^{-1} (see spectrum detail reported in Fig. 4.6c). This difference is evidence of a modification of the silica structure. Signals at ca. 760 and 910 cm^{-1} can be attributed to the symmetric and asymmetric stretching modes of $Si-O^-$ species, respectively [98, 101, 106]. Upon ageing, the peak at 760 cm^{-1} decreased relatively in absorbance with respect to its neighbouring signal (maybe due to a partial overlapping of the two), and the one at 910 cm^{-1} shifted towards lower wavenumbers. In addition, signals ascribable to the transverse optical (TO) and longitudinal optical (LO) components of the asymmetric stretching of $Si-O-Si$ gained strength, resulting in a peak at about 950 cm^{-1} and a shoulder around 1130 cm^{-1}, respectively. These bands fall at slightly different wavenumbers compared to those reported in the literature [43, 98, 103, 106, 107] probably due to the different structure of the glass under study. As explained in [106], the signal in the region between ca. $900-1000$ cm^{-1} given by $Si-O-Si$ asymmetric vibration is more sensitive to structural changes, its wavenumber being affected by the bond angles among bridging oxygens and silicon. Nonetheless, changes in IR spectra of silicate glasses upon ageing similar to the ones observed in the present study are reported in the literature. In particular, very similar features were observed by Palomar

et al. [101] for potash-lime silicate glasses after corrosion tests. Such evolution of IR spectra may suggest that a dealkalinisation process followed by the condensation of silanol groups has occurred at the surface of PA0noK glass. Thereby, a porous silica alteration layer has probably formed.

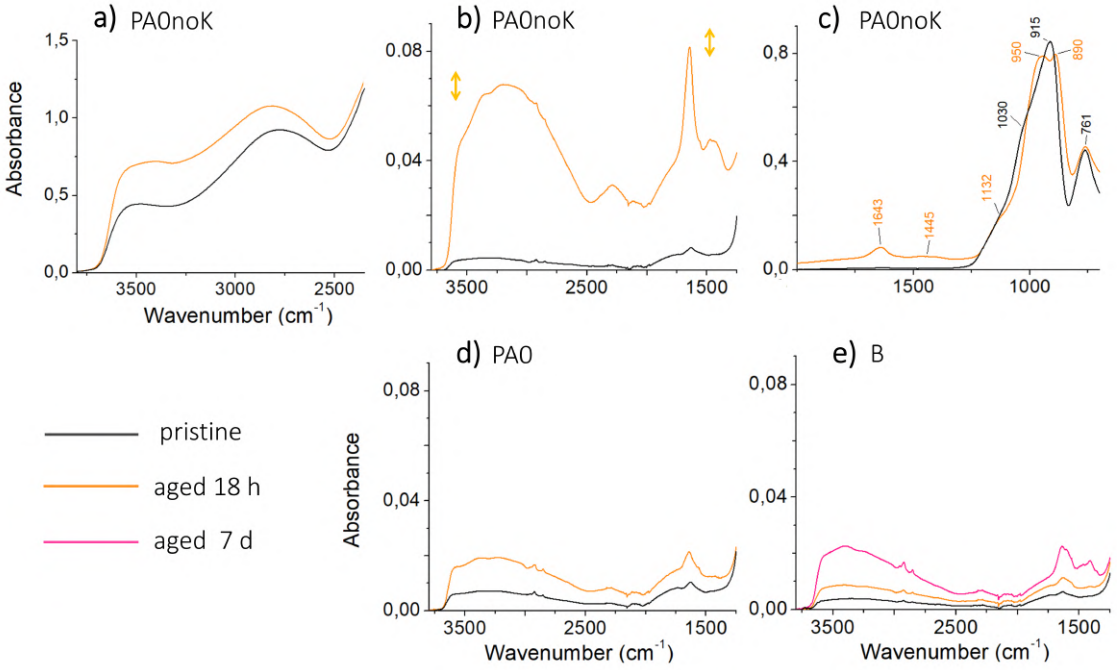

Figure 4.6: IR spectra details of glass before and after 18 hours-ageing at 80°C 80 RH% registered **(a)** in transmission for PA0noK and in ATR mode for **(b)** and **(c)** for PA0noK, **(d)** PA0 and **(e)** B. Regions at high wavenumbers are shown in **(a,b,d,e)** for focusing on glass hydration upon ageing, while the $2000-700$ cm^{-1} interval is reported in **(c)** to show structural changes occurred for PA0noK. The yellow arrows in **(b)** indicate the extent of absorbance variation between the three measurements on the sample (not shown in the other spectra because too narrow).

The effect of longer ageings at 80°C and 80 RH% was evaluated thanks to Raman spectra acquired on flakes. The hydration occurred in altered glass was assessed on account of the strong $O-H$ stretching bands in the range between 2000 and 4000 cm^{-1} [8, 20, 28, 108, 109]. These were quite intense, especially for PA0noK, and characterised by a maximum close to 3500 cm^{-1} followed by multiple shoulders at lower wavenumbers (Fig. 4.7a,b). The region between 100 and 1800 cm^{-1} gives information on the glass structure as signals for bending and stretching modes of $Si-O-Si$ species can be found in the ranges $300-700$ cm^{-1} and $800-1100$ cm^{-1}, respectively [6, 8, 12, 91, 109–119]. As can be seen in Fig. 4.7c,d, spectra registered for the flakes differred considerably from the ones acquired on pristine glass samples. The unaged materials presented two main peaks at about 545 and 1100 cm^{-1},

ascribable, respectively, to the bending and stretching of Q^3 species [6, 91, 114, 116–119]. Moreover, two small signals could be detected at ca. 780 and 950 cm^{-1}. The former may be caused by the motion of Si against its tetrahedral oxygen cage. This is commonly registered at 800 cm^{-1}, but is reported to shift to lower wavenumbers when the content of alkalis in the structure is high [6, 113, 115, 116]. Alternatively, the signal at 780 cm^{-1} may be ascribed to the $Si-O-Si$ symmetric stretching of Q^n-Q^m adjacent tetrahedra with a degree of polymerization higher than Q^1-Q^2 [119]. The band at 950 cm^{-1} is associated with $Si-O$ stretching of Q^2 species [6, 91, 111, 116–118].

Spectra collected on flakes exhibited the same signals described above but with lower intensities, pointing to a decrease in Q^3 species content. The structure of altered glass resulted to be quite different compared to the one of the pristine material: a more continuous network seems to have formed. This is suggested by the signal at ca. 120 cm^{-1}, which could be given by such medium-range ordering of the network and hence be recognised as the so-called Boson peak [110, 115, 120]. In addition, the emergence of the weak band at about 450 cm^{-1} could be due to a partial repolymerisation of the network [9, 20, 28, 91, 104]. The same signal enabled the distinction of PA2 glass from PA0 and PA0noK pristine samples, as can be noticed from Fig. 4.7e. Since the first is characterised by a lower amount of alkali ions compared to the other two, a structure richer in Q^4 species is likely to be the reason of the band at 450 cm^{-1}. The neighbouring signal, assigned to Q^3 species bending, decreased in intensity and maintained its position at 545 cm^{-1} for PA0 flakes, while shifted to ca. 535 cm^{-1} in the case of aged PA0noK. Both the drop in intensity and the change towards lower wavenumbers have been observed in previous studies and may be caused by the diminishing of alkali content [6, 91, 110, 115]. Concurrently with such modification, a new peak has risen around 660 cm^{-1} with ageing. This is possibly related to the $Si-O-Si$ symmetric bending in depolymerised portions of the glass structure consisting of Q^2 species comparable to those of pyroxenes [28, 91, 121]. Furthermore, the weak band at 950 cm^{-1} was substituted with another around 910^{-1}, commonly ascribed to $Si-OH$ stretching [8, 91, 119].

The range $1000-1100$ cm^{-1} displayed significant modifications: the peak detected for the pristine glass at about 1100 cm^{-1} turned into a shoulder of a broader and more complex band. Its centre being around 1030 cm^{-1}, such signal may point to the presence of Q^3 species where non-bridging oxygens (NBOs) are involved in strong hydrogen bonds. As a consequence of these intra-molecular interactions, the $Si-NBO$ bond is probably weakened, thereby leading to the downshift of the signal at 1100 cm^{-1} to lower wavenumbers [8, 9, 12, 91, 114]. Furthermore, an increase in content of Q^2 species, whose stretching signal lies at ca. 950 cm^{-1}, might have contributed to the broadening of the band at 1030 cm^{-1}.

The sharp peaks registered in the range $1020 - 1080$ cm^{-1} can be attributed to the symmetric stretching mode of CO_3^{2-} and, therefore, likely testify for the formation of carbonate salts. The signal at ca. 1060 cm^{-1} was common to all the spectra acquired for flakes and may be ascribed to an hydrate acid sodium carbonate. The peak location matches well with that of the main signal of Trona [122], a mineral that was also identified on artificially aged glass samples by Fanny Alloteau [35]. Spectra registered for flakes formed after a 3-days ageing on PA0noK presented a stronger signal at about 1078 cm^{-1}, which could be assigned to Pirssonite [35, 122] or sodium carbonate [123, 124]. The peak at 1025 cm^{-1} found for PA0 glass might indicate the formation of potassium carbonate or other similar salts [123]. It is worth noticing that the described peaks are well visible mainly in the spectra acquired on flakes formed after the 3-days ageing. This is reasonably related to the time gap between the end of the ageing test and the Raman analyses rather than the duration of the ageing itself. While samples subjected to the 7 and 14 days artificial ageings were analysed with Raman after about 40 days, measurements on those aged for 3 days were performed only when 71 days had passed. Thus, bigger salts were probably present on the latter group of samples at the time of the spectra acquisitions compared to the other two.

EDX results, summarised in Table 4.2, confirmed the hydration of the altered glass. Weight percentages of water ranging from 10 to 15 % resulted to be included in flakes. Such quantities are related to the water that is tightly bound as H_2O and OH groups, as samples are introduced in vacuum for SEM-EDX investigations and physisorbed water is lost through evaporation. Contrarily to what may be expected, the content of bound water resulted to be less in the samples aged for 14 days compared to that of samples aged for 3 days. On this note, it is worth pointing out that different time lags had passed for the two groups of samples between the end of the ageing test and EDX analyses (13 days for the 3-days ageing versus one month for the 14-days ageing). Glass alteration continues even after the accelerated ageing test with different processes which, for instance, lead to salts growth. Therefore, it is not convenient to draw conclusions from such comparison and the values for bound water content would better be taken only as a confirm that a remarkable hydration has occurred in the studied glass. Below the flakes, the material resulted to be comparable to unaged glass, given its null content of bound H_2O. A quantity of about 2 wt% of water was calculated to be present in the surface layer of pristine glass reference samples: this might be due to the very high sensitivity of the studied material, which let the natural short ageing prior to the analyses be enough for the samples to undergo a mild hydration.

Considering that it remains constant with atmospheric ageing, the quantity of silicon in the glass was used to normalise the % atomic quantities for sodium, potassium and calcium. The

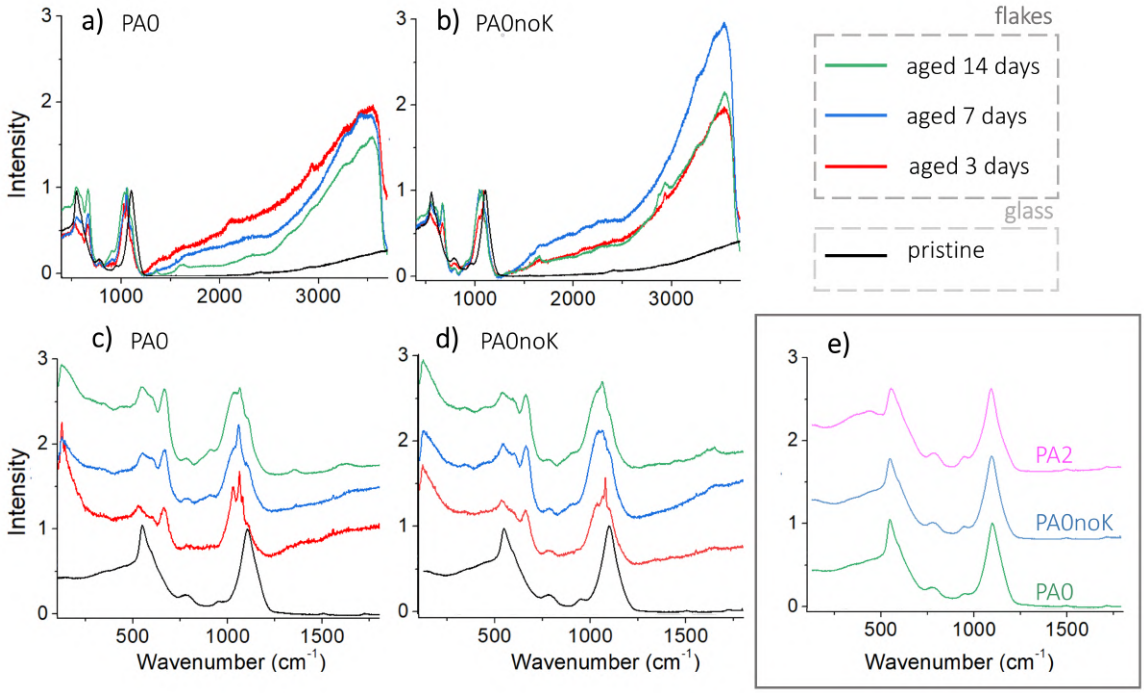

Figure 4.7: Normalised Raman spectra collected on pristine glass and on flakes formed after the ageing tests at 80°C and 80 RH% for different periods of time (3, 7 and 14 days). Spectra are shown in the whole wavenumber range allowed by the instrumentation in **(a)** and **(b)** and in the region between 100 and 1800 cm^{-1} in **(c)** and **(d)** for PA0 and PA0noK, respectively. Raman spectra in the range $100 - 1800$ cm^{-1} registered for pristine glass of the different compositions PA2, PA0 and PA0noK, are shown in **(e)**. In **(c,d,e)**, spectra are arbitrarily stacked to facilitate their visualisation.

ratios Na/Si, K/Si and Ca/Si are reported in Table 4.2: they resulted to be quite consistent, regardless the level of ageing and the location of measurement. This suggests the depletion in alkali or alkaline earth ions occurred with the 3 and 14 days atmospheric ageings at 80°C and 80 RH% was not extensive. Yet, a slight enrichment in sodium and calcium could be noticed for the hydrated glass compared to the pristine material. The fact that this was more evident for Ca^{2+} than for Na^{+}, while no change was detected for K^{+}, is in accordance with what reported by Alloteau et al.: these ions are driven towards the surface at different degrees, $Ca^{2+} > Na^{+} > K^{+}$ [91].

TGA results confirmed that PA0 and PA0noK glass underwent an hydration process that made them include around 10%wt of bound water (Table 4.3 and Fig. 4.8a). Once again, the higher sensitivity of PA0noK compared to PA0 was highlighted, as the percentage of bound water was higher for the former than for the latter glass type. Interestingly, the level of hydration did not change considerably with the different duration of ageing for PA0. The

same observation may be applicable for PA1 and PA2 as well, yet in this case the percentage of bound water is so low that it is hard to tell if the registered variations are meaningful.

The distinction between very stable and unstable glass compositions was observed with

Table 4.2: EDX results for PA0 and PA0noK pristine and aged samples, where A = above flakes and B = below flakes. The normalised atomic percentage of oxygen in the samples is reported both in its measured and calculated value, the former being the instrumental result and the latter being derived from the oxides stoichiometry. Ratios between the % atomic quantities of Na, K and Ca over the one of Si are also reported, to allow comparisons among the different measurements. The normalised weight percentage of water was calculated starting from the difference $O_{calc} - O_{meas}$ and is reported in the last column.

Sample	Ageing Duration	Location	O meas	O calc	Na/Si	K/Si	Ca/Si	H_2O wt%
PA0	3 days	A	65.72	49.21	0.34	0.21	0.09	14.31
		B	59.03	59.64	0.31	0.21	0.08	-0.51
	14 days	A	64.88	49.89	0.37	0.20	0.10	12.96
		B	59.11	59.26	0.32	0.21	0.10	-0.12
	Pristine	-	60.67	57.69	0.30	0.20	0.09	2.53
PA0noK	3 days	A	65.60	49.13	0.54	0.02	0.11	14.68
		B	59.41	59.58	0.47	0.02	0.11	-0.14
	14 days	A	63.92	52.16	0.53	0.00	0.09	10.47
	Pristine	-	60.24	58.26	0.51	0.00	0.08	1.74

Table 4.3: Weight percentage (%wt) content of bound water calculated for powder samples aged 3 and 14 days at 80°C and 80 RH% based on TGA results. PK and PA0noK samples aged 3 days were not analysed with this technique. For details on how these data were calculated, see paragraph 3.3.5

	% bound water				
Sample	PK	PA0noK	PA0	PA1	PA2
Aged 3 days	-	-	9.79	0.22	0.03
Aged 14 days	14.5	11.8	9.90	0.41	0.01

TGA analyses, as PK, PA0noK and PA0 samples were found to include a significantly higher percentage of bound water compared to PA1 and PA2. This is in accordance also with what was observed with the naked eye and with the microscope. Aged glass powders were visibly different depending on their hydration level: those of unstable compositions were clustered together in quite stiff opaque blocks, whereas those of more stable types appeared as unaltered and could be handled more easily. After the 14-days ageing, PK powder had formed a block with an icy appearance. An initial hypothesis about it envisaged the aged material consisting of several salts. Nonetheless, as the carbonate weight percentage on the total mass measured with TGA was only the 0.08%, such possibility was excluded. Consistent with TGA results, the peculiar appearance of PK was attributed to a more severe hydration of the glass. The

microscope images taken after the 3-days ageing test and reported in Fig. 4.8b provide an example of different aspects of the aged powders. While PA0 granules were smoothed and bound together, those of PA1 and PA2 appeared disconnected and characterised by sharp edges, as they were before the ageing test. Possibly, the adhesion among grains for the unstable compositions stemmed from the formation of hydrogen bondings merging the hydrated layers together.

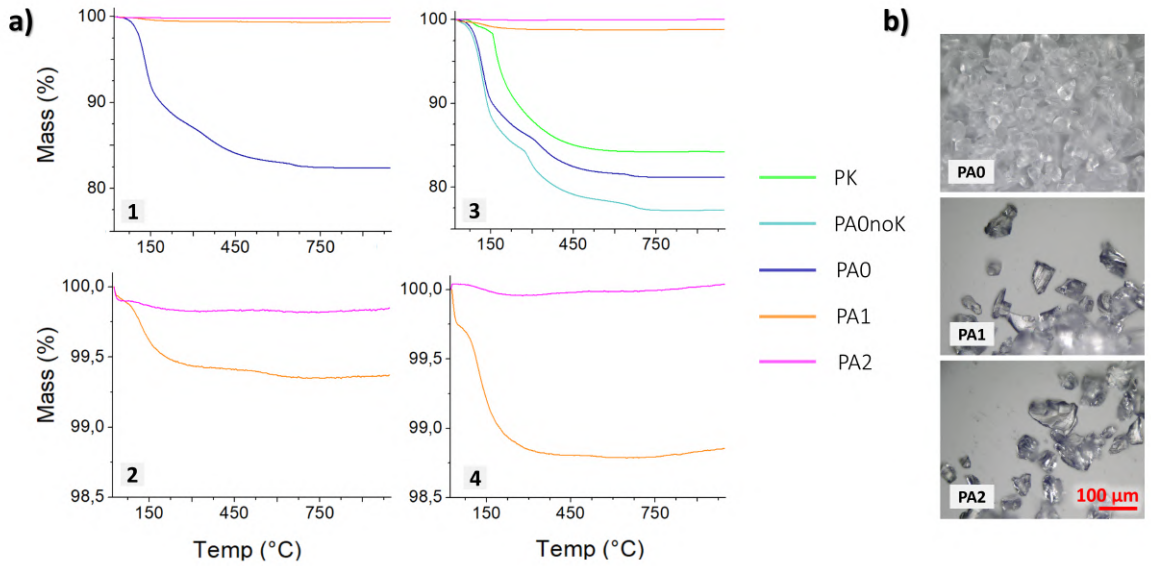

Figure 4.8: **(a)** TGA curves registered for powder samples aged 3 days (1,2, compositions PA0, PA1 and PA2) and 14 days (3,4, compositions PK,PA0noK, PA0, PA1 and PA2). Images 2 and 4 are reported with a different scale to 1 and 2 to better visualise the curves registered for the stable compositions PA1 and PA2. The T range from 150 to 600 °C was considered for the loss of bound water, the region below 150°C and the one between 600 and 800°C were related to physisorbed water and carbonates, respectively. **(b)** OM images taken on glass powders aged for 3 days at 80°C and 80 RH% of samples PA0, PA1 and PA2.

4.1.2 The temperature effect on atmospheric artificial ageing

By carrying out the 14-days, 80 RH% ageing at 60°C instead of 80°C, the role of the temperature on glass alteration kinetics could be questioned. The results were visibly different, as no flakes formation took place, the most unstable compositions included. Instead, a multitude of salts crystallised on the samples during the ageing test in the oven. OM observations revealed the presence of circular species of dimensions ranging from 1 (PA2) to $20-25$ μm (PA0 and PA0noK) which were spread quite uniformely throughout the glass surface (Fig. 4.9). Once again, the higher sensitivity of PA0noK compared to PA0 was revealed. Not only was the average salt dimension larger, but also cracking and iridescence phenomena

could be noticed (Fig. 4.9c and d, respectively). The substantial presence of salts might have prevented flakes from forming. This could be explained by considering that the hydrated layer alkalinity was probably lessened by salts formation (as OH^- ions are consumed by reacting with acid gases of the atmosphere). The silicate network hydrolysis was therefore slowed down and so was the in-depth hydration for the surface exposed to the atmospheric environment. Indeed, flaking occurred only on the side of PA0noK samples that laid on the holding plate. As this was in contact with the sample holder, its interaction with carbon dioxide present in the atmosphere was largely mitigated and hence it was not affected by salts crystallisation as much as the other side. Interestingly, the most stable compositions among the three tested with this experiment presented the same signs of alteration as the others, even if at a lower degree: salts formed on PA2 were at least one order of magnitude smaller than those detected on PA0 and PA0noK. Even if the polishing scratches constituted favourable sites for salts growth (Fig. 4.9e), the crystallisation phenomenon affected the whole surface of the samples (Fig. 4.9f).

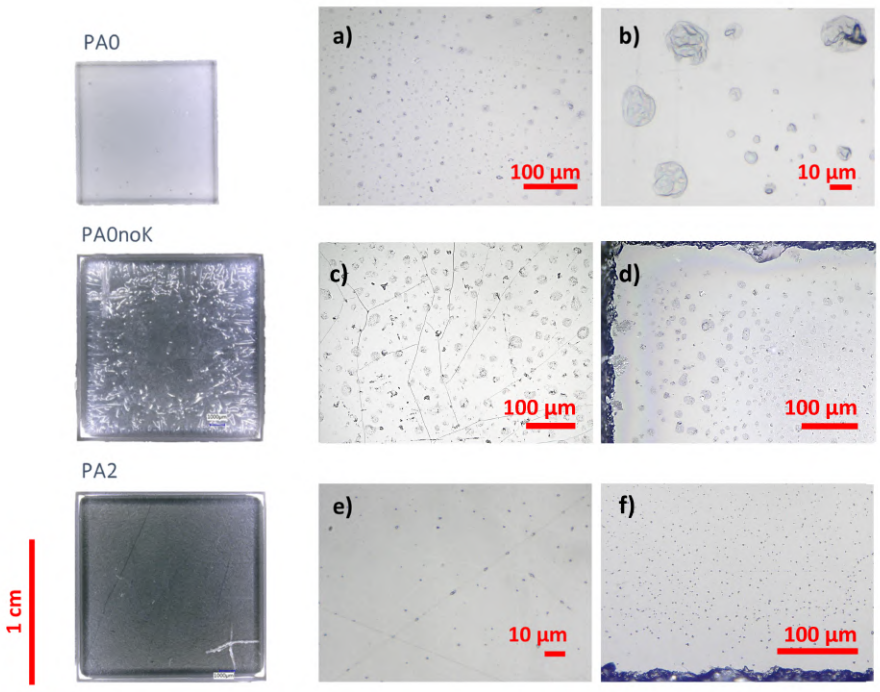

Figure 4.9: OM images taken on PA0, PA0noK and PA2 samples after a 14-days artificial ageing at 60°C and 80 RH%. At the left side, OM images at low magnification (1 cm scale) are reported to display the entire samples, whereas at the right side salts formed upon ageing are shown in detail (10-100 μm scale). **(a,b)** Salts of different dimensions formed on PA0; **(c,d)** salts formed on PA0noK with focus on **(c)** cracks spread on the surface and **(d)** iridescence along the edges; **(e,f)** small salts visible on PA2 samples.

SEM observations helped revealing that the rounded structures seen through optical microscopy (Fig. 4.9) actually consisted of moisture drops. As salts were highly hygroscopic, the water surrounding them did not evaporate at atmospheric pressure. Only the high vacuum used for SEM analyses determined the removal of the loosely bound water and hence the visualisation of the underlying crystals. Some examples of these are reported in Fig. 4.10a and b, where their needle-shaped structure can be noticed. Besides such quite large clusters, considerably smaller salts were found to be spread all over the samples surface, as can be seen in Fig. 4.10c. The fragile glass of PA0noK composition was severely damaged by the conditions of SEM analyses: the electron beam used for the observation was sufficient for causing an extensive cracking of the material (Fig. 4.10 d and e). This hindered a thorough investigation on the sample, but allowed to assess that the scratches from sample polishing could be seen even below the flakes (Fig. 4.10f), as it was previously noticed (see paragraph 4.1.1).

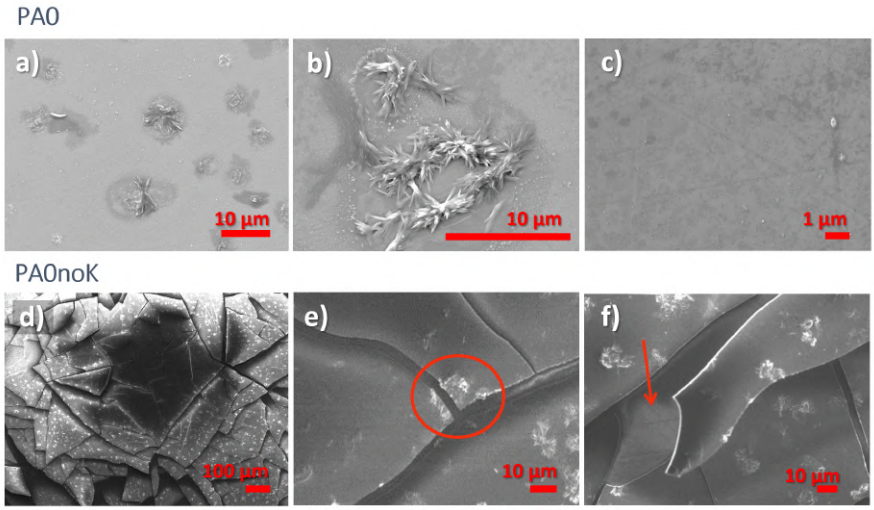

Figure 4.10: SEM images of PA0 and PA0noK samples after a 14-days artificial ageing at 60°C and 80 RH%. **(a,b,c)** Salts of different dimensions formed on PA0; **(d,e,f)** cracks formed during SEM observation in PA0noK. In **(e)** the red circle highlights an evidence of cracking after salt formation, while in **(f)** the arrow points at the scratches visible below a flake.

Given the absence of flakes, IR acquisitions could be performed. Spectra collected in transmission mode presented some changes upon ageing for PA0noK glass only. As can be noticed by looking at Fig. 4.11a, the increase in absorbance of the O H-related signals were dramatically bigger compared to those registered for the 18h ageing at 80°C, 80 RH%. Moreover, the relative intensities of the two bands changed, the one at higher wavenumbers

gaining strength with respect to the other and presenting a new maximum at ca. 3390 cm^{-1}. The rise in intensity of the band at ca. 3500 cm^{-1} might indicate an increase in the so-called "free" OH groups due to a change in the silica network structure, whereas the feature at 3390 cm^{-1} may be associated with molecular water, either deriving from the hydration of the glass or related to the hygroscopic alteration salts [9, 96, 97].

ATR-FTIR spectra confirmed the difference in sensitivity among the studied glass compositions: the most prone to alteration resulted to be PA0noK, followed by PA0 and PA2, the latter undergoing a negligible hydration. Indeed, ATR-FTIR spectra revealed a tremendous increase in intensity of the OH-related bands for the first glass type, a minor one for the second and null for the last, as can be seen in Fig. 4.11b,d and e. As it was observed for PA0noK aged 18h at 80°C, 80 RH%, new peaks were registered after the ageing test in the region $1400 - 1350$ cm^{-1} for PA0 and PA0noK. Moreover, the signal at about 1600 cm^{-1} gained complexity, displaying multiple sharp maxima. These two effects are ascribable to the salts formed on the samples: the absorptions at ca. 1400 cm^{-1} probably originate from the carbonate stretching modes and those at ca. 1600 cm^{-1} from the water adsorbed and bound in the salt structure (as well as in the hydrated layer). In the range $1200 - 700$ cm^{-1},

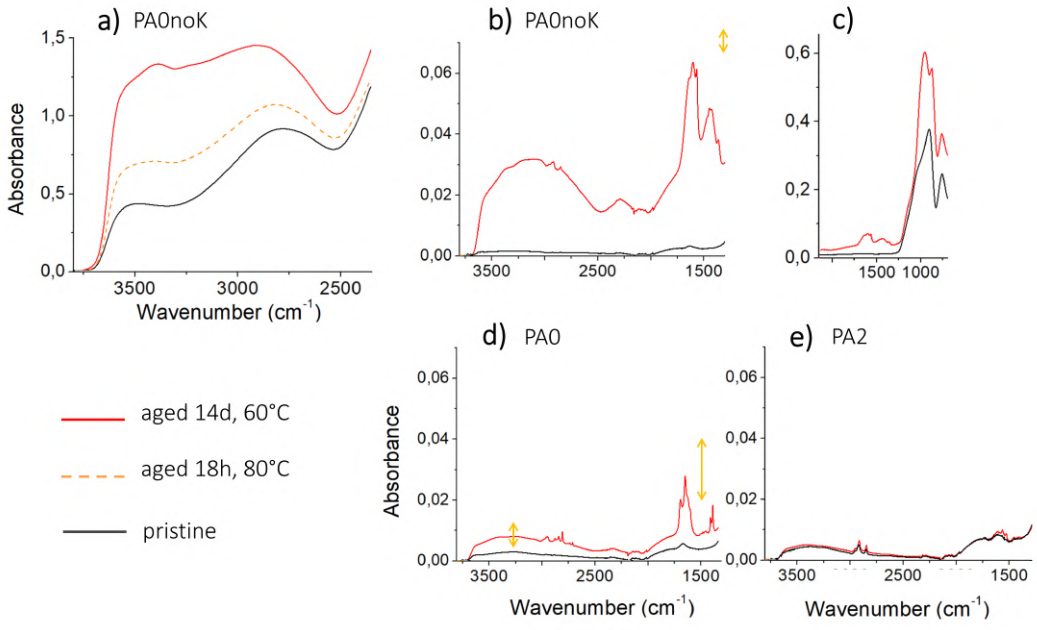

Figure 4.11: IR spectra acquired on PA0noK, PA0 and PA2 samples before (black) and after (red) a 14-days artificial ageing at 60°C and 80 RH%. For PA0noK glass, the IR spectrum in transmission is reported in **(a)** and two details of the ATR-FTIR spectra are shown in **(b,c)**. In **(a)** the spectrum obtained for the ageing of 18h at 80°C is shown with an orange dashed line for a comparison. The ATR-FTIR spectra of PA0 and PA2 are reported in **(d)** and **(e)**, respectively.

PA0noK presented changes in signals similar to those observed for the 18h, 80°C, 80 RH% ageing (Fig. 4.11c). In this case, the peak at ca. 950 cm^{-1} resulted more intense with respect to that at about 870 cm^{-1}. This might indicate the glass reached a more advanced state of alteration entailing the condensation of silanol groups after a dealkalinisation process.

Salts formed as ageing products were detected through Raman acquisitions as well. Spectra registered for PA0noK and PA0 after the 60°C ageing presented characteristic signals of hydrated carbonates in the ranges $1350 - 1440$ cm^{-1} and $2700 - 2950$ cm^{-1}. The former set of peaks is attributable to the asymmetric stretching mode of CO_3^{2-} species, whereas the latter to the $O - H$ stretching of salts hydration water [104, 123, 125–127]. In Fig. 4.12, the spectra are shown in comparison with the ones of pristine glass and with those registered for the 14-days, 80 RH% ageing at 80°C. Immediately noticeable is the difference of absorbance among the three spectra in the high wavenumbers range: the intensity of the $O - H$ stretching band is substantially higher for the samples aged at 80°C compared to those aged at 60°C. Furthermore, some differences can be detected at low wavenumbers. The peaks at ca. 1030 and 1060 cm^{-1}, related, respectively, to Q^3 and Q^2 species and to the symmetric stretching mode of CO_3^{2-} (see section 4.1.1), were detected for PA0noK aged at 60°C, but not for PA0. No further signs of alteration could be noticed at low wavenumbers, the spectra resembling closely those of the reference glass. This indicates that, the duration and the RH% kept constant, by lowering the temperature of ageing the hydration of glass results less severe, while the formation of salts is favoured. Still, it is of great importance to point out that Raman acquisitions were performed on detached flakes - and hence on the hydrated layer only - for the 80°C ageing, and on plate samples for the 60°C ageing. For the latter, the influence of the underlying bulk glass may have played a role in the resulting spectra, so that the evidence of alteration phenomena occurred on the surface layers were substantially mitigated.

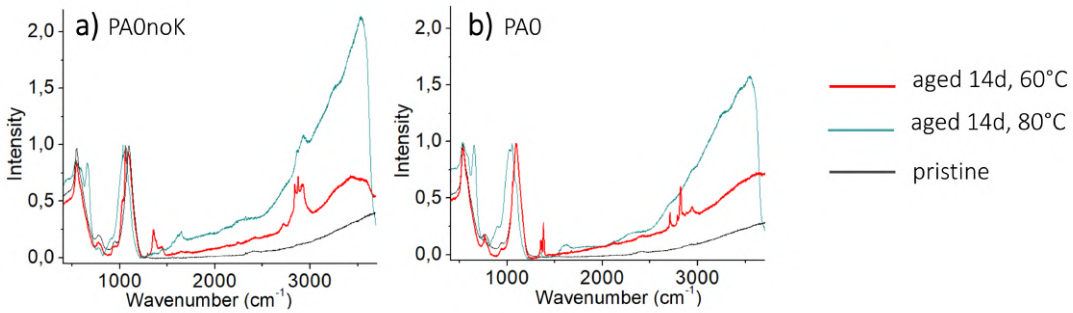

Figure 4.12: Raman spectra acquired on **(a)** PA0noK and **(b)** PA0 samples after 14-days, 80 RH% artificial ageings at 60°C (red) and 80°C (green). Spectra of the pristine materials are also shown in black as a comparison.

4.2 Dissolution experiment

The outcomes of the artificial ageing observed with the dissolution experiment were significantly different from those obtained under atmospheric conditions. Still, the composition effect on the degree of alteration could be recognised based on the results. Once retrieved from the PTFE containers, the plate sample of PA2 glass appeared unchanged, whereas those of PA0noK and PA0 were partially covered by the powder of identical composition that was immersed in their same water (calibrated powder, aged in the PTFE containers with the plate samples). This was quite tightly attached to the surface of the plate samples, indicating that the immersed glass had probably undergone an alteration process which favoured the adhesion between the two (Fig. 4.13a,b). Nevertheless, the powder could be removed from the plate samples surface by gently rubbing with the dry nonwoven cleanroom wipers. Besides this, no flakes or salts were detected through naked eye and OM observations (Fig. 4.13c).

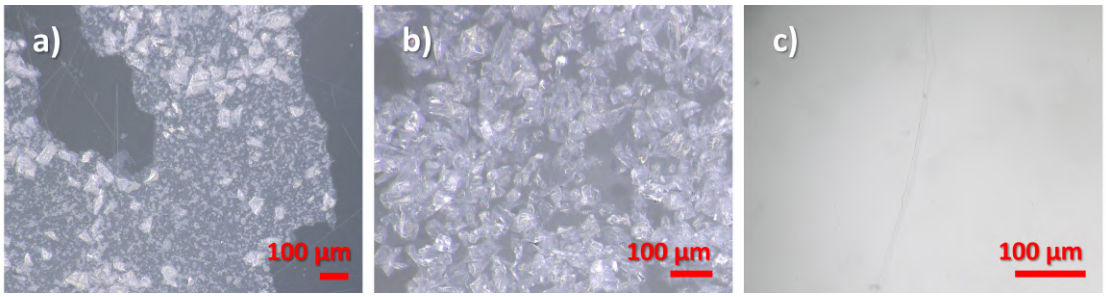

Figure 4.13: OM images of the powder adhering on plate samples surface of **(a)** PA0noK and **(b)** PA0 and **(c)** surface of PA0noK plate sample clean from any powder.

The hydration of glasses PA0noK and PA0 was assessed thanks to IR investigations. The spectra collected for PA2 after the ageing test coincided with those of the pristine glass, whereas for the other two compositions evident changes were observed (Fig. 4.14). OH-related signals increased in intensity both in transmission and ATR-FTIR spectra, indicating a thorough hydration had affected the surface of the material. Transmission bands for PA0noK were interestingly less intense compared to those registered after the atmospheric ageing of 14 days at 80°C. This might suggest that the hydration process is slower under immersion conditions. Nonetheless, the opposite phenomenon was noticed for PA0, whose negligible variation with the atmospheric ageing was replaced with a considerable change with the dissolution experiment. As can be seen in Fig. 4.14b, the band at higher wavenumbers ascribed to the "free" OH groups and molecular water gained more intensity with respect to the other, as it had been observed for PA0noK glass after the 14-days atmospheric ageing at 60°C, 80 RH% (section 4.1.2). Molecular water may be the key factor in the hydration under immersion

conditions. Not only did the high-wavenumber transmission band increase more in intensity compared to the one at lower wavenumbers, but also the ATR-FTIR signal at about 1640 cm^{-1} assigned to molecular water bending resulted quite strong for the spectra of PA0noK and PA0 aged under immersion conditions (Fig. 4.14d, e). Both for PA0noK and PA0 composition some changes with respect to the pristine glass were noticed in the low wavenumber range. These were pretty close to the ones observed for PA0noK glass after the atmospheric ageing tests: the peak at ca. 910 cm^{-1} was substituted by signals at 985 cm^{-1}, 885 and 1155 cm^{-1}. Yet, the relative intensities were not the same, indicating an altered material with a different structure had formed with the ageing under immersion conditions. The feature attributed to the asymmetric $Si-O^{-}$ stretching at ca. 885 cm^{-1} substantially diminished in intensity and appeared as a shoulder of the more intense peak at 985 cm^{-1}. Such analytical result is probably given by the presence of an altered layer formed through the ageing of glass in warm water. Being characterised by a different silica structure compared to the one of pristine glass, this is likely to consist of the porous, amorphous and hydrated layer that in the literature is alternatively called leached layer, hydrated glass or - more frequently - gel [7, 15, 37, 40, 43, 50].

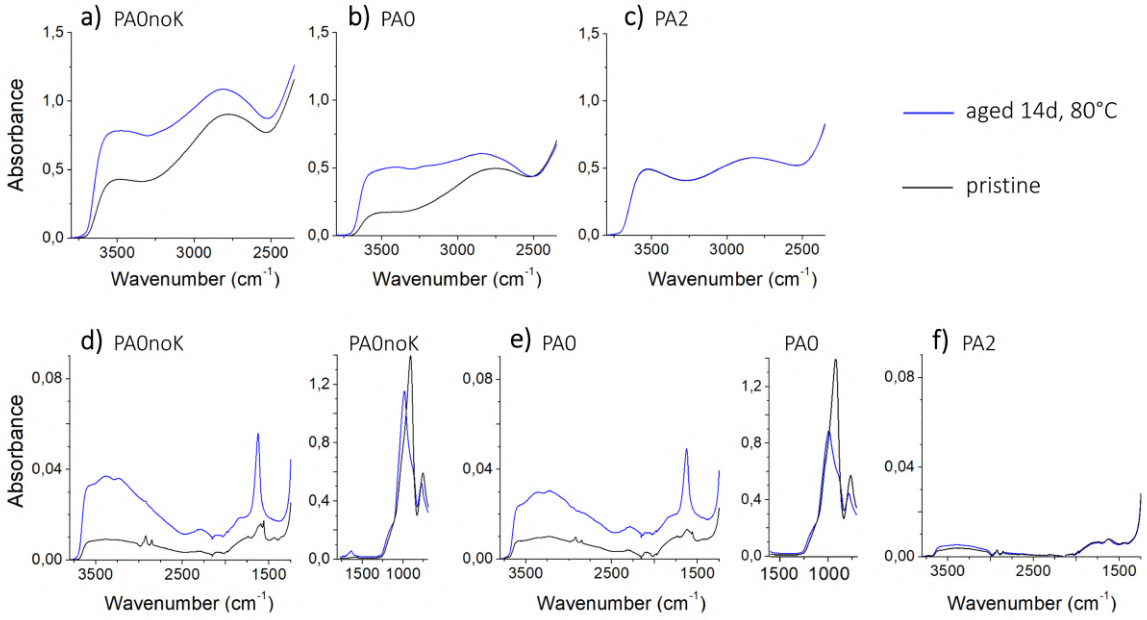

Figure 4.14: IR spectra of PA0noK, PA0 and PA0 before and after the dissolution experiment acquired in**(a)**, **(b)**, **(c)** transmission and **(d)**, **(e)** and **(f)** ATR mode.

While ATR-FTIR spectroscopy revealed the presence of the gel on PA0 and PA0noK glass, Raman spectroscopy did not allow for the same result. This is in accordance with the fact that

the former is a surface-sensitive technique, targeting approximately one micrometer of depth, whereas the latter is carried out using a green laser, which penetrates more in the samples due to glass transparency. As can be seen in Fig. 4.15, signals at low wavenumbers for the samples aged under immersion conditions coincided with those of the reference glass. Furthermore, the OH band at ca. 3500 cm^{-1} did not reach as high intensities as those registered for the flakes formed after the atmospheric ageing at 80°C and 80 RH%. The level of hydration was comparable to the one resulting from the samples aged under atmospheric conditions at 60°C (which were also analysed as plates since flakes did not form). Finally, no signals attributable to salts were detected.

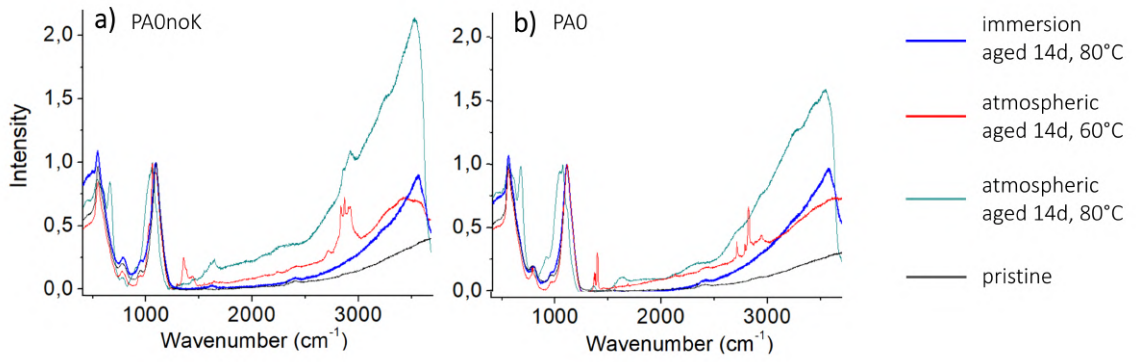

Figure 4.15: Raman spectra acquired on **(a)**PA0noK and **(b)** PA0 samples after the dissolution experiment (blue) and the 14-days ageings under atmospheric conditions with 80 RH%, 60°C (red) and 80°C (green). Spectra of the pristine materials are also shown in black as a comparison.

A comparison of the altered PA0noK glass resulting from ageing under immersion and atmospheric conditions can be made based on MAS NMR results. The ^{29}Si spectrum obtained for the pristine glass is shown in black in Fig. 4.16a and is characterised by a strong signal at about −90 ppm, an evident shoulder around −100 ppm and a smaller one at ca. −80 ppm. These can be respectively attributed to Q^3, Q^4 and Q^2 species present in the structure at different degrees, according to the signals intensity [13, 21, 35, 128]. The atmospheric alteration resulted in the lowering of the Q^4 signal, indicating a depolymerisation process took place, and the splitting of the Q^3 band into two maxima. The latter evidence suggests a new set of Q^3 species has arisen. In particular, the maximum at more negative chemical shifts probably testifies for a lowering in alkali content [21, 129]. More marked was the change for the alteration under immersion conditions: three signals were registered in the range between −90 and −100 ppm, their maxima lying at more negative chemical shifts compared to the pristine glass. The structure of the altered layer probably contains different Q^3 species due to a strong depletion in alkalis. Additionally, the occurred repolymerisation was attested by

the increase in intensity of two features attributable to Q^4 species.

The difference between atmospheric and immersion alteration was evident also with the registered ^{1}H spectra, reported in Fig. 4.16b,c. Three echo times (T_E) are shown to help signals attribution: by increasing their duration, the ^{1}H species involved in strong homonuclear dipolar couplings are not recovered and hence the spectrum is deprived of their signal. On this basis, the contribution at 5 ppm is generally agreed to be given by molecular water [13, 35]. The tailing at higher chemical shifts is instead related to the presence of silanol groups involved in hydrogen bondings: the stronger they are, the bigger the chemical shift [13, 35, 91]. Conversely, signals between +3 and 0 ppm are ascribable to isolated OH groups [35, 91]. By comparing Fig. 4.16b and c, it is possible to notice that after ageing under atmospheric conditions, both strongly H-bound silanol groups and isolated OH formed the altered material, the contribution of molecular water being rather small. Instead, the ageing under immersion conditions resulted in an altered layer containing mainly H_2O and loosely H-bound silanols. This is in accordance with the ^{29}Si spectrum, as it may point to the production of water as a byproduct of the condensation reactions, and at the minor presence of alkalis and therefore of NBOs involved in H-bondings. Overall, it is evident that the surrounding environment plays an important role in the alteration mechanisms, so that what is observed under immersion conditions cannot be fully extended to the atmospheric ageing, as it was well pointed out by Gin et al. [40].

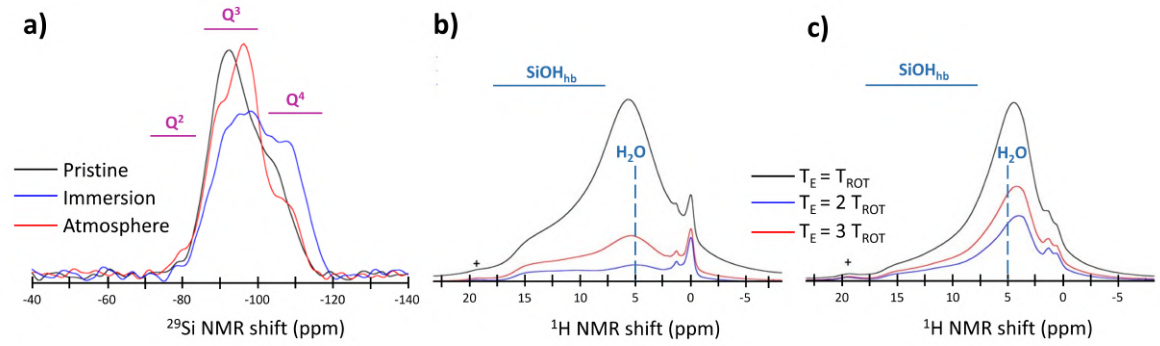

Figure 4.16: **(a)** ^{29}Si MAS NMR spectra of PA0noK glass powder before (black) and after ageing under immersion (blue) and atmospheric (red, 80 RH%) conditions at 80°C for 14 days. The ^{1}H MAS NMR spectra with different echo delays registered for PA0noK aged under atmospheric and immersion conditions are shown in **(b)** and **(c)**, respectively (hb = hydrogen bonded, + = probe signal).

ToF-SIMS results helped characterising the altered layer formed on the plate samples surface. As can be noticed by looking at Fig. 4.17, this was recognisable as the external portion of glass for which lower counts for alkali ions were registered (indicated by a dashed

red line in the images). The thickness of the leached layer could be inferred by considering the starting point of alkali content drop as the upper limit of the unaltered glass: for PA0 it resulted to be around 1.8 μm, whereas that of PA0noK approached 2.7 μm. Interestingly, the decrease in sodium was of similar entity for the two glasses (counts at the surface being inferior to those of the pristine material of 6 units), but the final content of Na in the gel formed in PA0 was lower than that of PA0noK. This is probably ascribable to the composition of such glasses: even if the loss in sodium is similar, PA0noK retains a non-negligible portion of these alkalis in its gel possibly due to their higher initial quantity.

The decrease in sodium was shown to be substantially stronger than that of potassium, indicating the higher mobility of the former. On the other hand, calcium and magnesium appeared to be retained in the glass structure. Given the porosity and the high degree of polymerisation of the alteration gel, it is likely that such metals were maintained in the network in the form of hydroxydes or carbonates, rather than as ions bound to NBOs. The amount of calcium appeared even higher for the altered layer compared to the pristine glass, and so was the case of silicon. This may be interpreted as an indication of the higher density of the gel compared to the underlying material, arising from the structure rearrangement occurring in parallel with the leaching of alkalis.

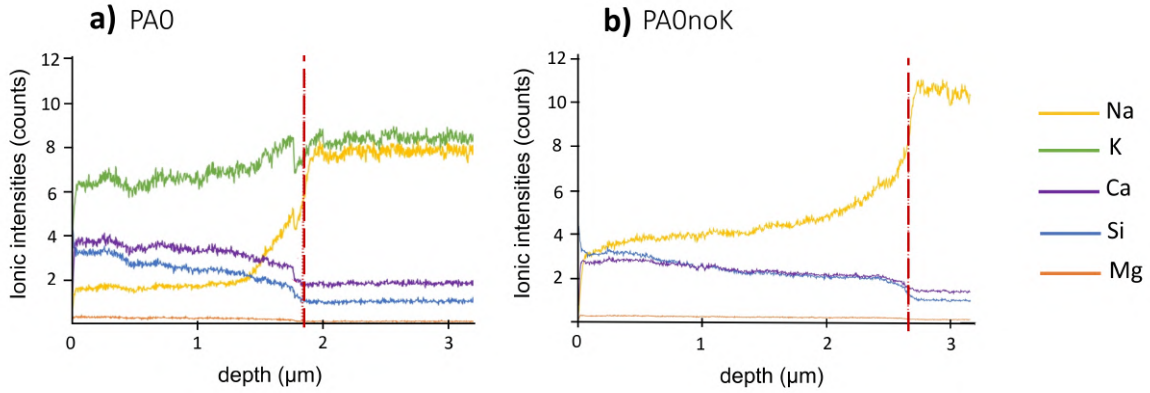

Figure 4.17: ToF-SIMS depth profiles of **(a)** PA0 and **(b)** PA0noK glass plates aged for 14 days at 80°C under immersion conditions. Si-normalised counts are displayed and the red dashed line highlights the limit between altered (left) and unaltered (right) glass. The depth scales were derived from the sputtering time by considering the dimensions of the craters, see section 3.3.4.

Not only did the ageing under immersion conditions cause the formation of an altered layer on the glass surface for the unstable compositions, but also it determined a progressive loss of material. This could be assessed thanks to ICP-AES analyses performed on water samples and involved the elements contained in the glass at different degrees, given the con-

curring reactions of ion exchange and of silica network hydrolysis [7, 39]. As can be seen in Fig. 4.18, the concentration of the major elements of glass in water changed throughout time following in most cases a semi-parabolic trend. After a quite fast rise in concentration in the first two days (up to the third point in the plots curves), the elements quantities in water increased progressively more slowly. As described in the introduction, such a fashion is generally described as a two-stage process, where stage 1 is associated to the so-called forward rate, and stage 2 to the residual rate [7, 37, 39, 46, 51, 52]. For PA0 and PA0noK, these two did not appear very different to one another, and the concentrations of elements in solution did not reach a completely steady state. Conversely, PA1 and PA2 glasses presented a visible change in the curves slope after two days of ageing: this may point either to the formation of a passivating alteration layer, or to the saturation of silica in the solution. To this end, it is relevant to remark that for both PA1 and PA2 the concentrations of Si reached values far below those of saturation at pH 10 [130] (see below for pH measurements). It is therefore possible to infer that the alteration layer for these compositions had passivating properties, which slowed down the proceeding of dissolution. Still, longer durations of ageing under immersion conditions would be beneficial to confirm or disprove such hypothesis and to investigate the extent of dissolution and interdiffusion processes for PA0 and PA0noK glasses. Noteworthy is the difference in scale between the unstable (PA0 and PA0noK) and the stable (PA1 and PA2) compositions. For the latter, Si concentrations in water reached ca. 70 ppm at most, which is about one quarter of the values registered for the other two glass types. Another key difference that can be noticed between unstable and stable compositions involves alkali ions: the concentrations of potassium and sodium registered for PA0 and PA0noK were quite high and comparable to those of silicon, whereas this was not the case for PA1 and PA2. For such more stable compositions, the quantities of Na and K in solution resulted pretty close to that of calcium, being considerably lower compared to the one of Si. This suggests that in PA0 and PA0noK a leaching process has taken place and caused the release of noteworthy quantities of alkalis. Magnesium resulted to be the most insoluble modifier ion in the glass structure, as its concentration in water was always very close or lower than the limit of detection (LOD, about 8.2×10^{-4} ppm for Mg).

The scatter plots built for the normalised mass loss reported at the bottom of Fig. 4.18 provided more accurate information for data interpretation. It is evident that the dissolution of PA0 and PA0noK was incongruent: Na and K were quickly leached while Si was more slowly dissolved. Conversely, for PA1 and PA2 the dissolution involved a very small portion of the material and was congruent, as Ca, Na, K and Si were dissolved at very close rates. It is interesting to notice that the curves for calcium and magnesium, respectively in unstable

and durable glasses presented a different outline compared to the others. The initial rise in mass loss followed by an immediate decrease might suggest that after reaching sursaturation in the solution, such elements precipitated as carbonates or hydroxydes.

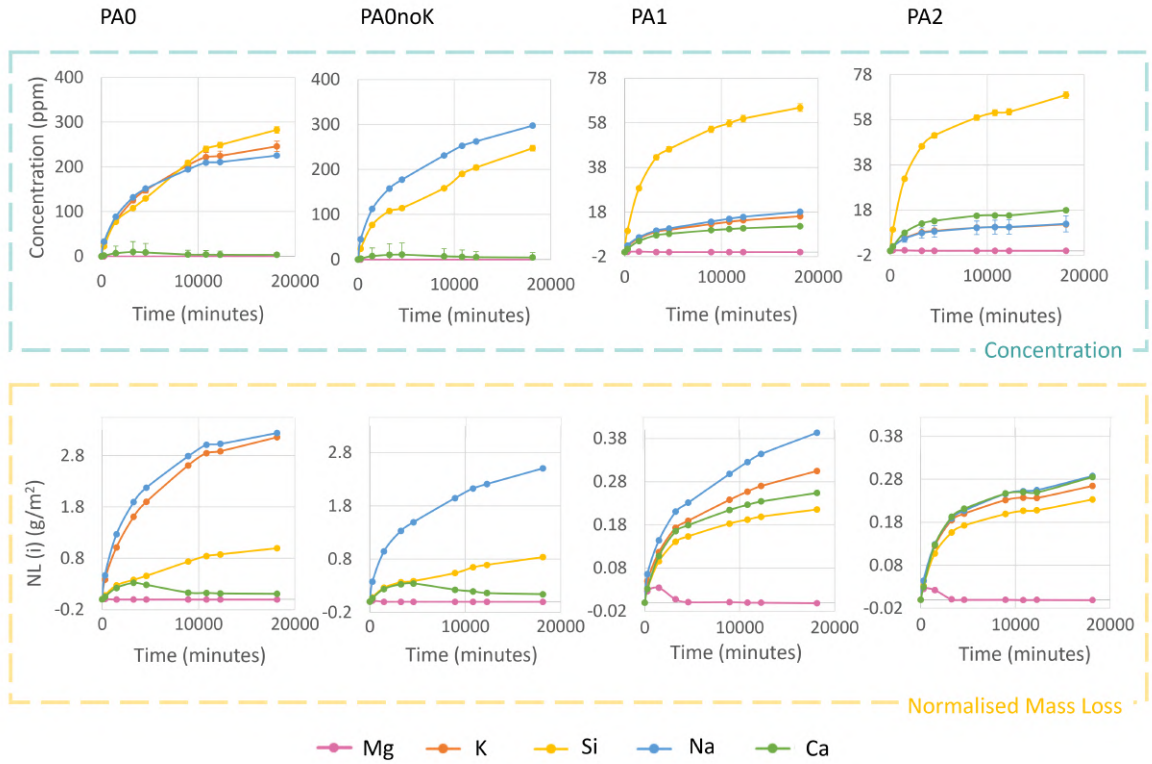

Figure 4.18: Results of ICP-AES analyses on the water samples of the dissolution experiment. At the top: plots of the concentration (ppm) in water of Mg, Si, Na, K and Ca versus time (minutes). At the bottom: plots of the normalised mass loss (NL, g/m^2) versus time (minutes). Notice that the concentration and NL scales for PA0 and PA0noK are different from those of PA1 and PA2 glasses. For concentration plots: (I) the LODs for the different elements are not shown, being them all close to zero and hence hard to visualise at these scales; (II) the absolute errors are shown as vertical lines for most of the elements, those of Ca for PA1 and PA2 and that of K for PA2 are not displayed as inexplicably wide, and others are not visible because too narrow.

With the aim of giving a more tangible meaning of ICP-AES results, the overall equivalent thicknesses $ET(Na)$ and $ET(Si)$ were calculated for each glass, starting from the normalised mass losses obtained for the last sampling. Such values can be taken as good approximations of the depth reached by the leaching process and of the dissolution of the glass network, respectively. Yet, when considering these simplifications, it is necessary to bear in mind that not all of the sodium involved in the alteration process is brought into solution, but may instead be displaced within the glass. Therefore, the extent of the leaching process is possibly

underestimated when considering the $ET(Na)$ values. Moreover, based on the porosity of the gel, part of the dissolved silica may come from greater depths in the altered layer and the equivalent thickness $ET(Si)$ might be greater than the actual depth of surface silica dissolution. For simplicity, it is assumed that most of the detected silicon was originally constituting the outermost layer of glass. The obtained results, reported in Table 4.4, make once again the difference between stable and unstable compositions quite evident, as a leached layer of 1 μm formed in the latter, while for the former the ion exchange process resulted to be limited to less than 0.2 μm. In both cases, the network dissolution involved only a thinner external layer, suggesting that what remained after the ageing process is a corroded glass which has lost a little of the outermost material and whose external altered layer is depleted in alkalis. By comparing the ET values obtained for PA0 and PA0noK, it is possible to notice that they were subjected to a similar dissolution process.

Table 4.4: Equivalent thickness (ET) calculated for silicon and sodium in PA0, PA0noK, PA1 and PA2 at the end of the 14-days ageing test under immersion conditions at 80°C. On the last column, the difference (Δ) $ET(Na)$ - $ET(Si)$ is reported.

Glass	ET (μm)		
	Si	Na	Δ
PA0	0.40	1.30	0.90
PA0noK	0.33	1.00	0.67
PA1	0.09	0.16	0.07
PA2	0.09	0.11	0.02

It is worth pointing out that the ICP-AES results reported in this work present some weaknesses, in that quite high RSE values were associated to some of the concentration measures for unknown reasons (see Fig. 4.18 caption), and the intensities registered for alkalis in the case of PA0 and PA0noK were too high compared to the calibration range. The experiment must therefore be repeated in future studies. Nonetheless, the results are reported here as they are quite consistent with the information gained with the other analytical techniques. In particular, the altered layer thickness estimated based on ToF-SIMS results was of the same magnitude order of the $ET(Na)$ obtained through ICP-AES. Considering the difference $ET(Na)$ - $ET(Si)$ (Δ in Table 4.4) would probably be more appropriate for such comparison, to estimate the portion of altered glass that remained on the sample (without the dissolved material), as it is done in ToF-SIMS. The latter technique indicated slightly higher values: this is reasonable, as ToF-SIMS profiles describe the in-depth change of alkalis amount, whereas ICP-AES data concern only the portion of elements that were completely removed from the glass. The latter measure therefore lacks part of the information related to the alkalis involved in the alteration that are displaced rather than leached out of the silica

network.

The leaching process was likely the cause of the dramatic rise in pH registered for all the glass compositions [7, 26, 31, 37, 43, 45, 47]. By looking at the plot reported in Fig. 4.19, it is possible to notice that after only 4 hours (first point in the curves) the pH was considerably higher compared to the initial conditions of neutrality and stabilisation was reached briefly after. The pH ranged between 11 and 12 for PA0noK and PA0 glasses, and between 9.5 and 10 for PA1 and PA2, in accordance with the different extent of the leaching process in unstable and stable compositions. These results are congruent with the calculated $ET(Si)$, as the more the environment of ageing is basic, the more the network dissolution is fostered [7, 26, 45].

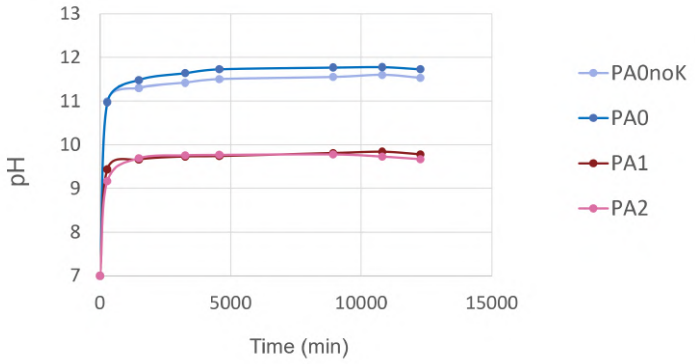

Figure 4.19: Scatter plot of the water pH measured for PA0, PA0noK, PA1 and PA2 during the ageing test under immersion conditions at 80°C.

4.3 Zinc salts treatment

Once applied to the samples and subsequently to a proper drying, the zinc-based protective deposit gave rise to the formation of crystals on the glass surface, regardless of its initial state - whether pre-aged or pristine. Based on what reported by Alloteau et al. in their study on the same protection treatment, such salts are likely zinc hydroxide nitrates [18]. Most of these were observed to be characterised by a needle-like morphology and to group either into irregular clusters or as star-shaped units. Besides this, a quite diverse range of morphologies was found, such as elongated, cubic or snowflake-like shapes. Some examples of these as well as of peculiar arrangements and different dimensions of salts detected on the samples surface are shown in Fig. 4.20. Quite structured distributions have formed, maybe due to the presence of defects on the surface which caused the crystallisation to occur in preferential sites. The

rounded structures of Fig. 4.20a and f likely stem from the formation of drops of the zinc salts protective onto the surface of glass. They may, hence, testify to an uneven spreading of the sprayed product. Furthermore, it is worth highlighting that on the same surfaces, both crystals with dimensions of the order of 10 μm are copresent with others appearing as tiny dots spread all around.

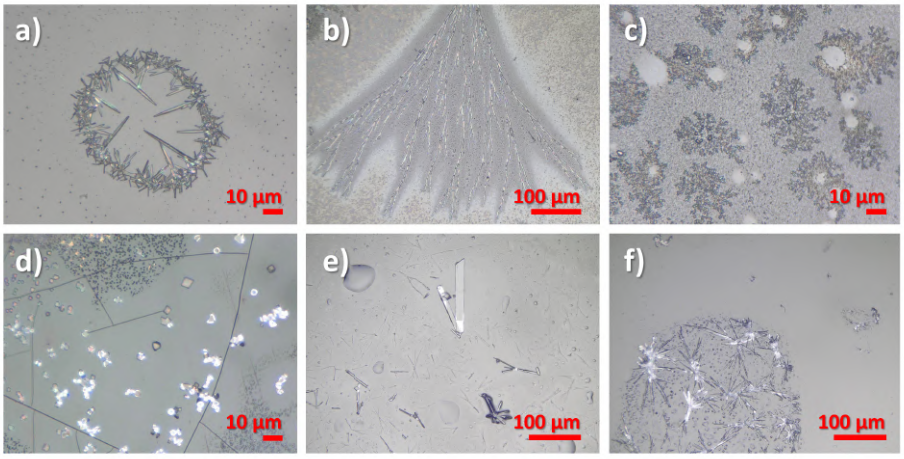

Figure 4.20: OM images of zinc salts deposited on glass plate samples observed to have peculiar morphologies or arrangements. They were detected in **(a)** B glass pre-aged and treated with rinsing and zinc, **(b,c)** PA0 glass pre-aged and treated with zinc, **(d)** PA0noK glass pre-aged and treated with rinsing and zinc, **(e)** B glass pre-aged and treated with zinc and **(f)** PA0noK glass treated with zinc.

Although the mentioned salt structures could not be perceived with the naked eye, a sort of opaque halo was observed on the surface of the treated samples. In Fig. 4.21 some examples are reported: by comparing how the plate samples looked before and after the treatment, it is possible to notice some differences, mainly for the glasses B and PA0noK. The effect on PA0 glass was probably the same, but hidden by the opacity effect of the unpolished back side. Overall, the material transparency was spoiled, albeit not drastically, and the uneven distributions of the protective on the samples surfaces could result evident.

As reported in paragraph 3.2.4, the salts formed on the samples surface after the zinc-based protection treatment resulted to be highly hygroscopic. For this reason, it was not possible to attain a perfectly dry material prior to the ageing test. Nevertheless, a quite good result was achieved by letting the samples dry for about 24 hours. In Fig. 4.22a and b the same salts cluster is shown before and after this period of time: while at first the crystals were largely covered by water and/or ethanol, they subsequently appeared almost completely dry and slightly bigger. Beyond the peculiar arrangements described above, a quite homogeneous

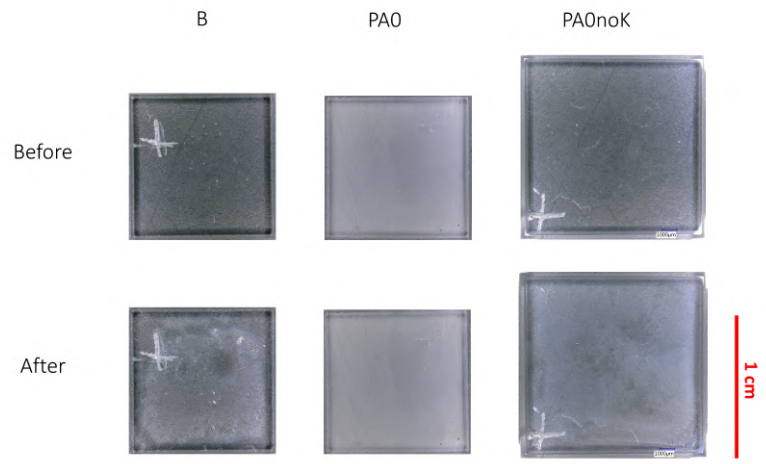

Figure 4.21: OM low-magnification images of sample plates of glasses B, PA0 and PA0noK before (top row) and after (bottom row) the application of the zinc-based protection treatment.

distribution of salts was observed in extended regions of the samples surfaces. One example is shown in Fig. 4.22c and d, which display images taken on PA0noK treated glass before and after the ageing test. By comparing these two, it is possible to notice that the number of salts has exponentially increased, whereas the drops observed before the ageing disappeared. The latter were probably sites of zinc salts nucleation, which occurred at the high temperature set in the climatic chamber together with crystal growth. Throughout ageing, both salts distribution and structure gained complexity and, in some cases, the formation of smaller crystals was observed to take place on pre-existing zinc salts (Fig. 4.22e and f).

The visual examination of aged samples was sufficient for noticing the protection treatments effects: in Fig. 4.23 low-magnification OM images of the samples after the different steps of the experiment are shown for comparison. For the stable glass composition B, the only visible output was the previously discussed opaque veil given by the zinc treatment, as no further evident changes took place with the ageing process. Different was the case of the other two glass types, for which the flaking phenomenon was key for highlighting the protection efficacy. As it was already observed by Alloteau et al. [18, 70], the zinc treatment resulted to have good results when applied on pristine glass (not pre-aged): only very few flakes formed, contrarily to the untreated glass, which gave rise to thick lamellae after ageing. Yet, the samples protected with zinc did go through a significant alteration, as extensive cracking was observed on the surface (details in Fig. 4.24a and b). In the case of PA0noK glass, zinc salts became somehow more evident after ageing (Fig. 4.23), probably because of the gain in density and complexity described above.

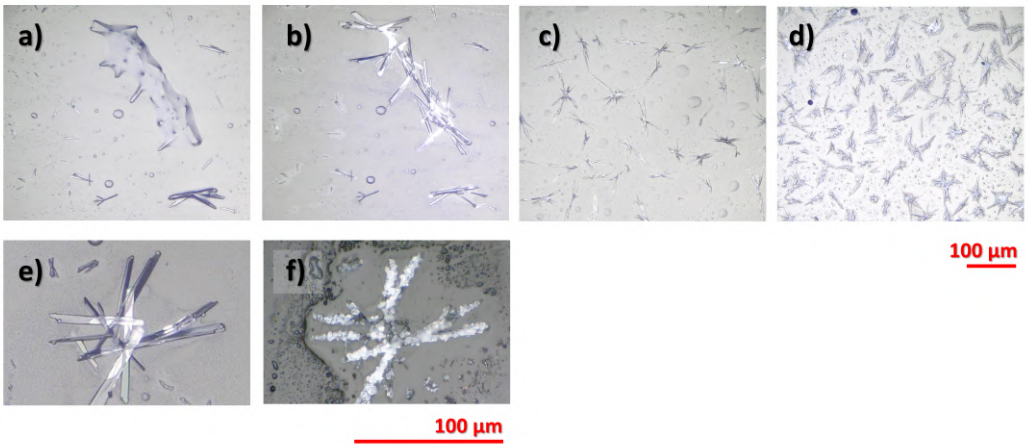

Figure 4.22: OM images of zinc salts deposited on glass plate samples. In **(a)** and **(b)** they are shown, respectively, right after the deposition and after one day of drying, whereas in **(c)** and **(d)** they are shown after the deposition and after the 7-days ageing, respectively. A detail of one cluster of acicular zinc salts is shown **(e)** before and **(f)** after ageing. The dimension scale at the top is for **(a,b,c,d)**, that at the bottom for **(e,f)**.

In contrast to what observed for the pristine samples, the zinc protection alone was not sufficient for preventing the pre-aged samples from flaking. By adding the rinsing step, tremendously better results were attained, as flakes did not form in either of the glasses. Yet, the surface was not preserved in its entirety, as both fine craquelures were detected in the central area of the surface (those of PA0noK are shown in Fig. 4.24c), and some short but noteworthy cracks were observed along the edges of the plate samples. The latter phenomenon is likely evidence of the border effect, which caused the protection to not completely cover the margins of plates. Whilst the combination of rinsing and zinc treatment gave quite satisfactory results for both the unstable compositions, the rinsing step alone was efficient only for PA0noK. PA0 instead presented rather big flakes.

Both the inefficacy on pre-aged samples of the zinc salt treatment and the beneficial impact of the rinsing step are in accordance with Alloteau et al. [13, 18]. The authors also mentioned a variation in the protective performance based on the composition of the glass onto which it was applied [13]: this was supported by the present results as the conditions of the treated PA0noK glass were generally better than those of PA0 after ageing. Besides, the rinsing step turned out to better help the durability of PA0noK rather than that of PA0 glass. Not only was the rinsed and zinc-treated sample of PA0noK better preserved after ageing than PA0, but also no flakes formed for the former composition in the case of rinsing only, whereas for the latter there was no difference among the results seen for the rinsed and not-rinsed samples. Alkalis were probably better removed from the hydrated layer of PA0noK than in PA0, maybe

due to differences in their network structure and to the fact that potassium (present in PA0 and not in PA0noK) is more hardly solvated and is therefore likely difficult to be rinsed away.

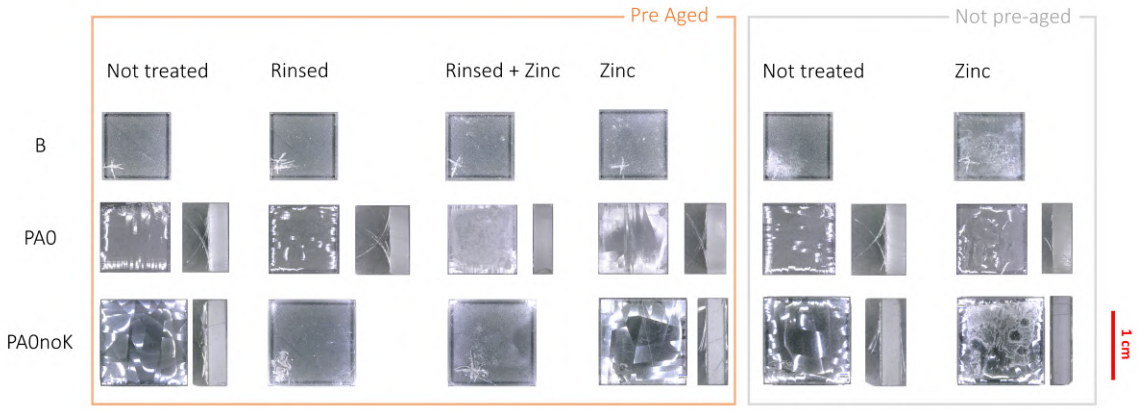

Figure 4.23: Low magnification OM images of B, PA0 and PA0noK samples after the 7-days atmospheric ageing at 80°C and 80 RH%. At the left, the ones that were aged for 18 hours prior to the treatments are grouped with an orange square. The surface of interest is shown for all the plate samples, and the side photograph is reported for some of them. In the latter case, the surface of interest is the one at the left.

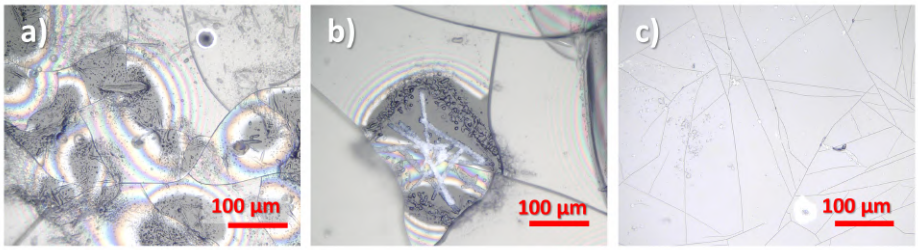

Figure 4.24: OM images taken on 7-days aged treated samples presenting cracks on their surface: **(a)** PA0noK zinc-salts treated and aged (not pre-aged), **(b)** PA0 zinc-salts treated and aged (not pre-aged) and **(c)** PA0noK pre-aged, rinsed, zinc-salts treated and aged.

Infrared spectra registered in transmission mode resulted to be consistent with what observed through visual examination. As can be seen in Fig. 4.25, the hydration level was determined to be noteworthy for PA0noK, substantial for PA0 and negligible for B glass. For the first, it is interesting to notice that after the 7-days ageing the treated glass did not far exceed in hydration the pre-aged one. Moreover, the combination of rinsing and zinc-based treatment was confirmed to be more effective in glass protection compared to rinsing alone. Quite astonishing is the result obtained for PA0 glass: if on one hand no difference could be detected between the spectrum of the pristine glass and that of the pre-aged one, on the other a tremendous variation was seen for the samples aged 7 days after pre-ageing, rinsing and zinc

treatment (violet line). Not only have signals grown in intensity, but they have also merged into a unique broad band, suggesting the presence of a large variety of OH-bearing structures in the bulk material, molecular water included. This is probably due to the conditions of the sample surface: it is possible to state rather confidently that even if not heavily, cracking had occurred and was the reason for the opaque appearance noticed with OM (see Fig. 4.23). As such inhomogeneities on the surface likely affect the optical path of the IR beam, such result would better not be taken into account for comparisons on the hydration levels. For the same reason, infrared spectra were not collected for samples for which the presence of cracks or flakes was evident.

Further insights on the samples hydration were introduced by ATR-FTIR spectra. Their interpretation resulted to be rather challenging, especially for PA0noK and PA0 glass, given the scarce reproducibility of the same intrumental contact. The latter may stem from the inhomogeneity of the samples surface after zinc treatment and ageing and was testified by the different intensities of the bands in the range $1200 - 700$ cm^{-1}: the poorer the adhesion of the sample to the probe, the lower the intensity of the signals. In the case of PA0noK (Fig. 4.25d), the rinsed and aged sample gave too-low-a signal to be compared to the others, while the rinsed, zinc treated and aged sample interestingly resulted slightly less hydrated than the pre-aged one. By looking at the low-wavenumbers range, it is possible to assess that a structural change has occurred for all the three: the pre-aged, the rinsed and the treated (R+Z) samples.

No changes in the OH or Si-O-related bands were detected for PA0: such result is unexpected, particularly in the case of the sample aged for 7 days. Given the issue indicated for the related transmission spectra for PA0, poor reliability can be attributed to this result. The surfaces of unstable glasses are so complex and fragile after the 7-days ageing that it is not convenient to take into account the obtained ATR-FTIR results for an evaluation of the hydration level, the information derived from OM observations being more reliable.

Contrarily, spectra acquired for B glass provided new insights on the efficacy of the different treatments, which could not be noticed through microscopy investigations. The differences detected for the band at 3500 cm^{-1} were in accordance with expectations: the untreated samples aged for 7 days (red full and dashed lines) and that only rinsed prior to the ageing test resulted to be the most hydrated, whereas the protective effect of zinc salts let the other samples have an IR response comparable to that of the pre-aged samples.

Finally, ATR-FTIR analyses allowed for the detection of zinc salts crystallised on the samples surface, in the case when the treatment was applied. One or more peaks were registered in the region between 1425 and 1330 cm^{-1} and are ascribable to zinc nitrates and carbonates

[131–133].

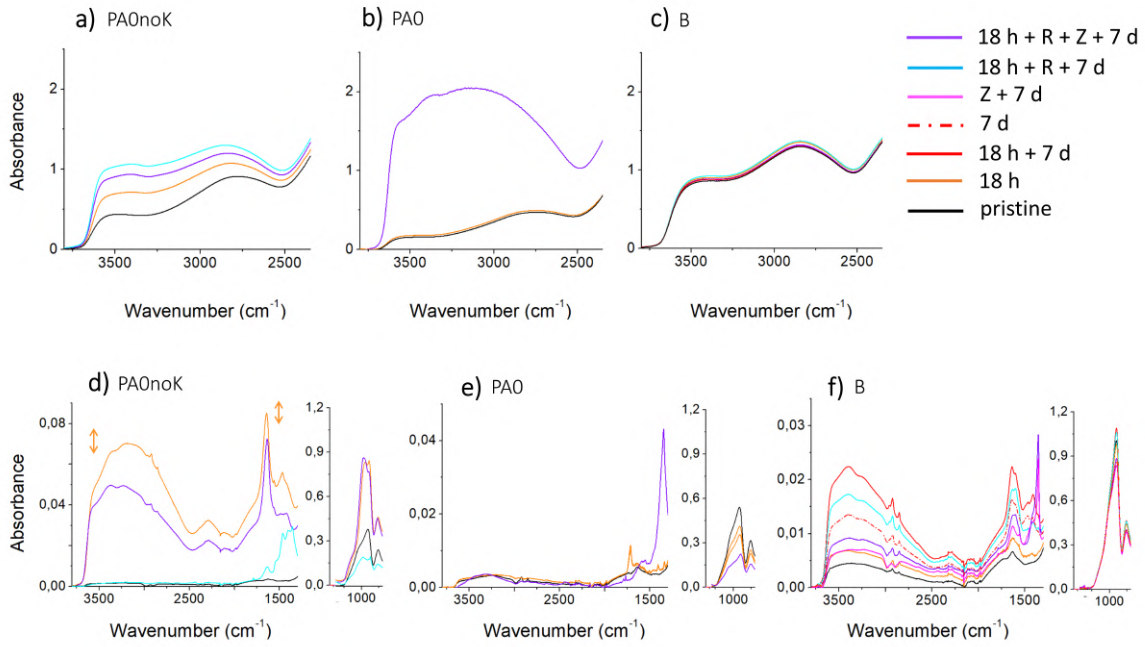

Figure 4.25: IR spectra acquired in transmission and ATR modes on **(a,d)** PA0noK, **(b,e)** PA0 and **(c,f)** B samples before and after pre-ageing or 7-days ageing subsequently to the protection treatments. In the legend *18 h* stands for the pre-ageing, *R* for rinsed, *Z* for zinc salt treated and *7 d* for the 7-days ageing test. Note that the absorbance scales are different to one another for high-wavenumbers ATR-FTIR spectra.

4.4 Synthesis of silica NPs

During the syntheses SN50, SN100 and SN200, the formation of a suspension was evident to the naked eye as the initially transparent and uncoloured solution became progressively opaque and whitish. In Fig. 4.26, photographs taken at different times on SN200 show that for such synthesis, about 10 minutes after the start of the process were sufficient for noticing a change in the appearance. As expected, the bigger the diameter, the duller the suspension. Not only were SN200 NPs big enough to render the synthesis batch markedly white, but also they presented peculiar interactions with the visible light during the washing process: the deposition disks formed at the tubes bottom through centrifugation appeared iridescent. On the other hand NPs formation could barely be noticed with the unaided eye for SN25, SN25a and SN25b. SN100a also resulted in a rather transparent suspension, suggesting quite small particles had formed. Nonetheless, the scattering effect arising when shining a laser beam through the synthesis batch attested the formation of NPs. The washing process resulted

quite arduous for SN25a: if not mixed constantly and thoroughly, the suspension gave quickly rise to hard and transparent agglomerates.

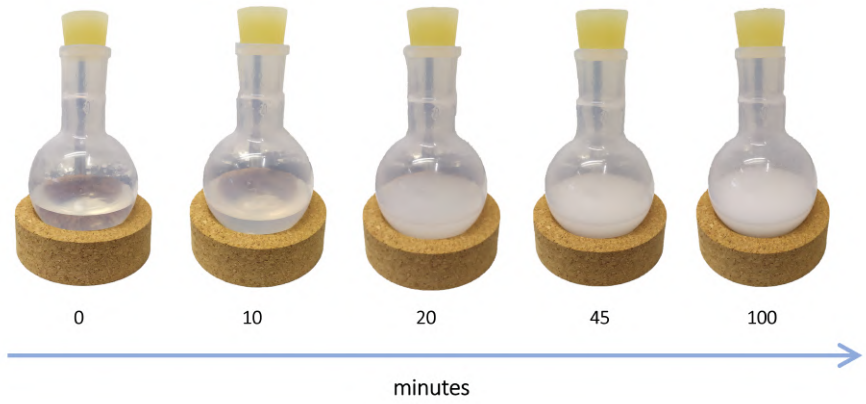

Figure 4.26: Evolution throughout time of the synthesis batch. Photographs of the flask were taken at some minutes distance during the synthesis of 200 nm silica NPs to show the visible changes in transparency towards opacity.

TEM images revealed that the syntheses SN50, SN100 and SN200 resulted in quite spherical NPs having consistent sizes. Among these, some that well represent the average outputs are shown in Fig. 4.27. By comparing the images acquired for the particles washed with the Amicon filters and those cleaned through simple centrifugation, it seems that the latter protocol produced inhomogeneously spread dispersions in the case of SN50.

As expected based on the fairly transparent batch appearance, SN100a synthesis resulted in NPs with smaller diameters compared to SN100 (Fig. 4.27). The obtained suspension was rather unevenly spread and contained particles with different sizes: whilst the majority of the NPs had diameters ranging between 20 and 40 nm, some were measured to be around 100 nm wide. Their shape was also slightly diverse, but not too far from sphericity. Such results likely stemmed from the lower concentration of both catalyst and reactants in the solvent: as a consequence, the kinetics was slowed down so that in the 24 hours of reaction the majority of NPs did not grow as much as in SN100.

More irregular shapes were observed for the NPs of SN25 syntheses (Fig. 4.28). These were very rarely spherical and more often rough and elongated, so that measuring their dimensions was more challenging. Whilst analogous results were obtained in with SN25 and SN25b, in the case of SN25a a very different structure was observed: particles of sizes in the order of 10 nm were entangled together in a complex network which, at higher dimensions scale, appeared as irregular stains. The obtained material can be considered as a gel, whose structure is indeed

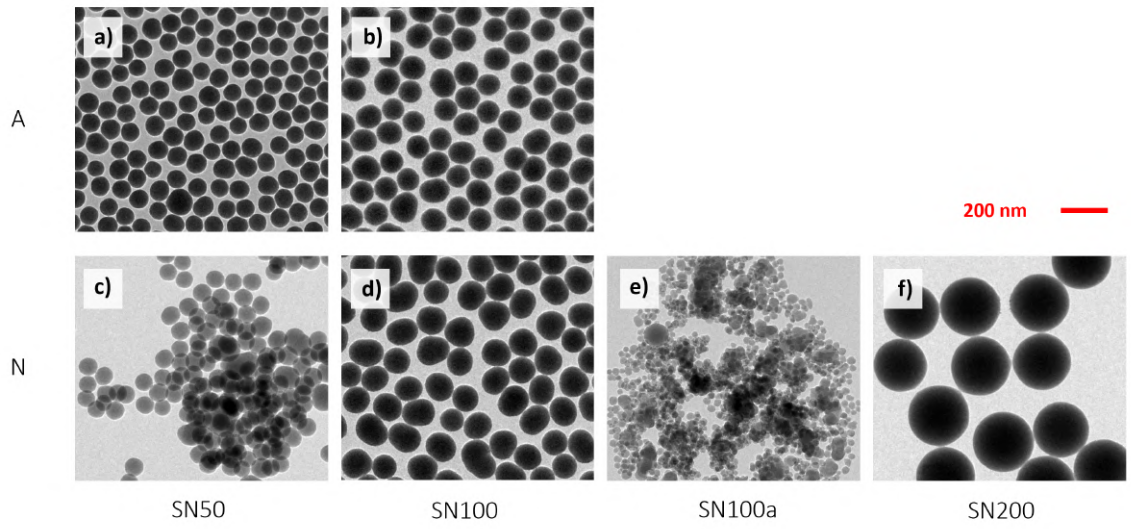

Figure 4.27: TEM images of silica nanoparticles obtained with the syntheses SN50, SN100, SN100a and SN200. NPs washed using the Amicon filters (A) are shown on the top row **(a,b)**, whereas those cleaned by normal centrifugation (N) are displayed on the bottom row **(c - f)**. The common scale is specified in red.

very close to the one shown by Buckley and Greenblatt in [134]. It is presumable that at a certain stage of the synthesis process, the formation of NP chains was favoured rather than the particles growth. A similar aggregation tendency was observed for the syntheses SN25 and SN25b, as can be noticed by looking at the images reported on the top row of Fig. 4.28: NPs were sometimes found to be arranged in chain-like structures which laid out either linearly or in rings.

TEM images were taken also on a sample of washing waste solution. In order to question the permeability of the Amicon filters, the sample was taken from the liquid collected at the bottom of the centrifuge tube during the washing of SN50. Aggregates of silica NPs were found, some examples of which are reported in Fig. 4.29. Particles were either small (about 20 nm diameter) and irregular, or bigger (ca. 70 nm d) and rather spherical. This testifies for a loss of material, even if quite limited and probably substantially lower compared to that of the other washing method.

Starting from TEM images, a dimensional study was performed for the syntheses whose output consisted of recognisable nanoparticles: SN25a and SN100a were therefore excluded. As can be seen in Fig. 4.30, in all the cases a quite symmetrical size distribution was obtained. This is attested also by the closeness or even coincidence of mean and median values, reported in Table 4.5. For SN25 and SN25b syntheses, the resulting size distributions were quite narrow

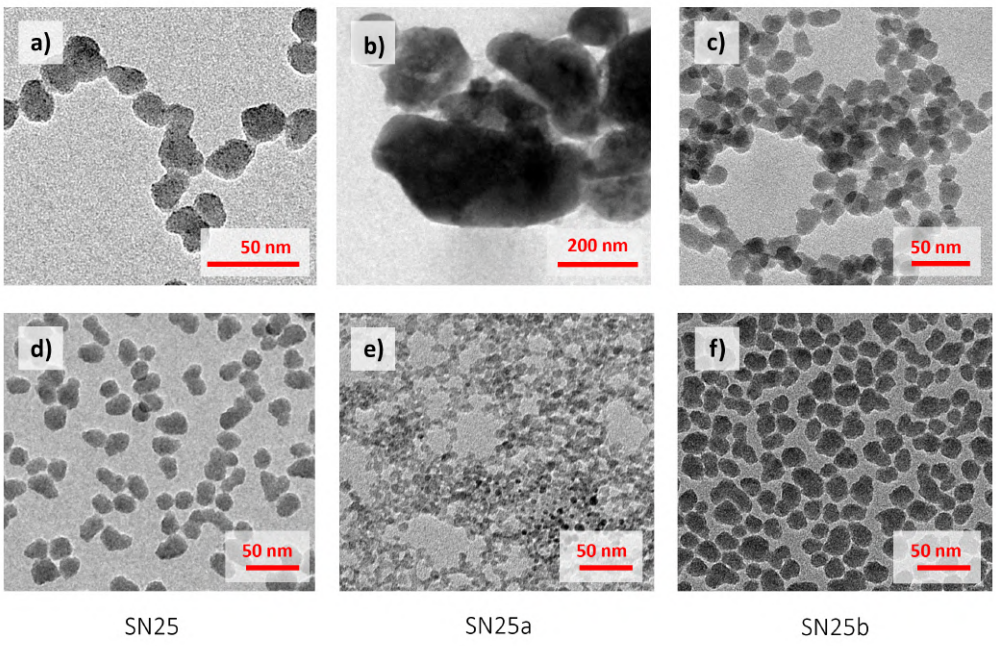

Figure 4.28: TEM images of the outputs of the syntheses SN25, SN25a and SN25b. Peculiar features are shown on the top row **(a - c)**, whereas representative pictures of the three are displayed on the bottom row **(d - f)**.

and the mean diameter did not deviate much from the expected value: 18-21 nm versus the theoretical 25 nm. Different was the outcome for the SN50 syntheses, for which average diameters of 76, 103 and 78 nm were measured. Interestingly, the two SN50 syntheses washed with the Amicon filters resulted in very different distributions, both having a bigger standard deviation compared to that washed with the normal centrifugation. This might indicate a scarce reproducibility of the protocol and should be further investigated through repeated experiments. The opposite scenario arose for SN100 syntheses: fairly narrow distributions with means of 105 and 106 nm were obtained with the Amicon filters washing, whereas the other method resulted in NPs with an average diameter of 115 nm and a slightly higher standard deviation for the size distribution. Finally, NPs spanning from about 210 to 300 nm were obtained with SN200 syntheses. With mean values ranging between 254 and 256 nm, the measured diameters resulted to be quite spread. Yet, in this case the three synthesis repetitions gave very similar outputs, suggesting the repeatability of the protocol.

Information about the suspensions homogeneity and stability was obtained thanks to DLS analyses, which were performed on all the syntheses outputs (see Fig. 4.31 and Table 4.5). The difference of SN25a from SN25 and SN25b appeared evident, as one single peak centered

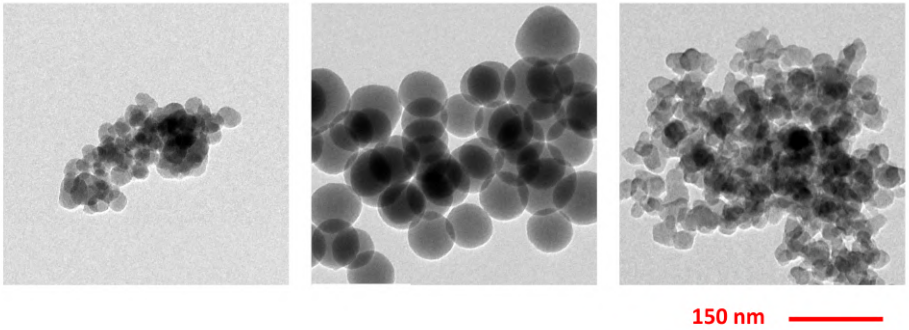

Figure 4.29: TEM images of NP clusters found in the sample of liquid waste taken during the washing with Amicon filters of a SN50 synthesis.

at 198 nm was registered for the former, while the other two presented a main signal around 30 nm and an additional one bigger of two orders of magnitude. Considering what was observed through TEM, the result obtained for SN25a is surprising: it seems that aggregates with a rather constant dimension were present in suspension. This may indicate that the gel had not completely formed and was composed of discrete units that well divided under stirring. The results obtained for SN25 and SN25b suggest that both well dispersed particles and aggregates of different dimensions were present in the suspension, attesting for the high tendency to cluster of the NPs. The outputs obtained for SN50 and SN100 syntheses resulted to be very similar to one another: single features centered at about 140 nm were registered for NPs washed with the Amicon filters, whereas multiple peaks characterised the products that were cleaned with normal centrifuge tubes. These outputs are likely deriving from the high RCF selected for concentrating the particles at the bottom of the centrifuge tubes. If on the one hand this allowed for the solvent removal and minimised the related loss of product, on the other it entailed a repetitive packing of NPs and therefore favoured aggregation. Moreover, the fact that particles were first dried and then suspended again in water may have played a role. It is reasonable that more evenly spread NPs were obtained by using Amicon filters, as a lower speed of centrifugation was employed and the suspension state was preserved throughout the washing protocol. The DLS result obtained for SN100a was in agreement with what observed through TEM: mainly ca. 490 nm wide aggregates formed. Finally, SN200 synthesis was confirmed to be quite repeatable, as a peak centered at about 300 nm was registered in all the three reiterations.

By comparing TEM and DLS data reported in Table 4.5, it is evident that higher dimensions were indicated by the latter technique. In that case, the measure is related to the hydrodynamic diameter, which is generally bigger than the particle actual dimension [68, 135].

While the main DLS signals are rather consistent with the mean diameters measured on TEM images, the additional features at bigger sizes gave further information on NPs aggregation, occurred for the 25 nm particles and for SN50 and SN100 NPs washed with the normal centrifuge tubes. The experimental yield resulted quite high for all the syntheses but SN100a, for which the low concentrations of catalyst and reagents determined the impossibility of accomplishing the synthesis process in 24 hours. In most of the other cases, values higher than 100 were obtained: this may either derive from the approximation of the NPs mass to the theoretical grams of $Si\,O_2$ produced in the reactions of TEOS with water, or point to the incomplete drying of the synthesised NPs prior to their weighing. Under the first hypothesis, it is reasonable that the highest yield value was registered for the synthesis SN25b: the different structure of the gel likely caused the high mass measured for the product. Similarly, it is presumable that in the other syntheses the final output was not only made of pure silica, due to a partial hydration or an incomplete reaction. For these reasons, it is hardly possible to gain further information from such data and more experiments are needed to determine whether the Amicon filters (A) or the normal centrifuge (N) protocols is more convenient for washing the NPs.

Table 4.5: Summary of TEM and DLS results. Mean, median and standard deviation (SD) of 300 diameter measurements per sample are reported for the dimensional analysis conducted based on TEM results. The standard deviation was calculated as $SD = \sqrt{\frac{\sum_{i=1}^{n}(x_i-\bar{x})^2}{N}}$. For DLS, the dimensions corresponding to the curves maxima are reported in ascending order as dimension (d) 1 and 2. The calculated experimental yields are also reported as percentages in the last row.

Synthesis		**SN25**		**SN25a**	**SN25b**	**SN50**			**SN100**			**SN100b**	**SN200**		
Washing		**A**		**A**	**A**	**A**		**N**	**A**		**N**	**N**	**N**		
TEM	**Mean**	20	21	-	18	76	103	78	106	105	115	-	256	255	254
	Median	20	21	-	18	76	102	78	105	105	113	-	255	256	254
	SD	3	4	-	3	6	13	5	7	6	9	-	12	11	13
DLS	**d1**	28	32	198	32	136	146	108	146	146	170	108	311	267	267
	d2	146	361	-	361	-	-	489	-	-	1209	489	-	-	-
Yield	%	89	143	190	171	96	93	99	97	98	95	4	105	110	109

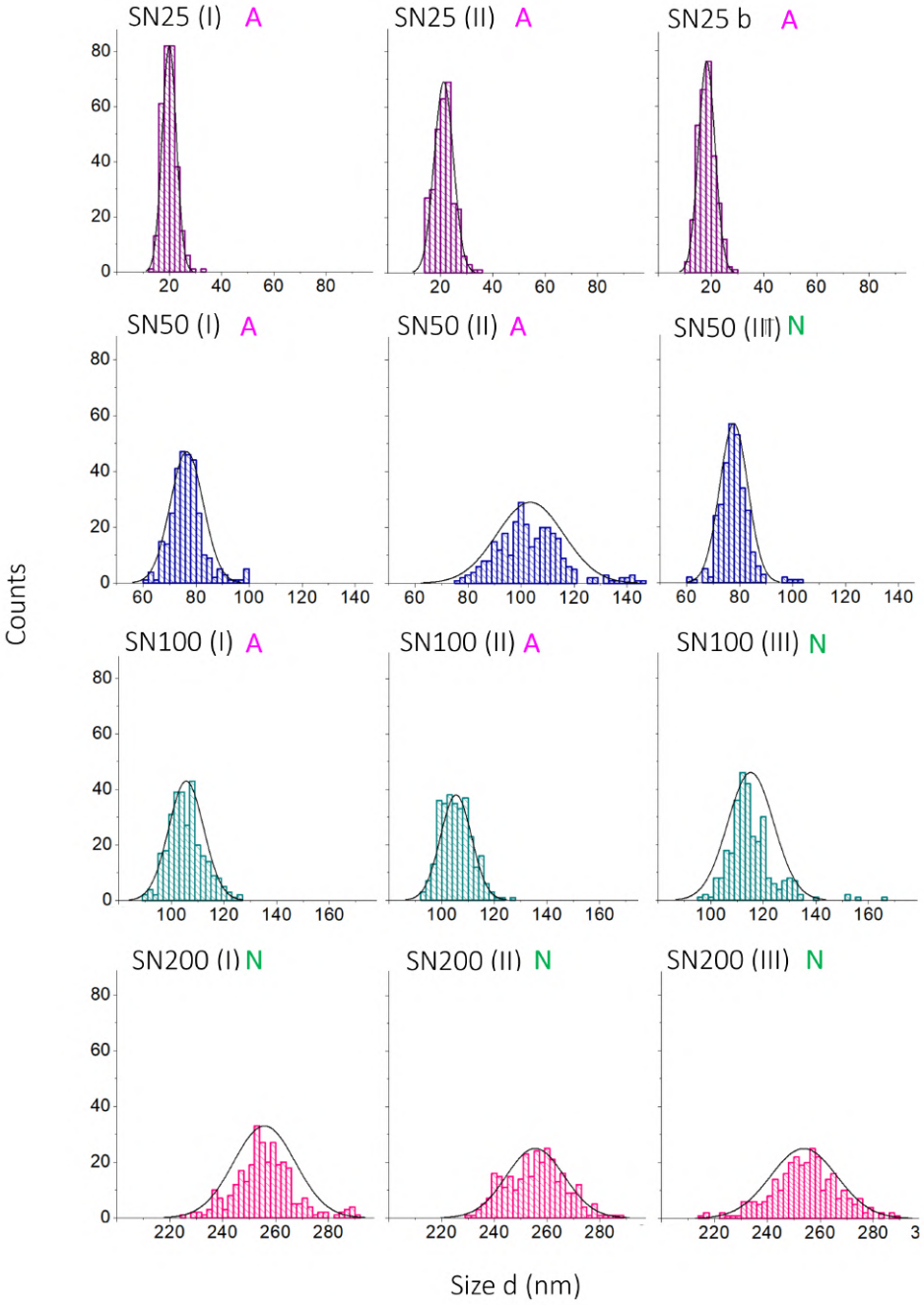

Figure 4.30: Histograms and normal curves built starting from 300 diameter values per synthesis, measured on TEM images. The name of the synthesis is specified at the top left of each histogram, together with a roman number in brackets to distinguish the duplicates and/or triplicates, and the washing method used (A = Amicon filters, N = normal centrifuges). The same scale for both size and counts was chosen for all the graphs to favour comparisons.

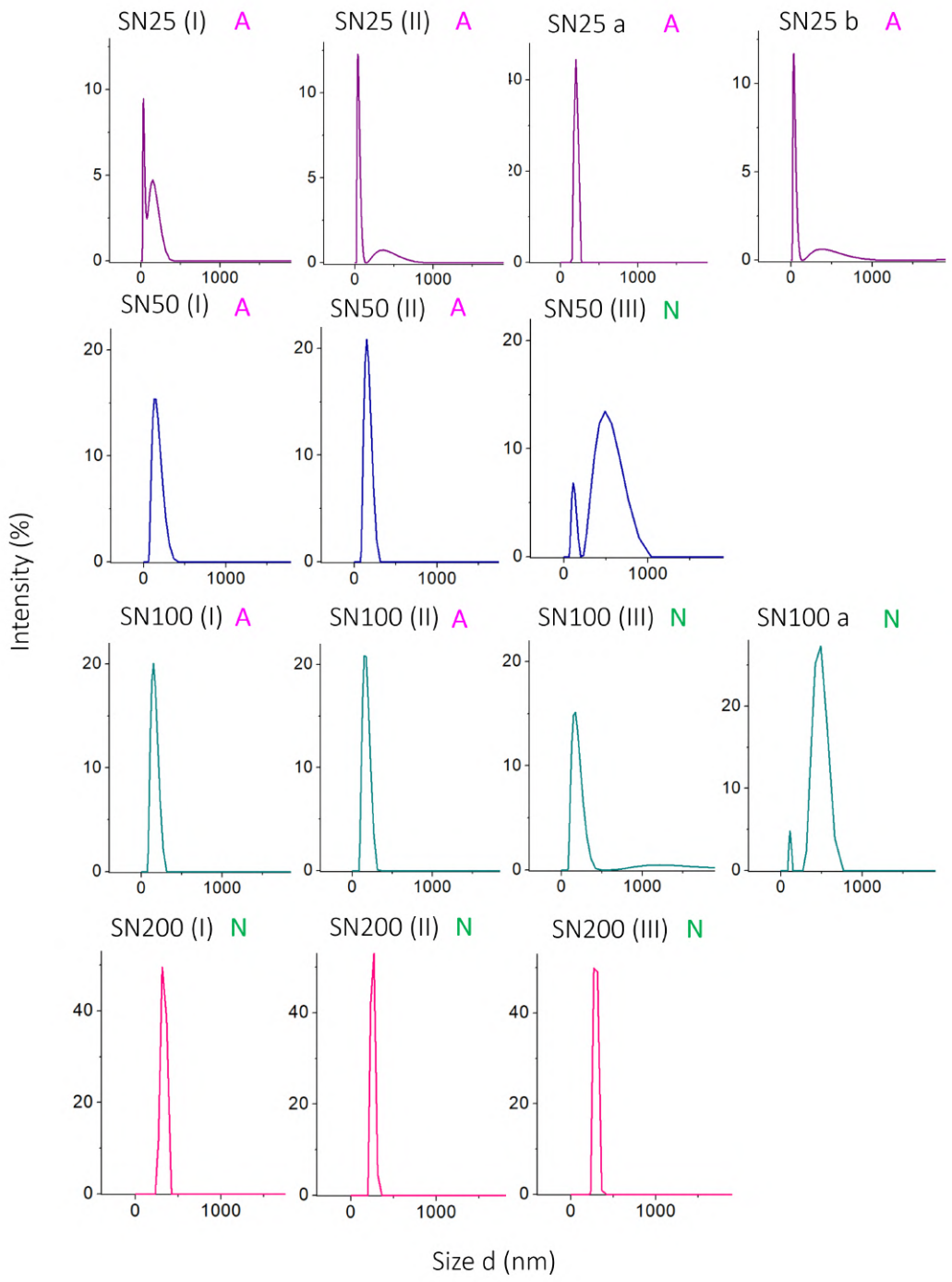

Figure 4.31: DLS results obtained for all the syntheses of silica NPs. The name of the synthesis is specified at the top left of each histogram, together with a roman number in brackets to distinguish the duplicates and/or triplicates, and the washing method used (A = Amicon filters, N = normal centrifuges).

5. Discussions

The experiments conducted in this multifaceted study included the investigation of different aspects of glass durability and conservation. By merging the information gained through the analytical techniques employed, some hypotheses on the alteration mechanisms could be inferred and proposals for protectives development may be brought forward.

5.1 Glass alteration

The ageing tests clearly showed that the composition played a fundamental role in glass alteration. PA0noK, PA0 and PK were determined to be very sensitive compared to PA1, PA2 and B glass, so that the former three can be defined as *unstable* and the others as *stable* compositions. A severe alteration process took place for the unstable glass under atmospheric conditions and determined the formation of a hydrated layer having a different silica structure with respect to the pristine glass. This became progressively thicker as the ageing process was extended and, once a certain level of hydration was reached, it peeled off in the form of flakes. The trend described by the gain in flakes thickness with the increase of ageing duration (see Fig. 4.3) suggested a linear kinetics of hydration, meaning that the rate associated to this process was constant over time. Such an observation leads to exclude the possibility that hydration is controlled by ion exchange. The latter, being a diffusion-limited reaction with a square root dependency on time, could not match with the experimental evidence. Conversely, hydrolysis was possibly the rate-controlling reaction as it is a surface-limited reaction linearly dependent on time [42].

Three days of artificial ageing at 80°C and 80 RH% were enough for flaking to occur, whereas 18 hours under the same environmental conditions resulted insufficient. In the latter case, only PA0noK glass was assessed to have undergone a significant hydration and silica network modification. For such composition, flakes were measured to be thicker compared to those formed in PA0, suggesting the alteration process takes place more quickly in PA0noK. Such evidence could be explained by taking into account how the composition determines the glass structure. The only difference between PA0 and PA0noK consists of the potassium amount with respect to that of sodium: it is likely that a deficiency of the former results in a more open glass structure, whereas the alternation of K and Na ions favours a rather closed and packed arrangement. Under this assumption, water penetrates more easily into the glass network of PA0noK, which is, therefore, promptly exposed to alteration processes.

Hydration, ion exchange and hydrolysis can take place and lead to the formation of silanols, the redistribution of network modifiers and the recondensation of Si-OH groups into a new silica structure. In PA0 glass, the same scenario possibly unfolds, albeit as a secondary phase. First, water penentration into the glass network has to occur: as PA0 structure is probably quite tight and complex, it is reasonable that water mainly interacts with such a glass through relatively slow hydrolysis reactions. Once the structure is opened, the alteration process is likely analogous to the one observed for PA0noK. By all means, the fact that PA0noK glass resulted to be slightly less durable than PA0 suggests that K_2O is not the reason for the instability of mixed alkali glasses. Being loosely bound to NBOs and relatively easily hydrated, Na^+ is probably the main actor in the ion exchange process under atmospheric conditions, and is leached across the network. Yet, this phenomenon was observed to occur rather slowly and to induce movements that only partially let modifier ions reach the material surface. Salts formation took place mainly during storage after the accelerated ageing tests, and the content of alkali and alkaline earth ions in the glass were assessed to remain rather constant.

Ion exchange was observed to be favoured at lower temperatures of atmospheric ageing. At 60°C and 80 RH%, all the studied glass gave rise to salts crystallisation as a result of the interaction of leached network modifiers and the atmospheric agents. Given that the experiments were conducted under controlled atmosphere, no pollutants were involved except CO_2, hence carbonates were detected on the samples surface. These were bigger for unstable compositions, suggesting that the leaching process has occurred more quickly and, therefore, a longer time was available for salts growth. Once again, PA0noK was confirmed as the most sensitive among the studied glasses: the salts that arose on its surface were the biggest to be observed and the ion exchange process was associated to a non-negligible change in the silica structure. Thus, hydration had occurred anyway, albeit at a lower degree compared to the ageing at 80°C. The migration of a larger quantity of network modifiers towards the surface has probably prejudiced the water to deeply penetrate in glass, so that the thickness of the resulting alteration layer was very limited. Whilst for PA0noK the latter could be detected through Raman and rendered the sample surface very fragile to pressure changes, it was not measurable in PA0.

It is evident that temperature constitutes a crucial parameter for the relative kinetics of the mechanisms involved in glass alteration. A change of twenty degrees was sufficient for a reversal of the situation observed at 80°C: ion migration became predominant with respect to glass hydration (the latter process being anyway necessary for the former to occur). On this basis, it is presumable that a very different balance of phenomena arises at room temperature. The present considerations on artificial accelerated ageing entail a distancing from the real

cases. Yet, they are beneficial for a more accurate understanding of how different processes are interwoven in the complex phenomenon of glass atmospheric alteration.

The ageing under immersion conditions was confirmed to determine considerably different outputs compared to those resulting from a humid atmospheric environment. Despite the same processes are implicated in the two situations, they occur following different kinetics due to the distinct amount of water involved. As the latter likely penetrates in the glass structure through NBOs channels, it is possible that, when glass is exposed to the atmospheric environment, the displacement of alkalis is limited by the strong hydrogen bonds in which they are involved. Conversely, the release in water of network modifiers can occur under immersion conditions. A quite fast loss of alkalis was attested for PA0noK and PA0 glass, as the solutions in which they were immersed were subjected to a quick rise in pH. The silica network dissolution, therefore, was favoured and occurred in conjuction with the leaching process. The phenomenon could be described as incongruent, since the layer of material depleted in alkalis was found to be thicker than the portion of silica network dissolved in water. Common to all the ions and valid for all the glass composition was the kinetics of dissolution: in no case was this linear, as a rate drop could be always observed - whether evident or rather small. This suggests the alteration process unfolds quite differently under immersion compared to atmospheric conditions. In particular, when glass is immersed in liquid water, passivation (gel) and affinity effects (saturation in Si of the solution) limit the progression of hydration, which affects only a very thin surface layer (about 60 times smaller than under atmospheric conditions for the 14-days ageing, see Tables 4.1 and 4.4). Whilst the durable glasses presented a substantial drop in silica dissolution rate, suggesting a passivating gel had formed on their surface, the unstable compositions did not seem to have reached a steady state after the 14-days accelerated ageing. Interestingly, PA0 glass was slightly more affected by alteration under immersion conditions than PA0noK. Possibly, the presence of both Na and K ions in the structure of such glass render the leaching process more complex and, therefore, the resulting gel structure quite irregular. Conversely, PA0noK may form a tighter alteration layer: thanks to the facile extraction of sodium ions from its open structure, a rather homogeneous and packed gel could develop. Nonetheless, the speculative nature of these interpretations must be pointed out and more investigations are necessary to understand the origin of the obtained results. Yet, it is possible to safely argue that the composition effects on glass ageing hold also under immersion conditions, albeit determining distinct outputs. The differentiation between durable and unstable glasses determined for the atmospheric ageing was confirmed for the dissolution experiment. Still, the minor differences observed for the comparison between PA0 and PA0noK glass support the fact that alteration under humid

atmosphere and in liquid water are not equal. This was highlighted also by the chemical and structural characteristics of the hydrated layers formed under the two conditions: water was found mainly in the form of molecules in the gel resulting from immersion alteration, and of silanols in the hydrated layer formed when glass was exposed to the atmospheric environment.

Overall, this study confirmed the composition to be a critical parameter in glass alteration. The effect of the ratio R (alkaline earth on alkalis) on durability was verified to be substantial: the difference of ca. 0.5 dividing the values for PA1 and PA0 glasses (see Table 3.1) was sufficient to make the former composition be extremely more stable than the latter. On the other hand, the high durability of PA1 and PA2 hindered the implementation of new insights on the topic. Only TGA analyses allowed to assess that the latter composition (highest R value) was the most stable. Still, the difference between PA2 and PA1 was considerably smaller compared to that holding between PA1 and PA0. This suggests that, rather than a linear dependence of the durability on R, a more complex scenario is at the basis of such relation and, possibly, a threshold of very specific compositions separates stable and unstable glasses. In order to question these hypotheses, further studies involving R values ranging between those of PA0 and PA1 would be necessary.

Given the severe alteration observed for PA0noK glass, it became evident that the cause of glass sensitivity should not be attributed merely to the presence of potassium, but rather to its proportion with respect to the other elements contained in the material. The formation of a robust or open structure likely depends on the relative amounts of ions to be allocated in the silica network: the imbalance given by an excessive quantity of either potassium or sodium may hinder the formation of a tight and resistant structure. Magnesium and calcium seemed to be quite tightly bound to the silica network as their dissolution in water was limited and it was not possible to assess their presence in the alteration salts formed on the samples surface after atmospheric ageing. However, it was hypothesised that some precipitates were quickly formed under immersion conditions, and calcite salts were possibly present as small and hardly detectable crystals on atmospherically aged samples. In addition, it is not to be excluded that such ions may be leached more easily at lower temperatures of ageing.

5.2 Protection methods

The zinc-based protection treatment was assessed to be very uneven in distribution and in the shape and dimension of crystals it deposited on the glass surface. The method of application involving the use of commercial atomiser bottles turned out to be scarcely controllable. Additionally, it easily determined slight but perceivable changes in the surface appearance of

the treated glass. Sprayers customised to the specific requirements of objects protection may be beneficial for a more homogeneous and thinner product spread. A shorter drying time would probably be favoured as well. Nevertheless, the efficacy of the treatment was confirmed for pristine glass. Interestingly, the protection worked better for PA0noK compared to PA0 composition. It can be hypothesised that zinc ions are more easily chemisorbed at the former's surface thanks to its open silica structure. By becoming part of the glass network, zinc may have contributed to the structural modification detected for PA0noK. When applied to the pristine glass, a quite resistant surface material has likely formed, whereas the rinsing step was necessary for the pre-aged glass prior to the treatment in order to remove part of the displaced Na^+ from the hydrated layer and thereby give room for Zn^{2+}. Not only is it necessary to better investigate how the zinc treatment protects glass, but also the role of high temperatures in its functioning must be questioned in future research. If on one hand the treatment at room T may hinder the excessive growth of zinc salts on the surface and hence favour the preservation of transparency, on the other it could discourage zinc chemisorption and therefore mitigate the protective effect. Moreover, the presence of zinc salts on the surface could be problematic for glass durability: as surface defects and hygroscopic species, such crystalline species would likely constitute preferential sites for moisture condensation and therefore favour alteration processes.

More experiments are also needed to optimise the protocol for silica NPs synthesis. The change in ammonia concentration was assessed not to be sufficient for completely controlling the resulting size of the nanoparticles. Whilst for SN25 and SN100 syntheses the obtained diameters were close to the theoretical values, the same could not be said for SN50 and SN200, for which the resulting particles were bigger than expected. In addition, the shape of 25 nm particles was far from spherical and rather seemed to suggest that the NPs formation was not yet fully completed. The change in water and ethanol content either worsened or did not change the situation, so the protocol would better be modified by acting on other parameters. Considering that (1) the concentration of catalyst used for SN25 might have been too low for the synthesis process to accomplish and that (2) spherical NPs of dimensions close to 20 nm have been obtained when the SN100 synthesis was slowed down by augmenting the quantity of solvent (SN100a), a trial for spherical 25 nm particles synthesis may be performed by increasing the content of ammonia and decreasing the time of reaction. Moreover, the latter parameter may be further investigated to determine how it influences the shape and dimension of the particles and the production yield. With the aim of formulating a protection treatment for glass, it is fundamental to define the best synthesis conditions to obtain 25 and 50 nm NPs, as they are probably the most appropriate for obtaining a transparent

material which would respect the aesthetics of the treated objects. While the washing of such small particles would be problematic with mere centrifugations, Amicon filters enabled its accomplishment. However, as their use was assessed to be rather time consuming and laborious, the implementation of alternative methods is preferable. For this reason, a protocol based on the dialysis process will be tested in future studies. As water would slowly replace the synthesis solvent by diffusing through a semipermeable membrane, the suspension would not be subjected to the strong forces imposed by the centrifuge and aggregates formation would probably be minimised.

As an extension of the study of the two protection methods, the possibility of combining them could be investigated in the future. Zinc ions may be introduced in a silica-based coating to associate the strengthening action of the former with the hydrophobic character of the latter. Nonetheless, the development of both the protectives is still far from being accomplished. In particular, they should be optimised in a way to guarantee their efficacy together with the preservation of the glass aesthetics and integrity. In the case these objectives will be equally met by the two methods, the choice between one and the other could be driven by further criteria. In terms of amount of material and health hazard, the zinc-based method might be preferable, as the involved substances are required in very little quantities and are non-toxic. Silica NPs, instead, are claimed to be carcinogenic when dry and their synthesis requires a considerable investment of reagents, solvents and time. Nevertheless, the health hazard could be avoided by keeping the system in the form of suspension, as it was done in the present study when using the Amicon filters for NP washing. Moreover, the more is the silica-based coating optimised, the less will be the material needed for an effective protection. These aspects must be taken into account in the selection of conservation products and in the design of preservation protocols in order to meet as far as possible the requirements of environmental, social and economic sustainability.

6. Concluding remarks

Critical aspects of the alteration mechanisms and protective formulation for glass have been demonstrated in this work. As the composition was confirmed to be deeply involved in the material durability, it is envisaged that the conservation and protection measures may not be fully generalised to any glass. Conversely, these would better be customised based on the characteristics of the glass to be preserved, a thorough knowledge on the latter being a fundamental requirement for the implementation of the conservation protocol. On the other hand, a generalised understanding of the influence of both the composition and the environmental parameters on glass durability may lead to the formulation of useful guidelines for conservators. Storage conditions for ancient glass should be kept stable and monitored so that to avoid high temperatures and RH%, as well as excessive drying of the material. Moreover, glasses having compositions which were assessed experimentally to be unstable, should be object of special care. Further studies are needed to better understand how the reactions involved in the alteration process unfold and are influenced by both the glass characteristics and the environmental parameters. The experiments carried out in the present thesis could be underpinned by additional tests and repeated measurements on all the studied compositions. This would help verifying whether the hereby drawn hypotheses are reasonable and could meaningfully contribute to the widening of knowledge on glass alteration. The present work resulting from the fruitful collaboration of different research groups, well represents the synergetic international effort which runs behind such advancement. This contribution ties in with the large network of studies whose ultimate goal is the preservation of glass and the transmission of this collective Cultural Heritage to the future generations.

Bibliography

1. Melcher, M., Wiesinger, R. & Schreiner, M. Degradation of Glass Artifacts: Application of Modern Surface Analytical Techniques. *Acc. Chem. Res.* **43,** 916–926. ISSN: 0001-4842, 1520-4898 (June 2010).
2. Rodrigues, A., Fearn, S., Palomar, T. & Vilarigues, M. Early Stages of Surface Alteration of Soda-Rich-Silicate Glasses in the Museum Environment. *Corrosion Science* **143,** 362–375. ISSN: 0010938X (Oct. 2018).
3. Richet, P. Une Brève Histoire Du Verre. *Verre* **13** (2007).
4. Davison, S. *Conservation and Restoration of Glass* ISBN: 978-0-7506-4341-2 (Routledge, Abingdon, Oxon, 2011).
5. Zachariasen, W. H. The Atomic Arrangement in Glass. *J. Am. Chem. Soc.* **54,** 3841–3851. ISSN: 0002-7863, 1520-5126 (Oct. 1932).
6. Matson, D. W., Sharma, S. K. & Philpotts, J. A. The Structure of High-Silica Alkali-Silicate Glasses. A Raman Spectroscopic Investigation. *Journal of Non-Crystalline Solids* **58,** 323–352. ISSN: 00223093 (Nov. 1983).
7. Gin, S. *et al.* The Controversial Role of Inter-Diffusion in Glass Alteration. *Chemical Geology* **440,** 115–123. ISSN: 00092541 (Nov. 2016).
8. Zotov, N. & Keppler, H. The Influence of Water on the Structure of Hydrous Sodium Tetrasilicate Glasses. *American Mineralogist* **83,** 823–834. ISSN: 0003-004X (Aug. 1998).
9. Tournie, A., Ricciardi, P. & Colomban, P. Glass Corrosion Mechanisms: A Multiscale Analysis. *Solid State Ionics* **179,** 2142–2154. ISSN: 01672738 (Nov. 2008).
10. Robinet, L., Hall, C., Eremin, K., Fearn, S. & Tate, J. Alteration of Soda Silicate Glasses by Organic Pollutants in Museums: Mechanisms and Kinetics. *Journal of Non-Crystalline Solids* **355,** 1479–1488. ISSN: 00223093 (Aug. 2009).
11. Kunicki-Goldfinger, J. J. Unstable Historic Glass: Symptoms, Causes, Mechanisms and Conservation. *Studies in Conservation* **54,** 47–60. ISSN: 0039-3630, 2047-0584 (June 2009).
12. Rodrigues, A., Fearn, S. & Vilarigues, M. Historic K-rich Silicate Glass Surface Alteration: Behaviour of High-Silica Content Matrices. *Corrosion Science* **145,** 249–261. ISSN: 0010938X (Dec. 2018).
13. Alloteau, F. *et al.* Evidence for Different Behaviors of Atmospheric Glass Alteration as a Function of Glass Composition. *npj Mater Degrad* **4,** 36. ISSN: 2397-2106 (Dec. 2020).
14. De Bardi, M., Hutter, H., Schreiner, M. & Bertoncello, R. Sol- Gel Silica Coating for Potash Lime- Silica Stained Glass: Applicability and Protective Effect. *Journal of Non-Crystalline Solids* **390,** 45–50. ISSN: 00223093 (Apr. 2014).

15. Melcher, M. & Schreiner, M. in *Modern Methods for Analysing Archaeological and Historical Glass* (ed Janssens, K.) 609–651 (John Wiley & Sons Ltd, Oxford, UK, Jan. 2013). ISBN: 978-1-118-31423-4 978-0-470-51614-0.

16. De Bardi, M., Hutter, H., Schreiner, M. & Bertoncello, R. Potash-Lime-Silica Glass: Protection from Weathering. *Herit Sci* **3,** 22. ISSN: 2050-7445 (Dec. 2015).

17. Newton, R. The Weathering of Medieval Window Glass. *Journal of Glass Studies* **17,** 161–168 (1975).

18. Alloteau, F. *et al.* Efficacy of Zinc Salts to Protect Glass against Atmospheric Alteration. Part I: Effects of a Spraying Treatment. *J. Am. Ceram. Soc.* **104,** 2039–2051. ISSN: 0002-7820, 1551-2916 (May 2021).

19. Koob, S. P. *Conservation and Care of Glass Objects* ISBN: 978-1-904982-08-1 (Archetype Publications ; Published in association with the Corning Museum of Glass, London : Corning, N.Y, 2006).

20. Robinet, L., Coupry, C., Eremin, K. & Hall, C. Raman Investigation of the Structural Changes during Alteration of Historic Glasses by Organic Pollutants. *J. Raman Spectrosc.* **37,** 1278–1286. ISSN: 03770486, 10974555 (Nov. 2006).

21. Alloteau, F. *et al.* New Insight into Atmospheric Alteration of Alkali-Lime Silicate Glasses. *Corrosion Science* **122,** 12–25. ISSN: 0010938X (July 2017).

22. Robinet, L., Fearn, S. & Eremin, K. Understanding Glass Deterioration in Museum Collections: A Multi-Disciplinary Approach. *Glass and Ceramics* (2005).

23. Fearn, S., McPhail, D. S. & Oakley, V. Room Temperature Corrosion of Museum Glass: An Investigation Using Low-Energy SIMS. *Applied Surface Science* **231–232,** 510–514. ISSN: 01694332 (June 2004).

24. Brill, R. H. Crizzling - a Problem in Glass Conservation. *Studies in Conservation* **20,** 121–134. ISSN: 0039-3630, 2047-0584 (Jan. 1975).

25. Alloteau, F. *et al.* in *Glass Atmospheric Alteration: Cultural Heritage, Industrial and Nuclear Glasses* (Hermann Ed., Paris (France), 2019). ISBN: ISBN978-2705697945.

26. Fearn, S., McPhail, D., Hagenhoff, B. & Tallarek, E. TOF-SIMS Analysis of Corroding Museum Glass. *Applied Surface Science* **252,** 7136–7139. ISSN: 01694332 (July 2006).

27. Eremin, K., Cobo del Arco, B., Robinet, L. & Gibson, L. in *Annales Du 16th Congrès International d'Etude Historique Du Verre* (London, 2003).

28. Robinet, L., Eremin, K., Coupry, C., Hall, C. & Lacome, N. Effect of Organic Acid Vapors on the Alteration of Soda Silicate Glass. *Journal of Non-Crystalline Solids* **353,** 1546–1559. ISSN: 00223093 (June 2007).

29. Oakley, V. L., Ryan, J. L., McPhail, D. S. & Rogers, P. S. in *ICOM Committee for Conservation 11th Triennial Meeting Edinburgh, Scotland 1.-6. Sept. 1996: Preprints* Kongreß, ICOM Conservation, 11,1996 [Edinburgh], 839–844 (James & James, London, 1996). ISBN: 978-1-873936-50-4.

30. Lombardo, T. *et al.* Long Term Assessment of Atmospheric Decay of Stained Glass Windows. *Corrosion Engineering, Science and Technology* **45,** 420–424. ISSN: 1478-422X, 1743-2782 (Oct. 2010).

31. Majérus, O. *et al.* Glass Alteration in Atmospheric Conditions: Crossing Perspectives from Cultural Heritage, Glass Industry, and Nuclear Waste Management. *npj Mater Degrad* **4,** 27. ISSN: 2397-2106 (Dec. 2020).

32. Lombardo, T., Gentaz, L. & Loisel, C. Altération des verres - Cas des vitraux du Moyen Âge. *Techniques d'analyse* (June 2015).

33. Comite, V. *et al.* Degradation Products on Byzantine Glasses from Northern Tunisia. *Applied Sciences* **10,** 7523. ISSN: 2076-3417 (Oct. 2020).

34. Emami, M., Nekouei, S., Ahmadi, H., Pritzel, C. & Trettin, R. Iridescence in Ancient Glass: A Morphological and Chemical Investigation. *Int J Appl Glass Sci* **7,** 59–68. ISSN: 20411286 (Mar. 2016).

35. Alloteau, F. *Contribution à la compréhension des mécanismes de l'altération atmosphérique des verres et étude d'un traitement de protection à base de sels de zinc* Théèse de doctorat (Paris Sciences et Lettres PSL Research University, Paris, 2017).

36. Gin, S. *et al.* A General Mechanism for Gel Layer Formation on Borosilicate Glass under Aqueous Corrosion. *J. Phys. Chem. C* **124,** 5132–5144. ISSN: 1932-7447, 1932-7455 (Mar. 2020).

37. Fournier, M., Gin, S. & Frugier, P. Resumption of Nuclear Glass Alteration: State of the Art. *Journal of Nuclear Materials* **448,** 348–363. ISSN: 00223115 (May 2014).

38. Ojovan, M. I. On Alteration Rate Renewal Stage of Nuclear Waste Glass Corrosion. *MRS Advances* **5,** 111–120. ISSN: 2059-8521 (Jan. 2020).

39. Vienna, J. D., Ryan, J. V., Gin, S. & Inagaki, Y. Current Understanding and Remaining Challenges in Modeling Long-Term Degradation of Borosilicate Nuclear Waste Glasses. *Int J Appl Glass Sci* **4,** 283–294. ISSN: 20411286 (Dec. 2013).

40. Gin, S., Delaye, J.-M., Angeli, F. & Schuller, S. Aqueous Alteration of Silicate Glass: State of Knowledge and Perspectives. *npj Mater Degrad* **5,** 42. ISSN: 2397-2106 (Aug. 2021).

41. Barbana, F., Bertoncello, R., Milanese, L. & Sada, C. Alteration and Corrosion Phenomena in Roman Submerged Glass Fragments. *Journal of Non-Crystalline Solids* **337,** 136–141. ISSN: 00223093 (July 2004).

42. Doremus, R. H. Interdiffusion of Hydrogen and Alkali Ions in a Glass Surface. *Journal of Non-Crystalline Solids* **19,** 137–144 (1975).

43. Vilarigues, M. & da Silva, R. Characterization of Potash-Glass Corrosion in Aqueous Solution by Ion Beam and IR Spectroscopy. *Journal of Non-Crystalline Solids* **352,** 5368–5375. ISSN: 00223093 (Dec. 2006).

44. Scholze, H. Chemical Durability of Glasses. *Journal of Non-Crystalline Solids* **52,** 91–103. ISSN: 00223093 (Dec. 1982).

45. Bunker, B. Molecular Mechanisms for Corrosion of Silica and Silicate Glasses. *Journal of Non-Crystalline Solids* **179,** 300–308. ISSN: 00223093 (Nov. 1994).

46. Frugier, P. *et al.* SON68 Nuclear Glass Dissolution Kinetics: Current State of Knowledge and Basis of the New GRAAL Model. *Journal of Nuclear Materials* **380,** 8–21. ISSN: 00223115 (Oct. 2008).

47. Paul, A. in *Chemistry of Glasses* 108–147 (Springer Netherlands, Dordrecht, 1982). ISBN: 978-94-009-5920-0 978-94-009-5918-7.

48. Erigoni, A. & Diaz, U. Porous Silica-Based Organic-Inorganic Hybrid Catalysts: A Review. *Catalysts* **11,** 79. ISSN: 2073-4344 (Jan. 2021).

49. Melcher, M. & Schreiner, M. Leaching Studies on Naturally Weathered Potash-Lime–Silica Glasses. *Journal of Non-Crystalline Solids* **352,** 368–379. ISSN: 00223093 (May 2006).

50. Cailleteau, C. *et al.* Insight into Silicate-Glass Corrosion Mechanisms. *Nature Mater* **7,** 978–983. ISSN: 1476-1122, 1476-4660 (Dec. 2008).

51. Ngo, D., Liu, H., Kaya, H., Chen, Z. & Kim, S. H. Dissolution of Silica Component of Glass Network at Early Stage of Corrosion in Initially Silica-saturated Solution. *J Am Ceram Soc* **102,** 6649–6657. ISSN: 0002-7820, 1551-2916 (Nov. 2019).

52. Rajmohan, N., Frugier, P. & Gin, S. Composition Effects on Synthetic Glass Alteration Mechanisms: Part 1. Experiments. *Chemical Geology* **279,** 106–119. ISSN: 00092541 (Dec. 2010).

53. Cummings, K., Lanford, W. & Feldmann, M. Weathering of Glass in Moist and Polluted Air. *Nuclear Instruments and Methods in Physics Research Section B: Beam Interactions with Materials and Atoms* **136–138,** 858–862. ISSN: 0168583X (Mar. 1998).

54. Collin, M. *et al.* Molecular Dynamics Simulations of Water Structure and Diffusion in a 1 Nm Diameter Silica Nanopore as a Function of Surface Charge and Alkali Metal Counterion Identity. *J. Phys. Chem. C* **122,** 17764–17776. ISSN: 1932-7447, 1932-7455 (Aug. 2018).

55. Gentaz, L., Lombardo, T., Chabas, A., Loisel, C. & Verney-Carron, A. Impact of Neocrystallisations on the SiO2–K2O–CaO Glass Degradation Due to Atmospheric Dry Depositions. *Atmospheric Environment* **55,** 459–466. ISSN: 13522310 (Aug. 2012).

56. de Ferri, L., Lottici, P. P., Lorenzi, A., Montenero, A. & Vezzalini, G. Hybrid Sol–Gel Based Coatings for the Protection of Historical Window Glass. *J Sol-Gel Sci Technol* **66,** 253–263. ISSN: 0928-0707, 1573-4846 (May 2013).

57. Artesani, A., Di Turo, F., Zucchelli, M. & Traviglia, A. Recent Advances in Protective Coatings for Cultural Heritage–An Overview. *Coatings* **10,** 217. ISSN: 2079-6412 (Feb. 2020).

58. Yuan, Z., Chen, H. & Zhang, J. Facile Method to Prepare Lotus-Leaf-like Super-Hydrophobic Poly(Vinyl Chloride) Film. *Applied Surface Science* **254,** 1593–1598. ISSN: 01694332 (Jan. 2008).

59. Cassie, A. B. D. & Baxter, S. Wettability of Porous Surfaces. *Trans. Faraday Soc.* **40,** 546. ISSN: 0014-7672 (1944).

60. Yang, H. *et al.* Preparation of Lotus-Leaf-like Antibacterial Film Based on Mesoporous Silica Microcapsule-Supported Ag Nanoparticles. *RSC Adv.* **4,** 2793–2796. ISSN: 2046-2069 (2014).

61. Latthe, S., Terashima, C., Nakata, K. & Fujishima, A. Superhydrophobic Surfaces Developed by Mimicking Hierarchical Surface Morphology of Lotus Leaf. *Molecules* **19,** 4256–4283. ISSN: 1420-3049 (Apr. 2014).

62. Ebert, D. & Bhushan, B. Transparent, Superhydrophobic, and Wear-Resistant Coatings on Glass and Polymer Substrates Using SiO $_2$, ZnO, and ITO Nanoparticles. *Langmuir* **28,** 11391–11399. ISSN: 0743-7463, 1520-5827 (Aug. 2012).

63. Wang, X.-D. *et al.* Preparation of Spherical Silica Particles by St?Ber Process with High Concentration of Tetra-Ethyl-Orthosilicate. *Journal of Colloid and Interface Science* **341,** 23–29. ISSN: 00219797 (Jan. 2010).

64. Nozawa, K. *et al.* Smart Control of Monodisperse Stöber Silica Particles: Effect of Reactant Addition Rate on Growth Process. *Langmuir* **21,** 1516–1523. ISSN: 0743-7463, 1520-5827 (Feb. 2005).

65. Najafi, A. & Ghasemi, S. A Study of APC Surfactant Role on the Surface Characteristics, Size and Morphology Improvements of Synthesized Mesoporous Silica Nanopowder through a Sol-Gel Process. *Journal of Alloys and Compounds* **720,** 423–431. ISSN: 09258388 (Oct. 2017).

66. Stöber, W., Fink, A. & Bohn, E. Controlled Growth of Monodisperse Silica Spheres in the Micron Size Range. *Journal of Colloid and Interface Science* **26,** 62–69. ISSN: 00219797 (Jan. 1968).

67. Han, Y. *et al.* Unraveling the Growth Mechanism of Silica Particles in the Stöber Method: In Situ Seeded Growth Model. *Langmuir* **33,** 5879–5890. ISSN: 0743-7463, 1520-5827 (June 2017).

68. Green, D. *et al.* Size, Volume Fraction, and Nucleation of Stober Silica Nanoparticles. *Journal of Colloid and Interface Science* **266,** 346–358. ISSN: 00219797 (Oct. 2003).

69. Alloteau, F. *et al.* Efficacy of Zinc Salts to Protect Glass against Atmospheric Alteration. Part II: Possible Passivation Mechanisms. *J. Am. Ceram. Soc.* **104,** 2052–2065. ISSN: 0002-7820, 1551-2916 (May 2021).

70. Valbi, V. *Study of the Interaction between Glass Surfaces Altered in Atmospheric Conditions and a Zinc(II) Salts Deposit. Potentiality of a Zinc Salts Protective Treatment.* PhD thesis (Università di Bologna, 2015).

71. Barbe, F. & Le Roux, J. in *Glass Atmospheric Alteration: Cultural Heritage, Industrial and Nuclear Glasses (Eds Biron, I., Alloteau, F., Lehuédé, P., Majérus, O. & Caurant, D.)* 111–117 (Hermann, Paris, 2019). ISBN: 978-2-7056-9794-5.

72. Greenspan, L. Humidity Fixed Points of Binary Saturated Aqueous Solutions. *J. RES. NATL. BUR. STAN. SECT. A.* **81A,** 89. ISSN: 0022-4332 (Jan. 1977).

73. Tournié, A. *et al.* Impact of Boron Complexation by Tris Buffer on the Initial Dissolution Rate of Borosilicate Glasses. *Journal of Colloid and Interface Science* **400,** 161–167. ISSN: 00219797 (June 2013).

74. Walters, H. V. & Adams, P. B. Effects of Humidity on the Weathering of Glass. *Journal of Non-Crystalline Solids* **19,** 183–199 (1975).

75. Park, S. K., Kim, K. D. & Kim, H. T. Preparation of Silica Nanoparticles: Determination of the Optimal Synthesis Conditions for Small and Uniform Particles. *Colloids and Surfaces A: Physicochemical and Engineering Aspects* **197,** 7–17. ISSN: 09277757 (Feb. 2002).

76. Kharchenko, A., Myronyuk, O., Melnyk, L. & Sivolapov, P. Analysis of Methods of Regulation of Silicon Dioxide Particles Size Obtained by the Stober Method. *TAPR* **2,** 9–16. ISSN: 2312-8372, 2226-3780 (Dec. 2017).

77. Sivolapov, P., Myronyuk, O. & Baklan, D. Synthesis of Stober Silica Nanoparticles in Solvent Environments with Different Hansen Solubility Parameters. *Inorganic Chemistry Communications* **143,** 109769. ISSN: 13877003 (Sept. 2022).

78. Stucchi, N. M. E., Tesser, E., Zaccariello, G., Antonelli, F. & Benedetti, A. Evaluating Two Nanosilica Dimensional Range for the Consolidation of Degraded Silicate Stones. *Construction and Building Materials* **329,** 127191. ISSN: 09500618 (Apr. 2022).

79. Innocenzi, P. *The Sol-to-Gel Transition* ISBN: 978-3-030-20029-9 978-3-030-20030-5 (Springer International Publishing, Cham, 2019).

80. *50mL Centrifuge Tube & Cap* https://www.qualitybiological.com/product/tube-cap-50ml-centrifuge-tube-cap-bags-non-sterile-caps-and-tubes-packed-separately/.

81. *Amicon Ultra-15 Centrifugal Filter Unit* https://www.sigmaaldrich.com/IT/it/product/mm/ufc9050.

82. Sierra-Fernandez, A., Gomez-Villalba, L. S., Rabanal, M. E. & Fort, R. New Nanomaterials for Applications in Conservation and Restoration of Stony Materials: A Review. *Mater. construcc.* **67,** 107. ISSN: 1988-3226, 0465-2746 (Jan. 2017).

83. Amma, S.-i., Kim, S. H. & Pantano, C. G. Analysis of Water and Hydroxyl Species in Soda Lime Glass Surfaces Using Attenuated Total Reflection (ATR)-IR Spectroscopy. *J. Am. Ceram. Soc.* **99** (ed Mauro, J.) 128–134. ISSN: 0002-7820, 1551-2916 (Jan. 2016).

84. Lowenstern, J. B. & Pitcher, B. W. Analysis of H2O in Silicate Glass Using Attenuated Total Reflectance (ATR) Micro-FTIR Spectroscopy. *American Mineralogist* **98,** 1660–1668. ISSN: 0003-004X (Oct. 2013).

85. Collin, M. *et al.* Structure of International Simple Glass and Properties of Passivating Layer Formed in Circumneutral pH Conditions. *npj Mater Degrad* **2,** 4. ISSN: 2397-2106 (Dec. 2018).

86. Majérus, O., Gérardin, T., Manolescu, G., Barboux, P. & Caurant, D. Effect of Aqueous Mg^{2+} and Ca^{2+} Cations on the Dissolution Kinetics and Alteration Layer of Sodium Borosilicate Glasses at Neutral pH Buffered with Tris/HCl. *Physics and Chemistry of Glasses* **55** (2014).

87. Gin, S. *et al.* The Fate of Silicon during Glass Corrosion under Alkaline Conditions: A Mechanistic and Kinetic Study with the International Simple Glass. *Geochimica et Cosmochimica Acta* **151,** 68–85. ISSN: 00167037 (Feb. 2015).

88. Inagaki, Y. *et al.* Aqueous Alteration of Japanese Simulated Waste Glass P0798: Effects of Alteration-Phase Formation on Alteration Rate and Cesium Retention. *Journal of Nuclear Materials* **354,** 171–184. ISSN: 00223115 (Aug. 2006).

89. Gin, S., Ribet, I. & Couillard, M. Role and Properties of the Gel Formed during Nuclear Glass Alteration: Importance of Gel Formation Conditions. *Journal of Nuclear Materials* **298,** 1–10. ISSN: 00223115 (Sept. 2001).

90. Panalytical, M. *Intensity-Volume-Number. Which Size Is Correct?* 2010.

91. Alloteau, F. *et al.* Temperature-Dependent Mechanisms of the Atmospheric Alteration of a Mixed-Alkali Lime Silicate Glass. *Corrosion Science* **159,** 108129. ISSN: 0010938X (Oct. 2019).

92. Charlaix, E. & Ciccotti, M. in *Handbook of Nanophysics* (CRC Press, 2009).

93. Falcone, R., Licenziati, F., Orsega, E. F. & Verità, M. The Dependence of the Weathering of Soda-Lime-Silica Glass on Environmental Parameters: A Preliminary Investigation. *Glass Technology: European Journal of Glass Science and Technology Part A* **52,** 23–29 (Feb. 2011).

94. Silverstein, R. M., Webster, F. X. & Kiemle, D. J. *Spectrometric Identification of Organic Compounds* 7th ed. Includes index. ISBN: 978-0-471-39362-7 978-0-471-42913-5 (John Wiley & Sons, Hoboken, NJ, 2005).

95. Navarra, G., Iliopoulos, I., Militello, V., Rotolo, S. & Leone, M. OH-related Infrared Absorption Bands in Oxide Glasses. *Journal of Non-Crystalline Solids* **351,** 1796–1800. ISSN: 00223093 (July 2005).

96. Efimov, A. M., Pogareva, V. G. & Shashkin, A. V. Water-Related Bands in the IR Absorption Spectra of Silicate Glasses. *Journal of Non-Crystalline Solids* **332,** 93–114. ISSN: 00223093 (Dec. 2003).

97. Suzuki, T., Konishi, J., Yamamoto, K., Ogura, S. & Fukutani, K. Practical IR Extinction Coefficients of Water in Soda Lime Aluminosilicate Glasses Determined by Nuclear Reaction Analysis. *Journal of Non-Crystalline Solids* **382,** 66–69. ISSN: 00223093 (Dec. 2013).

98. Davis, K. & Tomozawa, M. An Infrared Spectroscopic Study of Water-Related Species in Silica Glasses. *Journal of Non-Crystalline Solids* **201,** 177–198. ISSN: 00223093 (June 1996).

99. Bartholomew, R., Butler, B., Hoover, H. & Wu, C. Infrared Spectra of a Water-Containing Glass. *Journal of the American Ceramic Society* **63,** 481–485 (1980).

100. Arévalo, R., Mosa, J., Aparicio, M. & Palomar, T. The Stability of the Ravenscroft's Glass. Influence of the Composition and the Environment. *Journal of Non-Crystalline Solids* **565,** 120854. ISSN: 00223093 (Aug. 2021).

101. Palomar, T., Chabas, A., Bastidas, D. M., de la Fuente, D. & Verney-Carron, A. Effect of Marine Aerosols on the Alteration of Silicate Glasses. *Journal of Non-Crystalline Solids* **471,** 328–337. ISSN: 00223093 (Sept. 2017).

102. Hosseinpour, S. & Johnson, M. Vibrational Spectroscopy in Studies of Atmospheric Corrosion. *Materials* **10,** 413. ISSN: 1996-1944 (Apr. 2017).

103. Abo-Naf, S. M., El Batal, F. H. & Azooz, M. A. Characterization of Some Glasses in the System SiO2, Na2O·RO by Infrared Spectroscopy. *Materials Chemistry and Physics* **77,** 846–852. ISSN: 02540584 (Jan. 2003).

104. Aguiar, H., Serra, J., González, P. & León, B. Structural Study of Sol–Gel Silicate Glasses by IR and Raman Spectroscopies. *Journal of Non-Crystalline Solids* **355,** 475–480. ISSN: 00223093 (Apr. 2009).

105. Duran, A., Serna, C., Fornes, V. & Fernandez Navarro, J. Structural Considerations about SiO2 Glasses Prepared by Sol-Gel. *Journal of Non-Crystalline Solids* **82,** 69–77. ISSN: 00223093 (June 1986).

106. Lee, Y.-K., Peng, Y. L. & Tomozawa, M. IR Reflection Spectroscopy of a Soda-Lime Glass Surface during Ion-Exchange. *Journal of Non-Crystalline Solids* **222,** 125–130. ISSN: 00223093 (Dec. 1997).

107. Geotti-Bianchini, F., Preo, M., Guglielmi, M. & Pantano, C. G. Infrared Reflectance Spectra of Semi-Transparent SiO2 Rich Films on Silicate Glasses: Influence of the Substrate and Film Thickness. *Journal of Non-Crystalline Solids* **321,** 110–119. ISSN: 00223093 (June 2003).

108. Bertoluzza, A., Fagnano, C., Antonietta Morelli, M., Gottardi, V. & Guglielmi, M. Raman and Infrared Spectra on Silica Gel Evolving toward Glass. *Journal of Non-Crystalline Solids* **48,** 117–128. ISSN: 00223093 (Mar. 1982).

109. Le Losq, C., Mysen, B. O. & Cody, G. D. Water and Magmas: Insights about the Water Solution Mechanisms in Alkali Silicate Melts from Infrared, Raman, and 29Si Solid-State NMR Spectroscopies. *Prog. in Earth and Planet. Sci.* **2,** 22. ISSN: 2197-4284 (Dec. 2015).

110. Hehlen, B., Neuville, D., Kilymis, D. & Ispas, S. Bimodal Distribution of Si–O–Si Angles in Sodo-Silicate Glasses. *Journal of Non-Crystalline Solids* **469,** 39–44. ISSN: 00223093 (Aug. 2017).

111. Mysen, B. Structure of H_2 O-saturated Peralkaline Aluminosilicate Melt and Coexisting Aluminosilicate-Saturated Aqueous Fluid Determined in-Situ to 800°C and ∼800MPa. *Geochimica et Cosmochimica Acta* **74,** 4123–4139. ISSN: 00167037 (July 2010).

112. Ando, M. F. *et al.* Boson Peak, Heterogeneity and Intermediate-Range Order in Binary SiO2-Al2O3 Glasses. *Sci Rep* **8,** 5394. ISSN: 2045-2322 (Dec. 2018).

113. McMillan, P. Structural Studies of Silicate Glasses and Melts-Applications and Limitations of Raman Spectroscopy. *Raman Spectroscopy* **69,** 622–644 (1984).

114. Ferri, L. *et al.* Raman Study of Model Glass with Medieval Compositions: Artificial Weathering and Comparison with Ancient Samples. *J. Raman Spectrosc.* **43,** 1817–1823. ISSN: 0377-0486, 1097-4555 (Nov. 2012).

115. Furukawa, T., Fox, K. E. & White, W. B. Raman Spectroscopic Investigation of the Structure of Silicate Glasses. III. Raman Intensities and Structural Units in Sodium Silicate Glasses. *The Journal of Chemical Physics* **75,** 3226–3237. ISSN: 0021-9606, 1089-7690 (Oct. 1981).

116. Robinet, L., Coupry, C., Eremin, K. & Hall, C. The Use of Raman Spectrometry to Predict the Stability of Historic Glasses. *J. Raman Spectrosc.* **37,** 789–797. ISSN: 0377-0486, 1097-4555 (July 2006).

117. Cesaratto, A. *et al.* Characterization of Archeological Glasses by Micro-Raman Spectroscopy. *J. Raman Spectrosc.* **41,** 1682–1687. ISSN: 03770486 (Dec. 2010).

118. Tan, J., Zhao, S., Wang, W., Davies, G. & Mo, X. The Effect of Cooling Rate on the Structure of Sodium Silicate Glass. *Materials Science and Engineering: B* **106,** 295–299. ISSN: 09215107 (Feb. 2004).

119. Spiekermann, G., Steele-MacInnis, M., Schmidt, C. & Jahn, S. Vibrational Mode Frequencies of Silica Species in SiO_2-H_2O Liquids and Glasses from *Ab Initio* Molecular Dynamics. *The Journal of Chemical Physics* **136,** 154501. ISSN: 0021-9606, 1089-7690 (Apr. 2012).

120. Schroeder, J. *et al.* Raman Scattering and Boson Peaks in Glasses: Temperature and Pressure Effects. *Journal of Non-Crystalline Solids* **349,** 88–97. ISSN: 00223093 (Dec. 2004).

121. Ohashi, H. & Sekita, M. Raman Spectroscopic Study of the Si-O-Si Stretching Vibration in Clinopyroxenes. *J. Japan. Assoc. Min. Petr. Econ. Geol.* **77,** 455–459. ISSN: 0021-4825, 1883-0765 (1982).

122. Lafuente, B., Downs, R., Yang, H. & Stone, N. *RRUFF* https://rruff.info/.

123. Buzgar, N., Ionu, A. & Apopei, Ț. The Raman Study of Certain Carbonates. *Analele Stiintifice de Universitatii "Al. I. Cuza" Iasi* **55,** 97–112 (2009).

124. Burgio, L. & Clark, R. J. Library of FT-Raman Spectra of Pigments, Minerals, Pigment Media and Varnishes, and Supplement to Existing Library of Raman Spectra of Pigments with Visible Excitation. *Spectrochimica Acta Part A: Molecular and Biomolecular Spectroscopy* **57,** 1491–1521. ISSN: 13861425 (June 2001).

125. Koura, N. *et al.* Alkali Carbonates: Raman Spectroscopy, Ab Initio Calculations, and Structure. *Journal of Molecular Structure* **382,** 163–169. ISSN: 00222860 (Sept. 1996).

126. Frost, R. L. & Dickfos, M. Hydrated Double Carbonates – A Raman and Infrared Spectroscopic Study. *Polyhedron* **26,** 4503–4508. ISSN: 02775387 (Sept. 2007).

127. Coleyshaw, E. E., Crump, G. & Griffith, W. P. Vibrational Spectra of the Hydrated Carbonate Minerals Ikaite, Monohydrocalcite, Lansfordite and Nesquehonite. *Spectrochimica Acta Part A: Molecular and Biomolecular Spectroscopy* **59,** 2231–2239. ISSN: 13861425 (Aug. 2003).

128. Robert, E., Whittington, A., Fayon, F., Pichavant, M. & Massiot, D. Structural Characterization of Water-Bearing Silicate and Aluminosilicate Glasses by High-Resolution Solid-State NMR. *Chemical Geology* **174,** 291–305. ISSN: 00092541 (Apr. 2001).

129. Maekawa, H., Maekawa, T., Kawamura, K. & Yokokawa, T. The Structural Groups of Alkali Silicate Glasses Determined from 29Si MAS-NMR. *Journal of Non-Crystalline Solids* **127,** 53–64. ISSN: 00223093 (Jan. 1991).

130. Iler, R. K. *The Chemistry of Silica: Solubility, Polymerization, Colloid and Surface Properties, and Biochemistry* "A Wiley-Interscience publication." ISBN: 978-0-471-02404-0 (Wiley, New York, 1979).

131. Hester, R. E. & Scaife, C. W. J. Vibrational Spectra of Molten Salts. III. Infrared and Raman Spectra of Variably Hydrated Zinc Nitrate. *The Journal of Chemical Physics* **47,** 5253–5258. ISSN: 0021-9606, 1089-7690 (Dec. 1967).

132. Ju, Y., Du, Z., Xiao, C., Li, X. & Li, S. Novel Effect of Zinc Nitrate/Vanadyl Oxalate for Selective Catalytic Oxidation of α-Hydroxy Esters to α-Keto Esters with Molecular Oxygen: An In Situ ATR-IR Study. *Molecules* **24,** 1281. ISSN: 1420-3049 (Apr. 2019).

133. Winiarski, J., Tylus, W., Winiarska, K., Szczygieł, I. & Szczygieł, B. XPS and FT-IR Characterization of Selected Synthetic Corrosion Products of Zinc Expected in Neutral Environment Containing Chloride Ions. *Journal of Spectroscopy* **2018,** 1–14. ISSN: 2314-4920, 2314-4939 (July 2018).

134. Buckley, A. M. & Greenblatt, M. The Sol-Gel Preparation of Silica Gels. *J. Chem. Educ.* **71,** 599. ISSN: 0021-9584, 1938-1328 (July 1994).

135. Bogren, S. *et al.* Classification of Magnetic Nanoparticle Systems—Synthesis, Standardization and Analysis Methods in the NanoMag Project. *IJMS* **16,** 20308–20325. ISSN: 1422-0067 (Aug. 2015).

Acknowledgments

As a conclusion of this work, I would like to thank all the people that made its accomplishment possible. First of all, my supervisors Robert Carlyle Pullar, Odile Majérus, Giulia Franceschin and Arianna Traviglia for giving me the chance of taking part in this diverse project, in which I had the opportunity to greatly learn and grow. Not only could I finally participate in the fascinating study of glass, but also I had the possibility of getting closer to different environments of scientific research.

My words are probably not enough for expressing my gratitude to Odile Majérus, for all she taught me with great care and passion and for the motivation she gave me with her encouragements to pursue my interest in research. I could not have been luckier in having Thalie Law as internship mate in Paris. We shared challenges and adventures in great harmony and a lot of laughter. Very significant to me was also the kind and attentive support of Daniel Caurant, who has been a constant reference for the unfolding of the project. A big thanks goes to all the members of the équipes PCMTH and MPOE, who made the working environment be motivating, collaborative and joyful, and to the trainees *secrétariat*, which turned a little misfortune into a daily fun.

I will bear as a great example the admirable co-operation attitude which led a number of people at Chimie ParisTech to give us a precious help in the different steps of our research project. The inclusion of multiple analytical techniques was made possible by their guidance and availability, as well as that of researchers from different establishments. I would therefore like to thank Antoine Seyeux (IRCP) and Thibault Charpentier (CEA) for performing the ToF-SIMS and NMR measurements respectively; the C2RMF for the possibility of carrying out SEM-EDX investigations, and Gregory Lefevre, Alexandre Guillot, Julien Sanglerat, Patrick Gredin and Patrice Lehuédé for the training and support in the performing of FTIR, TGA, ICP-AES analyses and the employment of the climatic chamber and STRATAGem software.

The internship in Paris could not have taken place without the collaboration with Saint Gobain Research. My gratitude thereby goes to Amandine Serve, Sophie Papin and Hervé Montigaud, for the great teamwork they developed and for the chance they gave me of getting to know the research running behind the industry.

I would like to thank all the members of the conservation science group of the IIT for welcoming me in their team during my traineeship in Venice. I am particularly grateful to Giulia Franceschin, for her patient guidance during this whole thesis project and for all she taught me. Fundamental was the contribution of Neva Stucchi and Stefano Centenaro, who helped and supported me in the synthesis and study of silica nanoparticles. I would also like to thank Mauro Moglianetti, Roberta Zanini and Luigi Marasco for their help and Luca Leoncino for performing the TEM analyses.

A particular thanks then goes to the people who were not officially part of the project but have played key roles behind the scenes: Prof. Alvise Benedetti, who encouraged me to put myself on the line and gave me important life advice when I was in doubt of what to do next, Prof. Ligia Maria Moretto for her prompt listening, encouragement and guidance, and Giulia Moro, who gave me confidence in my potentials and helped me with the great passion she devotes to tutoring students.

I am also very grateful to Margherita, for teaching me how to use LaTeX, to my scout group Pablo Neruda for giving me the escapes in nature and simplicity I needed, and to my friends, for all the support, talks and sharing that guided me in this year of thesis. Finally, I would like to thank my family for the confidence and dedication they have instilled in me through the love and trust they constantly demonstrate and for their enthusiastic encouragement to follow my dreams.